Université de Neuchâtel - Faculté des Sciences

A study of meteoritic impact craters with the magnetotelluric method

par
WILHELM MASERO
Institut de Géologie

THÈSE
présentée à la Faculté des Sciences de l'Université de Neuchâtel
pour obtenir le grade de docteur ès sciences

Neuchâtel, 1995

IMPRIMATUR POUR LA THÈSE

A Study of Meteoritic Impact Craters with the Magnetotelluric Method

de M. Wilhelm Masero

UNIVERSITÉ DE NEUCHÂTEL

FACULTÉ DES SCIENCES

La Faculté des sciences de l'Université de Neuchâtel sur le rapport des membres du jury,

Messieurs G. Fischer, M. Burkhard , P.-A. Schnegg et A. Junge (Frankfort)

autorise l'impression de la présente thèse.

Neuchâtel, le 14 novembre 1995

Le doyen:

R. Dändliker

A study of meteoritic impact craters with the magnetotelluric method

by

Wilhelm Masero

Doctoral dissertation at the University of Neuchâtel, Switzerland, 1995

Abstract

Impact cratering played a major role in the evolution of the terrestrial planets. A simple comparison with the heavily cratered moon indicates that the major impact evidence on the Earth's landscape has been continuously erased by the action of erosion. Nevertheless, almost the entire knowledge about the deep aspects of impact craters comes from geological and geophysical investigations of known structures on our own planet's surface. In order to reveal some of the structural characteristics underneath large and complex impact craters a series of magnetotelluric (MT) soundings were carried out in two different locations, the Araguainha Dome in Central Brazil and the Serra da Cangalha in Northeast Brazil. In spite of their common meteoritic origin these investigations revealed distinct features for both structures.

With a diameter of 40 km the Araguainha Dome is the largest known impact site in South America. It is characterised by its appearance as a set of imbricated circles and a central uplift with a diameter of 18 km. A total of 25 MT soundings were carried out across the structure, along 5 radii. The MT responses in the period range from 0.001 to 1 s show one-dimensional behaviour, in contrast to the longer periods where data show, at periods between 1 and 10 s, a splitting of the apparent resistivity and phase curves of both polarizations, accompanied by a strong increase of the phase-sensitive regional skew parameter to values up to 0.5. This is believed to be caused by impact induced faulting and brecciation of the crust, reaching to depths of 3 to 7 km. The horizontal extent of this zone is 16 km, corresponding to about 40% of the total crater diameter at the surface. The long period data (periods $T > 10$ s) reveal an anomalous lower crust of enhanced conductivity at depths between 15 and 30 km, which is not related to the impact event. It is likely to be a feature typical of the basement in the area of the Araguainha structure.

The smaller Serra da Cangalha crater has a diameter of 13 km and its prominent feature is a central ring of mountains with a diameter of 3 to 4 km. The MT data indicate in general a one-dimensional conductivity distribution of the subsurface. Nevertheless, anisotropic MT responses in the period range between 0.01 and 0.1 s are observed at a few sites, all located in the vicinity of the centre. They reflect a fractured zone, which is no deeper than a few hundred metres and has a horizontal extension smaller than the total diameter of

the structure. In spite of the crater-like appearance of the Serra da Cangalha, the outcropping structure is considered to represent the root of a deeply eroded complex crater. The identification in the data of shallow impact effects favours this point of view. Additionally, the recognition at all MT sites of a good conducting layer at a depth of about 1100 m provides an accurate maximum depth for the impact disturbance in the surrounding bedrocks.

Introduction

Magnetotellurics (MT) is a geophysical technique which provides information about the electrical conductivity distribution of the Earth's underground. The method is based on the relationship between transient electric and magnetic fields, which are measured at the Earth's surface. The main source of the fields are natural fluctuations of the Earth's magnetic field, which occur over a wide spectrum of frequencies. The magnetic field variations diffuse into the Earth and induce electric currents, the so-called telluric currents, which in turn cause secondary magnetic fields. The first task when carrying out an MT sounding is to record the time-varying geoelectromagnetic fields. The recordings are processed into frequency-dependent responses and are then used for the interpretation of the Earth's conductivity. The depth of penetration of the method is controlled by the skin-effect, i.e., the recorded variations of the geoelectromagnetic fields give information concerning increasing depths as the period of the signal becomes longer.

The MT method was first and independently proposed by (Tikhonov, 1950) and (Cagniard, 1953) in the early fifties and is nowadays widely applied in the investigation of all sorts of geological and tectonic environments. A good collection of fifty-five papers with details on the historical development and state-of-the-art up to early 1980s on the MT method is given in the Society of Exploration Geophysicists book edited by Vozoff (1986).

In spite of the wide application of the method, only few MT surveys are known to have been carried out in areas of impact sites. The objectives of these studies were the determination of the deep electric structures associated with large impact events or the estimation of the depth of the floor of small craters. Zhang et al. (1990) observed in the Siljan crater (diameter D = 55 km), Sweden, a conductive zone, approximating the horizontal extent of the crater at a depth of 5 to 20 km. In Charlevoix (D = 46 km), Canada, a sub-horizontal conductor was interpreted by Mareschal and Chouteau (1990) as sub-horizontal faulting related to the impact at a depth of 1.5 km. High-frequency data revealed in the Colônia crater (D = 3.6 km), Brazil, a bowl-shaped depression, filled with 440 m of Quaternary sediments (Masero and Fontes, 1992).

The interest in studying impact structures has strongly increased over the last few decades. It has long been recognised that impact cratering processes played a major role in the formation and growth of the terrestrial planets and satellites, but only recently have the

effects of major impacts on the Earth's climatic and biologic evolution been considered (Melosh, 1989).

In contrast to the smaller and classic types of bowl-shaped simple craters, the Araguainha and the Serra da Cangalha structures, with diameters of respectively 40 km and 12 km, are complex craters with an uplifted central core of shocked rocks, surrounded by one or more concentric, peripheral depressions (Grieve et al., 1981). The transition from the simple to the complex form is a function of the diameter or impact energy and for terrestrial craters occurs at 1-2 km in sedimentary, and 3-4 km in crystalline targets.

Impact structures are indeed seen as laboratories for the study of the Earth's crust from which geophysics can draw a great deal of information. The main objective of this work is to reveal the deep structure of large and complex meteorite craters on the basis of MT measurements carried out at the Araguainha and Serra da Cangalha impact sites. Both structures lie in the Palaeozoic sediments of two large intracratonic basins, respectively the Paraná and the Parnaíba Basins. Their exact locations are 16° 46' S and 52° 59' W for the Araguainha crater, and 8° 05' S and 46° 52' W for the Serra da Cangalha crater. The MT method is well suited to provide a general picture of the basement of impact sites, as well as shape and extension of structures making up the crust, thus helping to secure a minimum value for the structural uplift of the crater floor during the impact event.

This work comprises four papers, which represent an overview and summary of the results and major aspects treated in the full length version of the dissertation *"A study of meteoritic impact craters with the magnetotelluric method"*.

The first paper, entitled *"A magnetotelluric investigation of the Araguainha impact crater in Mato Grosso-Goiás, central Brazil"*, deals with MT data in the frequency range from 1000 to 1 Hz collected in the region of the Araguainha crater. The paper starts with a description of the geological setting of the structure. For the high frequency range data analysis shows a one-dimensional (1-D) behaviour, whereas lower frequency data indicate multi-dimensional MT responses. The consideration of all four elements of the MT impedance tensor in the data analysis indicates the absence of strong galvanic distortion effects. However, static shift affected some of the sounding curves. The term "static" refers to the fact that it is a frequency-independent effect. It usually cannot be determined from MT data alone. A procedure is presented which successfully removes static shift by means of parametric constraints. These constraints are based on the radial distribution of the resistivity, believed to be caused by brecciation and fracturing of the target rocks during the impact. The 1-D modelling of the data allowed the determination of the thickness of the sediments covering the crystalline rocks in the area of the Araguainha structure, revealing the rise of the basement from an average depth of 1000 m to the surface within a circularly shaped area extending to a radius of 9 km from the centre of the structure.

The second paper *"Magnetotellurische Untersuchungen eines Meteoritenkraters"* treats the low frequency (< 1 Hz) range MT responses of the Araguainha region, which show

2-D and 3-D characteristics. The decomposition of the impedance tensor permitted to differentiate between a local and a regional distortion of the measured responses. The interpretation of the data was carried out in terms of a 2-D model, constituted of five vertical segments, which are symmetrically arranged with regard to the centre of the model. Because of the circular symmetry this corresponds to a thick disk, of which the 2-D model gives a vertical cut through an axial plane. The horizontal extension of this disk-shaped body is of 16 km and reaches to a depth of 7 km. The resistivity of the body varies from 20 to 500 Ωm and lies significantly below the bulk resistivity (5000 Ωm) of the surrounding basement rocks of the upper crust. Considerable brecciation and fracturing of the target rocks accompany crater formation and are believed to be the origin for this low resistivity. The lower portion of the 2-D model (15-30 km) is represented by a heterogeneous structure of alternating blocks of 2 Ωm and 2000 Ωm, which is not related to the impact event. This is likely to be a feature typical of the basement in the area of the Araguainha structure, characterised by the presence of a series of different Precambrian terrains. For instance, the continental dimensions of the Transbrazilian Lineament, which crosses the basement underneath the Araguainha structure, makes it a strong candidate for the origin of this lower crustal anomaly observed in the MT data.

The third paper *"Rotational properties of the magnetotelluric impedance tensor: the example of the Araguainha impact crater, Brazil"* describes a simple scheme for evaluating MT sounding results in terms of the three identical ellipses that the four elements of the MT impedance tensor define in the complex plane. It is shown that the orientation of the ellipses in the complex plane is strongly related to the directional properties of the structure. Structures with strong directionality yield ellipses whose major axes point towards the origin. For ellipses with their minor axes pointing to the origin, the structure is not very directional. A given structure can show these two kinds of behaviour simultaneously, though in different period ranges, i.e. in different depth ranges. However, for a structure characterised by circular symmetry like the Araguainha crater directional properties in different period bands must not forcibly be interpreted as different depth ranges, but rather as different lateral ranges. The circular structure will only manifest itself at frequencies sufficiently high for the skin-depth to be at most of the same order as the radius of the crater.

The fourth paper *"Magnetotelluric investigation of the Serra da Cangalha impact crater, Northeast Brazil"* presents the final results from MT investigations carried out in the sediments of the Parnaíba Basin, where the Serra da Cangalha impact structure is located. A geological description and a brief introduction to the MT method is given in the first part of the paper. Data analysis was performed with a special emphasis on the treatment of galvanic distortion effects caused by near-surface structures. Contrary to the Araguainha crater, most MT data indicate a generally undisturbed tabular distribution of the conductivity, thus requiring only the application of 1-D modelling routines. The identification at all MT models of a good conducting layer at a depth of about 1100 m provides an accurate maximum depth

for the impact effects in the sediments of the Parnaíba Basin. Like in the Araguainha structure, static shift was also successfully removed by means of a parametric constraint. In this case it was based on the identification of the good conducting layer in data sets free of static shift effects, and on the correlation of this layer with a sequence of over 350 m of good conducting Devonian shales in a borehole 70 km south of the Serra da Cangalha.

References

Cagniard, L., 1953. Basic theory of the magnetotelluric method of geophysical prospecting, *Geophysics*, **18**, 605-635.

Grieve, R.A.F., P.B. Robertson, and M.R. Dence, 1981. Constraints on the formation of ring impact structures, based on terrestrial data, in *Multi-Ring Basins, Proceedings of the Lunar Planet Science*, edited by P.H. Schultz, and R.B. Merrill, pp. 37-57, Pergamon, New York.

Mareschal, M., and M. Chouteau, 1990. A magnetotelluric investigation of the structural geology beneath Charlevoix Crater, Quebec, *Phys. Earth. planet. Inter.*, **60**, 120-131.

Masero, W., and S.L. Fontes, 1992. Geoelectrical studies of the Colônia impact structure, Santo Amaro, State of São Paulo - Brazil, *Rev. Bras. Geofis.*, **10**, 25-41.

Melosh, H.J., 1989. Impact Cratering: A Geologic Process, 245 pp., Oxford University Press, New York.

Tikhonov, A.N., 1950. On the investigation of electrical characteristics of deep strata of the Earth's crust (in Russian), *Dokl. Akad. Nauk SSSR*, **73**, 295-297.

Vozoff, K., ed., 1986. Magnetotelluric Methods. Soc. Expl. Geophys. Reprint Ser. 5, Soc. Expl. Geophys., Tulsa, Okla.

Zhang, P., T.M. Rasmussen, and L.B. Pedersen, 1988. Electric resistivity structure of the Siljan impact region, *J. Geophys. Res.*, **93**, 6485-6501.

This dissertation comprises the following four papers:

I.

Masero, W., P.-A. Schnegg, and S. L. Fontes, 1994. A magnetotelluric investigation of the Araguainha impact structure in Mato Grosso-Goiás, cenral Brazil, *Geophys. J. Int.*, **116**, 366-376.

II.

Masero, W., and P.-A. Schnegg, 1994. Magnetotellurische Untersuchungen eines Meteoritenkraters, *Protokoll Kolloquium Elektromagnetische Tiefenforschung*, Höchst im Odenwald, 114-120.

III.

Fischer, G., and W. Masero, 1994. Rotational properties of the magnetotelluric impedance tensor: the example of the Araguainha impact crater, Brazil, *Geophys. J. Int.*, **119**, 548-560.

IV.

Masero, W., P.-A. Schnegg, and S. L. Fontes, 1995. Magnetotelluric investigation of the Serra da Cangalha impact crater, Northeast Brazil, 13 pp., 3 tables, 16 figures, submitted to *J. Geomag. Geoelectr.*

I.

A magnetotelluric investigation of the Araguainha impact structure in Mato Grosso-Goiás, cenral Brazil

Masero, W., P.-A. Schnegg, and S. L. Fontes

Geophys. J. Int., **116**, 366-376, 1994

Geophys. J. Int. (1994) 116, 366–376

A magnetotelluric investigation of the Araguainha impact structure in Mato Grosso-Goiás, central Brazil

W. Masero,[1] P.-A. Schnegg[1] and S. L. Fontes[2]
[1]*Institut de Géologie, Université de Neuchâtel, CH-2007 Neuchâtel, Switzerland*
[2]*CNPq-Observatório Nacional, CEP 20291 Rio de Janeira, Brazil*

Accepted 1993 July 14. Received 1993 June 25; in original form 1993 April 13

SUMMARY

With a diameter of 40 km the Araguainha Dome is the largest known impact site in South America. The main characteristics of the structure is its appearance as a set of imbricated circles and a central uplift with a diameter of 9 km. 25 magnetotelluric (MT) soundings were completed across the structure, approximately defining five radial sections. The MT responses in the frequency range from 1000 to 1 Hz show 1-D behaviour, in contrast to the longer periods where data indicate a strong anisotropy and a decline of the resistivity. 1-D modelling of the high-frequency data reveals a well-defined symmetric crystalline basement ring at 1000 m depth between the radii of 9 and 20 km, which seems to drop deeper further away from the centre. Inside the ring and toward the centre, the top of the granites rises, outcropping at 1.5 to 2 km from the centre.

Key words: Araguainha Dome, complex impact crater, 1-D modelling, magnetotellurics, static shift.

1 INTRODUCTION

The Araguainha Dome is one of six meteorite impact structures known in Brazil and with an outer diameter of 40 km is the largest impact crater in that country (Crósta 1982). The structure is located in central Brazil between the states of Mato Grosso and Goiás, at the north-eastern border of the intracratonic Paraná basin (Fig. 1).

The interest in studying this kind of structure has increased strongly over the last few decades. It has long been accepted that impact cratering processes played a fundamental role in the formation and growth of the terrestrial planets and satellites. But the recognition that large impacts may have played an important role on the earth's climatic and biologic evolution has spurred the search for more evidence of such events (Melosh 1989).

In contrast to the smaller classical type of simple bowl-shaped craters, the Araguainha Dome is a complex crater with an uplifted central core of shocked rocks surrounded by one or more concentric, peripheral depressions (Grieve, Robertson & Dence 1981).

Experimental and numerical studies of impact-crater formation show that several excavation flow stages control the growth of a crater (Melosh 1989). The so-called transient crater is established just at the end of the excavation stage and is defined as the state of maximum depth of the cavity. The transient crater is gravitationally unstable and subjected to further collapses. The time-scale of crater collapse is similar to that of the excavation stage, ranging from a few tens of seconds to a few minutes. It is apparent that this modification takes place on time-scales very much shorter than most geologic processes. The modification stage comprises the formation of a central uplift, terraced walls and flat floors. Fig. 2 illustrates the major structural features of a complex crater.

Only few magnetotelluric (MT) surveys are known to have been carried out in areas of impact sites. The objective of these studies was the determination of the deep electric structures associated with large impact events, or the estimation of the depth of the floor of small craters. Zhang, Rasmussen & Pedersen (1988) concluded that the Siljan crater, Sweden, (diameter 55 km), includes a conductive zone, approximating the horizontal extent of the crater at a depth of 5 to 20 km. In Charlevoix (46 km), Canada, an almost horizontal conductor was interpreted by Mareschal & Chouteau (1990) as subhorizontal faulting related to the impact at a depth of 1.5 km. High-frequency data in the Colônia crater (3.6 km), Brazil, revealed a bowl-shaped depression filled with 440 m of Quaternary sediments (Masero & Fontes 1992).

The objective of the present work is to determine the

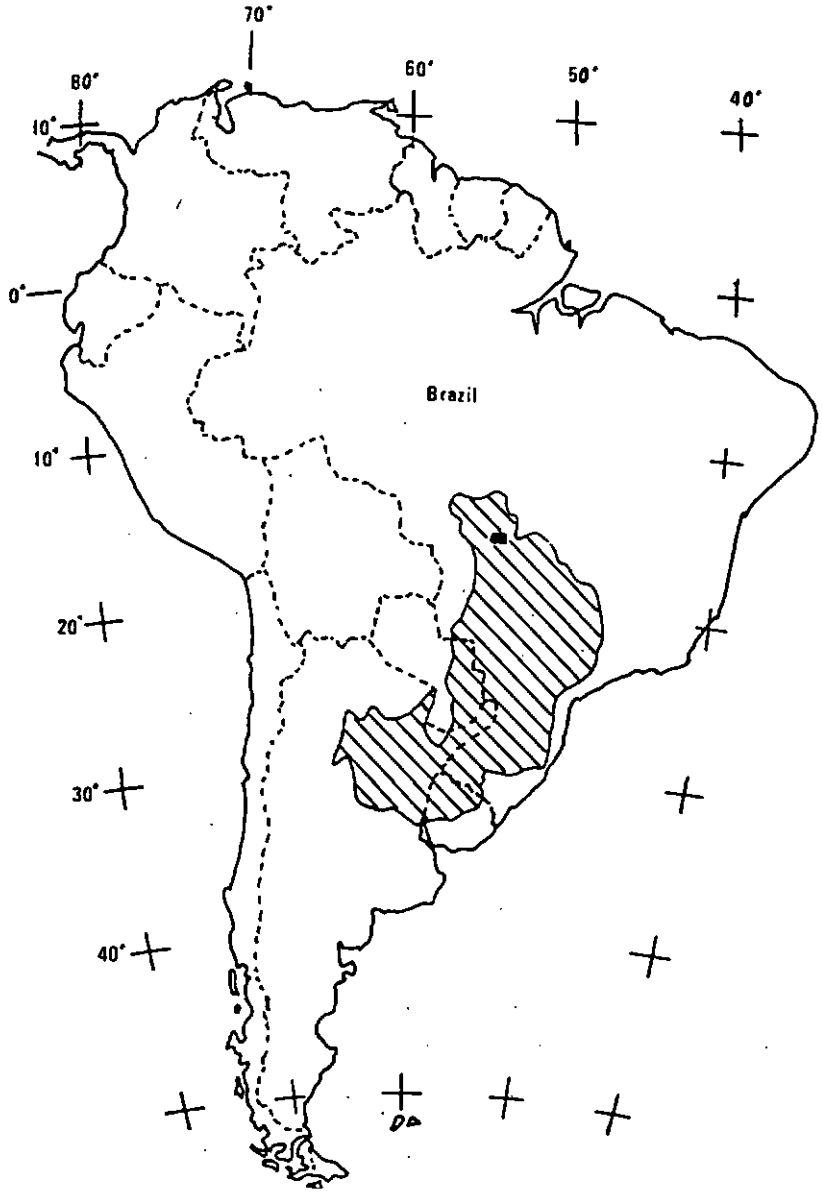

Figure 1. Paraná basin, shaded on map of South America (after Northfleet *et al.* 1969). The location of the Araguainha Dome is indicated by the small rectangle (not to scale).

depth to the crystalline basement and additionally to give an estimate of the uplift in the central region of the Araguainha Dome. For this purpose, MT measurements were made at 25 locations inside the structure. Static shift of apparent resistivities, due to near-surface heterogeneities, affected measurements at only a few sites. An attempt to remove these near-surface effects was undertaken by estimating a correction factor for each distorted site. This factor consists of two real, frequency-independent numbers operating on the undistorted regional electric fields at each site (Larsen 1977).

Further investigations with the purpose of revealing the deep structure underneath the Araguainha Dome are presently in progress with the help of 3-D modelling routines.

2 GEOLOGICAL SETTING

Northfleet, Medeiros & Muhlmann (1969) were the first to mention the Araguainha dome-like structure and interpreted it as a syenite (alkaline) intrusion related to the Cretaceous magmatism in the southern part of the Paraná basin. In the centre of the structure Silveira Filho and Ribeiro (1971, in: DNPM, 1975, p. 39) describe a block of crystalline basement surrounded by a ring of volcanic breccias and tuffs and tectonically deformed Palaeozoic sediments. They interpret the structure as a cryptovolcanic intrusion of Cretaceous age.

Dietz & French (1973) first identified the Araguainha Dome as an astrobleme—ancient meteoritic crater. The impact origin has been established by the discovery of shock-metamorphic effects near the centre of the structure (extensive development of planar deformation features—shock lamallae—in quartz grains and shatter cones in Devonian sandstones). Crósta, Gaspar & Candia (1981) and Theilen-Willige (1982) investigated the petrographic and geomorphologic aspects, supporting the hypothesis of an impact-generated structure. Recently Engelhardt, Matthaï & Walzebuck (1992) presented a detailed petrographic and geologic description of the alkali-feldspar

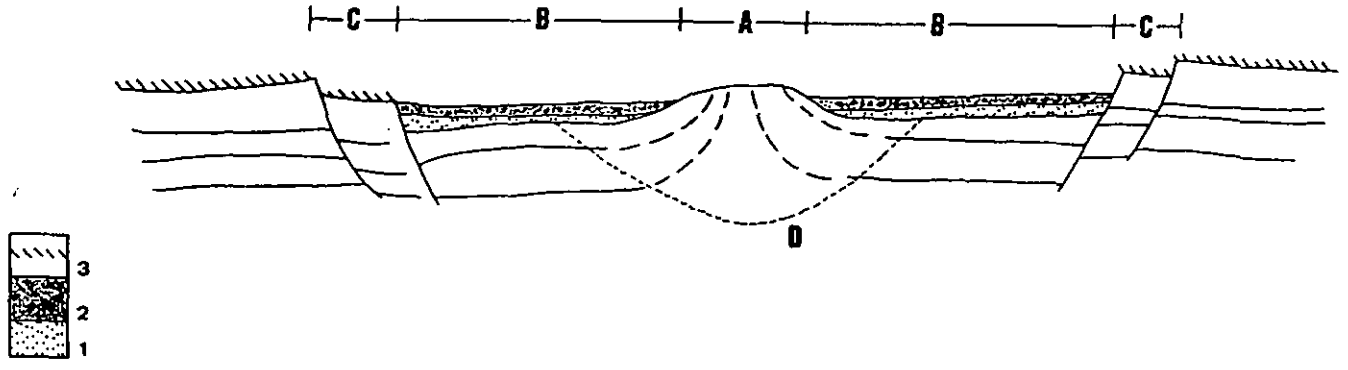

Figure 2. Schematic cross-section of a *complex crater*, showing (a) *the central uplift*, (b) *the flat crater floor*—corresponding to the horizontal extension of the transient crater—(c) the faulted rim zone, (d) the limit of major disruption and shock features in autochthonous rocks and the impact-related lithologies: (1) + (2) allochthonous and highly shocked material that did not escape the transient cavity by ejection—breccias and impact melt rocks; (3) fall-out ejecta (after Pilkington & Grieve 1992).

granite and impact breccias, with melt matrix, outcropping in the central uplifted area of the Araguainha Dome. They mention $^{40}Ar/^{39}Ar$ isotopic analyses on two different samples of impact melt rocks of the central area, which yield radiometric ages of 247+/−5.5 and 245.8+/−5.5 myr, indicating that the impact occurred close to the Permian–Triassic boundary. They also refer to $^{40}Ar/^{39}Ar$ isotopic analyses on unaltered biotites from the alkali–feldspar granite, which reveal a radiometric age of 480 myr. The same authors interpreted this as a cooling age when the alkali–feldspar granite, ascending from its deep intrusion level, passed the 300 °C isotherm. This age is consistent with the oldest known sediments—Devonian sandstones (Fig. 3)—covering the granitic basement.

The Araguainha Dome lies within the Palaeozoic sediments of the north-eastern border of the Paraná basin. According to an early aeromagnetic survey, the crystalline basement was believed to lie in the surrounding areas at a depth of 2000 m, rising within the structure to a depth of less than 500 m (Theilen-Willige 1982). A borehole in Alto Garças, located 60 km WSW of the area in focus, penetrated 1847 m of Upper Permian to Early Devonian sediments (Engelhardt *et al.* 1992). According to these authors, the basement underlying the Araguainha structure is probably covered by 1500 to 1800 m of sedimentary rocks. In the centre of the structure the pre-Devonian basement outcrops as an alkali–feldspar granite, leading to the central elevation and the dome-like structure.

The Araguainha structure is characterized by its annular aspect and an uplifted core with a diameter of about 9 km (Fig. 3). The innermost area of this central uplift is a small basin (diameter 3–4.5 km) occupied by alkali–feldspar granites and bordered by a ring of small hills, consisting of the same granitic rocks and the overlying impact breccias (Engelhardt *et al.* 1992). This central area is surrounded by another ring of higher hills, 8 to 9 km in diameter, formed by folded and steeply inclined Devonian sandstones. Around the central uplift Permo–Carboniferous sediments, mainly sandstones, are exposed in a series of semi-circular grabens formed by a ring fault system (Dietz & French 1973; Crósta *et al.* 1981).

3 MT SURVEY AND MT DATA

The MT fieldwork was carried out in July/August 1991 and July/August 1992 simultaneously by groups from the Observatoire Cantonal, Neuchâtel, Switzerland, and from the CNPq-Observátorio Nacional, Brazil. MT soundings were performed at a total of 25 different sites. They were placed across the structure approximately along five radii. The locations of all sites are shown on the geological map of the area surveyed (Fig. 3).

The MT data covers a range of periods from 0.001 to 1000 s. Since the aim of the present work is to investigate the depth of the crystalline basement, only the high-frequency data (0.001 to 3 s) are considered for interpretation. A discussion of the low-frequency data will be presented in a subsequent paper.

The MT method has already been described in detail by Fischer (1982) and Schnegg *et al.* (1983). The acquisition procedures of both groups participating in the survey were very similar, although they used different equipment. The soundings were performed at each site in three stages, where the first two covered the periods ranging from 0.001 to 0.2 s and 0.01 to 2 s. In order to cover the period interval from 0.6 to 1000 s, the signals were measured during approximately 12 hr. The third stage was usually performed during the night.

The telluric lines at each recording site were orientated in the direction of magnetic north and in the corresponding perpendicular E–W direction. Magnetic North is presently about 15° West of geographic North in the region of the Araguainha Dome. In order to present the MT results, the data were rotated in a manner such that the x direction corresponded to the azimuth (radial azimuth) with regard to the centre of the Araguainha Dome.

Figures 4 and 5 show rotated MT-tensor data of representative soundings carried out in the region of the Araguainha Dome, where Az stands for the rotation angle, which is the same as the radial azimuth. This direction is believed to be particularly appropriate for a structure showing circular symmetry. Also, the evident 3-D character of the MT data makes it impossible to determine a single and well-defined principal strike direction. Two differently defined skew parameters, the conventional one after Swift (1967) and the regional one after Bahr (1991), are used as structural dimension indicator (Figs 4 and 5). The regional skew is based on the phases of the impedance tensor and is sensitive to local distortion effects (see also next section) on the measured impedances. In the coordinate system of a regional 2-D structure and in the presence of local distortion

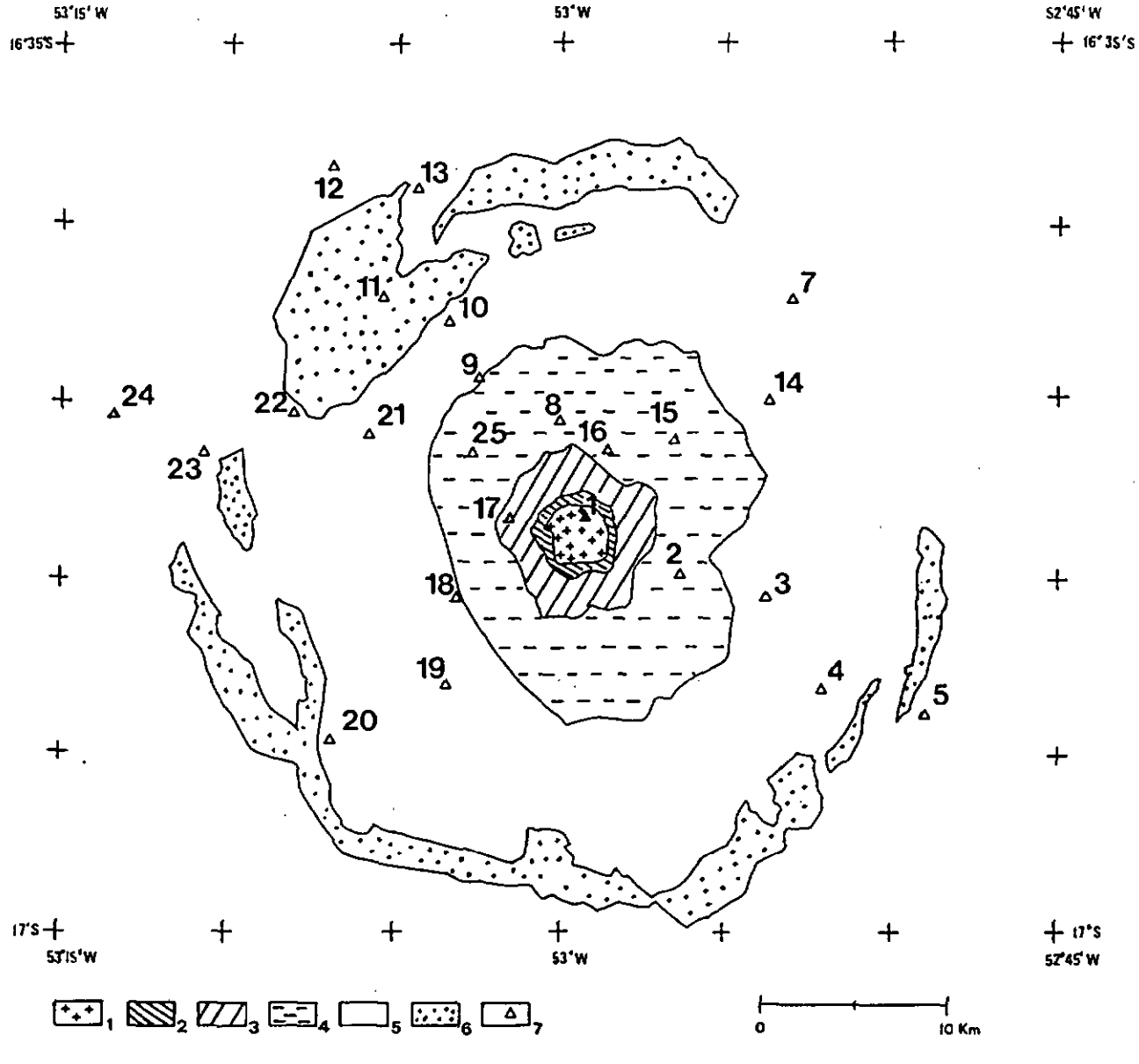

Figure 3. Simplified geologic map of the Araguainha structure (after Theilen-Willige 1981), showing the crystalline basement—alkali-feldspar granites (1), the impact breccias with melt matrix (2), the Palaeozoic sedimentary formations—Devonian Furnas (3) and Devonian Ponta Grossa (4), Upper Carboniferous to Lower Permian Aquidauana (5) and Permian Passa Dois (Palermo) (6) sandstones respectively, and the location of the MT sites (7).

the impedance element Z_{xx} has the same phase as Z_{yx}, and Z_{yy} the same phase as Z_{xy}. Therefore, the phases in each column of the impedance tensor are identical. Any departure from these conditions yields a regional skew larger than zero (Bahr 1991). The conventional skew after Swift (1967) would, in the presence of a local heterogeneity, only give the skew of the distortion tensor.

However, in a first attempt the representation of the impedance tensor in terms of four apparent resistivities and phases (Figs 4 and 5) does not indicate the presence of very strong galvanic distortion effects in our data. Of the examples in Figs 5 and 4, only site 1 shows appreciable evidence of local distortion, while the others seem much less affected (site 7 and 5) or are even without distortion (site 10).

Most of the MT data behave very much like the curves of sites 7 and 10 shown in Fig. 4 (localization see Fig. 3). For periods up to 0.1 s the apparent resistivity varies in most cases between 10 and 50 Ωm and the phases are equal to 45°. An evident increase of the apparent resistivity follows at periods longer than 0.1 s, accompanied by a drop of the phase. The MT responses of both polarizations are practically identical in the short-period range, i.e. they show no anisotropy, thus indicating 1-D behaviour of the structures. This changes between 1 and 10 s, where the apparent resistivity curves start to split, and between 10 and 100 s both curves drop to different resistivity levels. When we mention anisotropy, we mean an anisotropic MT response, and this does not imply an anisotropic resistivity medium. Both skews present very low values, ranging

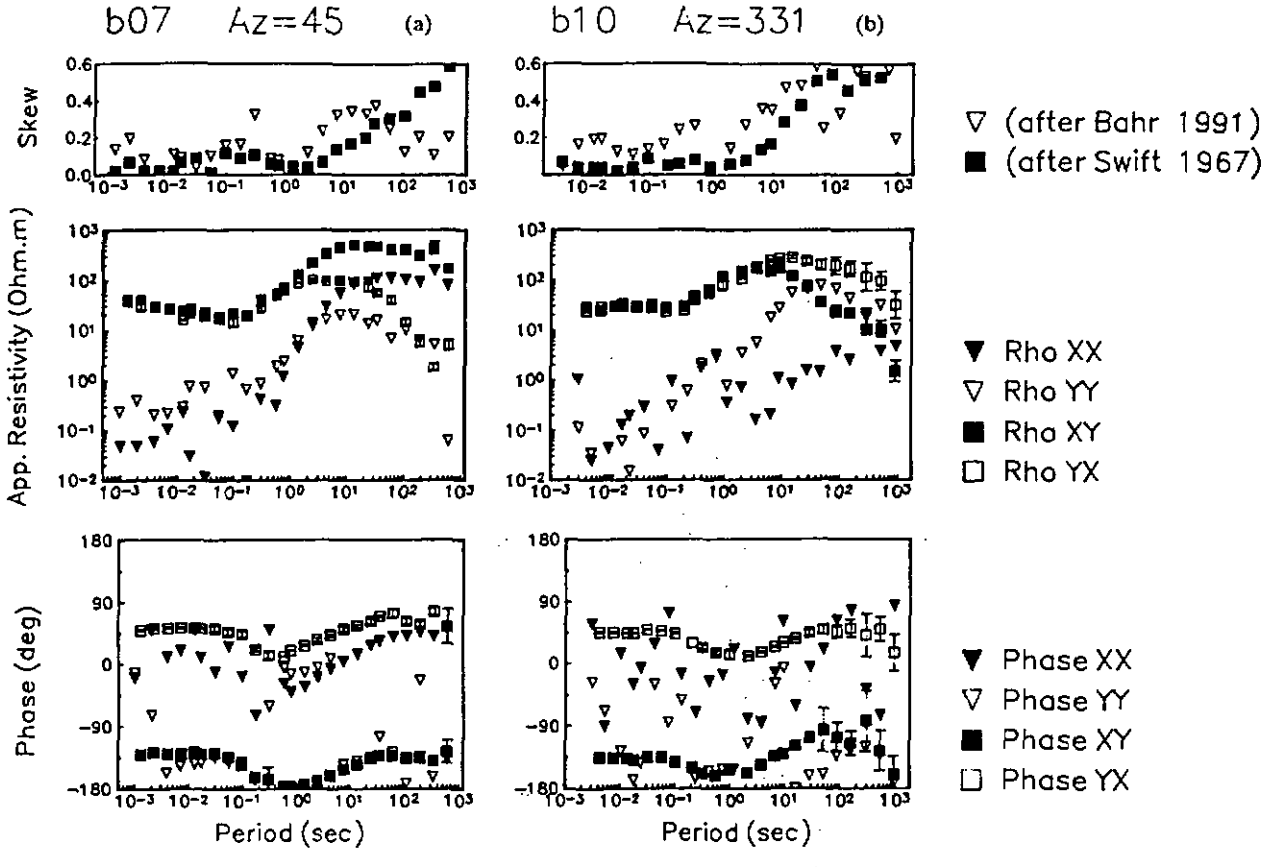

Figure 4. MT responses (phase, apparent resistivity and skew) at two selected sites located (a) 17 km and (b) 13 km away from the centre of the structure. Filled squares stand for electric field in the direction of the radial azimuth (Az), empty squares refer to the tangential direction, i.e. perpendicular to the radial azimuth.

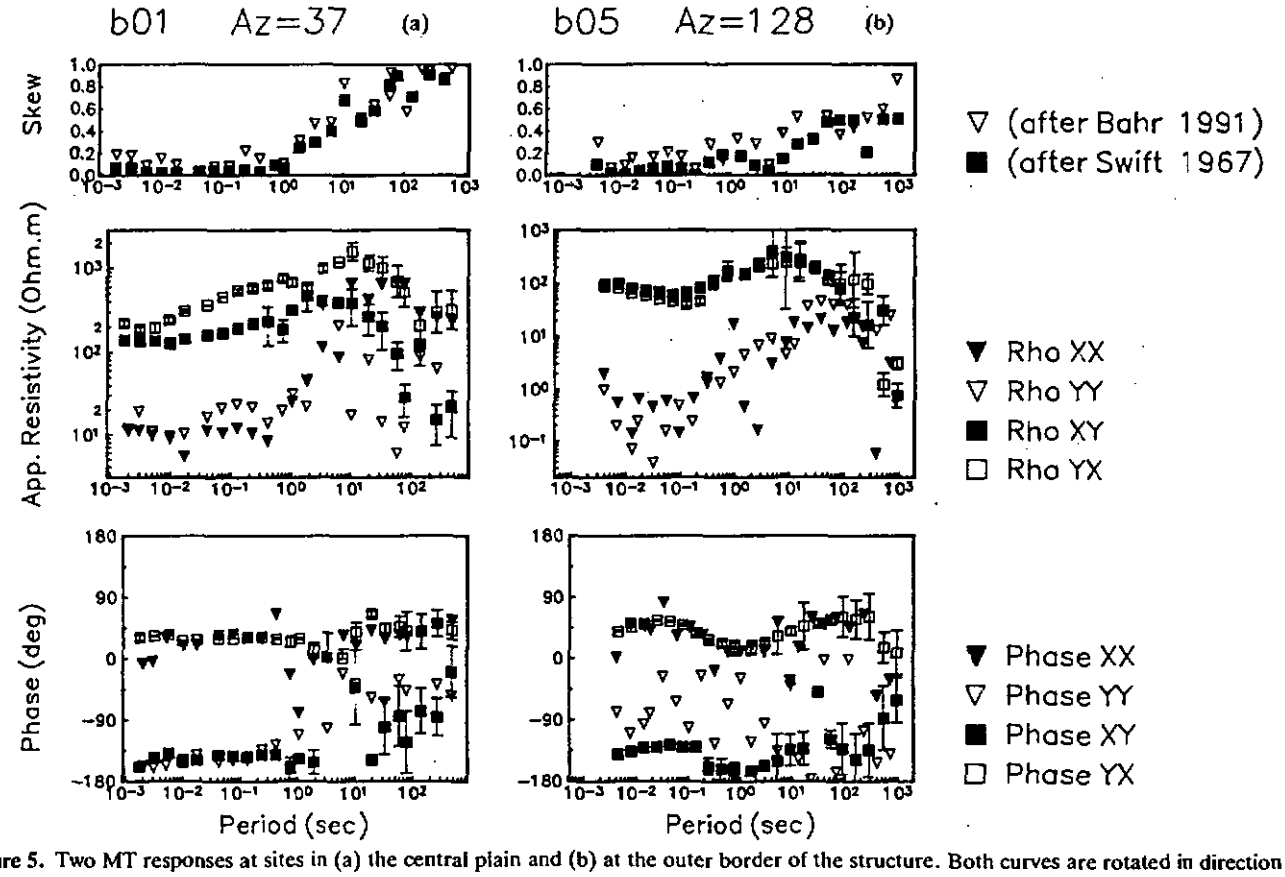

Figure 5. Two MT responses at sites in (a) the central plain and (b) at the outer border of the structure. Both curves are rotated in direction of the radial azimuth (Az).

between 0 and 0.1 for the short periods. However, they show a remarkable increase in the same period interval (above 1–10 s) where the splitting of the resistivity curves occurs. In general practice skew values smaller than 0.3 are taken to indicate that 3-D effects can be neglected. Taking this into account, the result of the soundings can be divided in two distinct parts, a first one containing the responses at the short periods, characterized by almost no difference between both polarizations and small skews, and a second part consisting of the long-period data with large anisotropies accompanied by a strong increase of the skew. It is now apparent that the responses in the periods between 0.001 s and 1 to 10 s show 1-D behaviour, in contrast to the longer periods, where data indicate 3-D structures and a decline of the resistivity.

The MT responses shown in Fig. 5 deviate in some respects from the ones just described. They are representative for soundings carried out in the centre (Fig. 5a) and at the outer margin of the Araguainha Dome (Fig. 5b), respectively. At the shorter periods the observed apparent resistivities are higher (around 200 to 300 Ωm) than those at most of the other sites. Another difference consists in the separation of the curves of both polarizations. This begins for site 1 around 0.01 s (Fig. 5a) and not, as mentioned above, for sites placed at a distance beyond about 4 km of the centre of the structure (Fig. 4), at periods between 1 and 10 s. The MT responses shown in Fig. 5(b) behave almost like the ones in Fig. 4, but the anisotropy at longer periods is practically absent or very small.

Therefore, the use of a 1-D inversion scheme to analyse the data from the short-period range (0.001 to 3 s) seems well justified for all sites lying inside the Araguainha Dome beyond a distance of 4 km from the centre.

4 1-D MODELLING AND REMOVAL OF STATIC-SHIFT EFFECTS

In order to determine the thickness of the sediments covering the crystalline basement in the area of the Araguainha Dome, 1-D modelling according to Fischer & Le Quang (1981) was applied on the high-frequency (0.001 to 3 s) data. Only MT data without static distortions were considered in this first step of 1-D modelling. For the five sites showing static-shift effects a correction involving the use of parametric constraints was first applied (see below).

The main invariant of the MT response $[\frac{1}{2}(Z_{xy} - Z_{yx})]$ was used to construct the layered 1-D models. The number of layers of the calculated models varies between two and four, including the half-space. For example, Fig. 6 shows the model obtained at site 8 and the model response for apparent resistivity and phase, together with the invariant of the observed data. The four-layer model at site 8 resolves the lower base of the good conducting (11 Ωm) sediment layers quite well. This interface lies on top of the considerably more resistive (1900 Ωm) crystalline basement. The model response fits the observed data (Fig. 6) very well, achieving small values for the standard deviations, given separately for the apparent resistivity (ε_ρ) and for the phase (ε_ϕ). In the site 8 model ε_ρ achieves a value of 0.024, which means that in the units given in Fischer *et al.* (1981) the calculated apparent resistivity is either 4.9 per cent too large or 4.6 per cent too small, whereas ε_ϕ is equal 0.018, corresponding to a deviation of the phase of just about 1°.

The resolution of the model parameters was determined by way of parameter trade-off analysis according to Fischer & Le Quang (1982), where the family of models is determined for which the standard deviation ε remains within 10 per cent of the minimum value ε_0. This is achieved by varying each of the model parameters (resistivity ρ and layer thickness d) to larger or smaller values. Under the constraint of the imposed variation, all the other parameters are adjusted to minimize ε. The set of limiting parameters is obtained when $\varepsilon = 1.1\ \varepsilon_0$. They can be expressed in terms of those of the best-fitting model. Fig. 7 shows three typical trade-off diagrams for every model parameter of the sites 4, 3 and 10. It is evident, that the layer on top of the basement is well constrained in these examples: for sites 3 and 10 the model parameters of this layer have variation ranges of the order of 10 per cent around their best-fitting values; for site

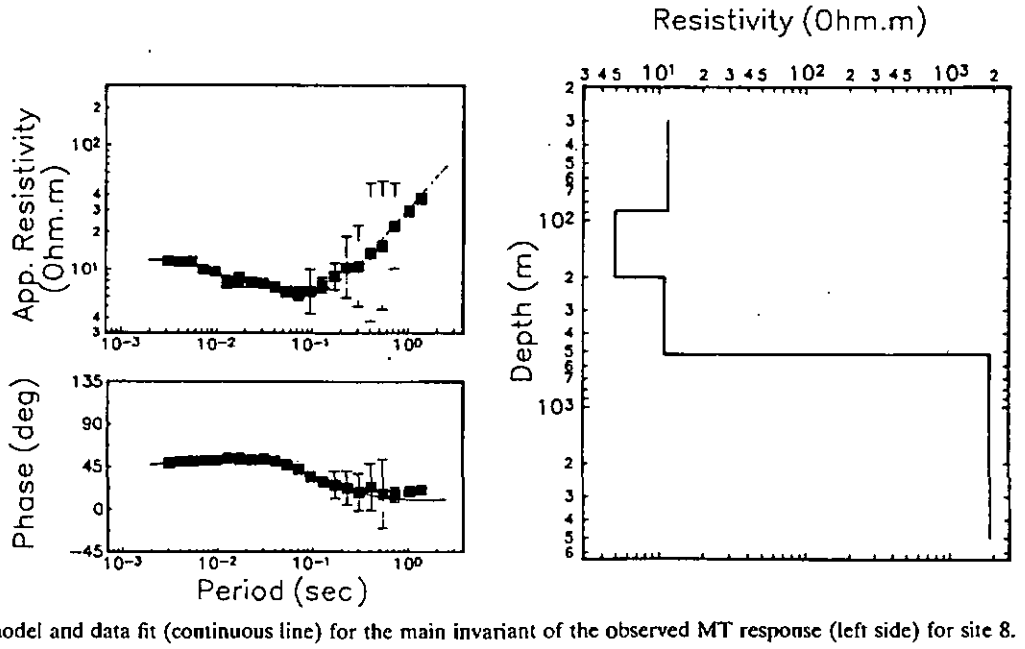

Figure 6. Best model and data fit (continuous line) for the main invariant of the observed MT response (left side) for site 8.

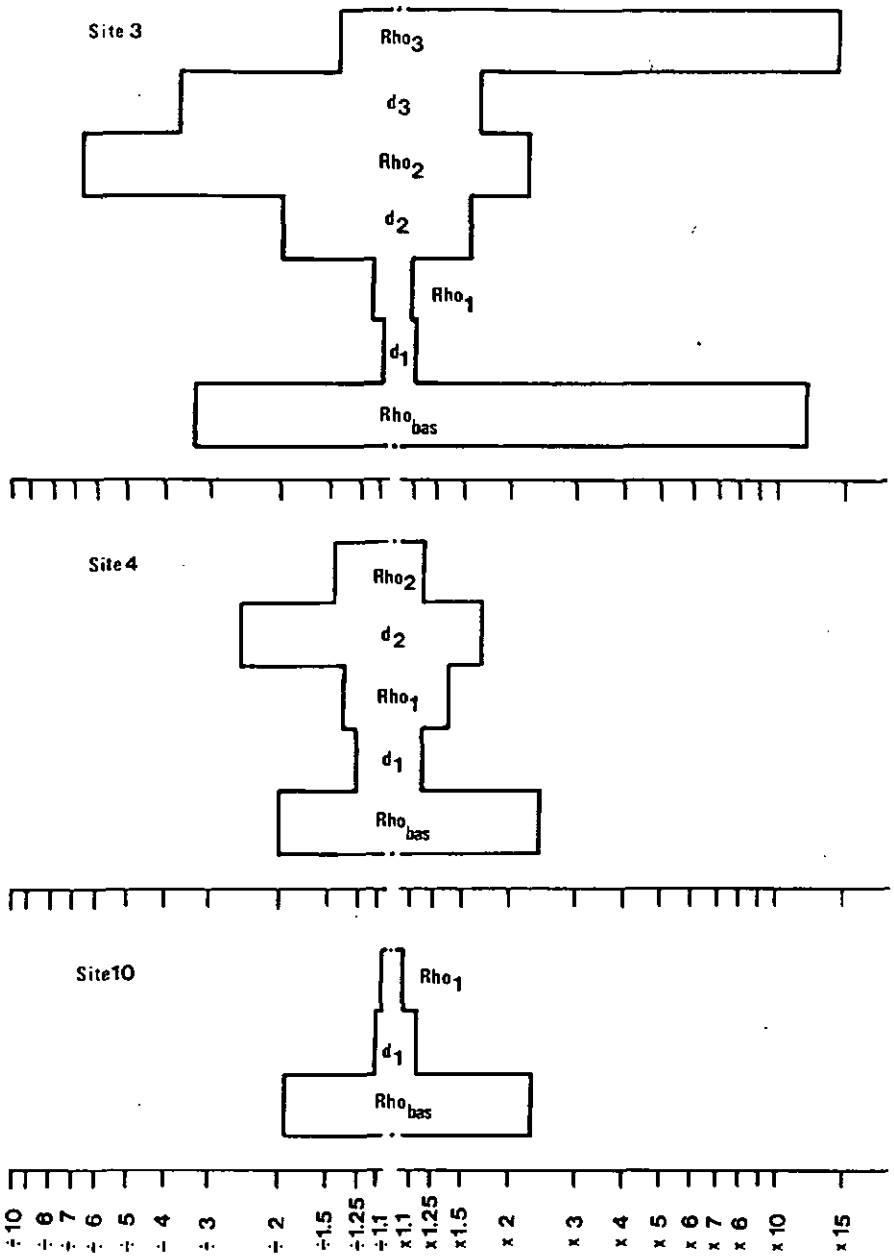

Figure 7. Trade-off diagram for the data and model of site 3, 4, 10. Vertical lines give the trade-off limits for each model parameter, i.e. the range within which it is possible to achieve $\varepsilon = 1.1\varepsilon_0$, where $\varepsilon_0 = [\frac{1}{2}(\varepsilon_\rho^2 + \varepsilon_\phi^2)]^{1/2}$ (Fischer *et al.* 1981).

4 the limits for the resistivity are +/− 20 per cent and for the thickness −40 per cent and +24 per cent. The other layers are all clearly less well resolved.

The resulting layered models of all 1-D inversions are summarized in Table 1, together with their separate standard deviations. Note that Table 1 also contains the layered models of the sites (underlined) where static distortion effects are present. The table includes results obtained after removal of the static shift. The process of static-shift removal is treated in the following paragraphs.

It is well known that local or near-surface inhomogeneities, often in the form of small-scale lateral-resistivity variations, are the reason for static shift in MT data. This problem is often referred to as near-surface distortion and has been treated in different numerical modelling studies (Wannamaker, Hohmann & Ward 1984; Park 1985) and regional MT investigations (Jones 1988; Beamish & Travassos 1992).

Small-scale lateral-resistivity variations can lead to striking deviations of the observed horizontal electric fields from the true regional values of interest. Static shift is frequency independent and consists of a parallel shift of the apparent resistivity curve when plotted in a logarithmic scale, without any corresponding change in the phase curve. The shape of the apparent resistivity curve is therefore retained.

A 2×2 real and frequency-independent tensor $\boldsymbol{C}$ relates the observed, distorted impedance tensor $\boldsymbol{Z}_m$ to the undistorted tensor $\boldsymbol{Z}$:

$$\boldsymbol{Z}_m = \boldsymbol{C}\boldsymbol{Z}. \tag{1}$$

As shown by Larsen (1977), for a 1-D earth, it is possible to determine this near-surface effect, i.e. the elements of $\boldsymbol{C}$ in

Table 1. Resistivities and depths of the layered models. ρ_1 and h_1 are the resistivity in Ωm and the depth in m to the base of this layer, i.e. to the top of the half-space, whereas indices 2 and 3 refer to the layers above. ρ_{bas} is the half-space resistivity, representing the Pre-Cambrian basement. The radial distance to the centre of the structure is given underneath the site number. ε_ρ and ε_ϕ are the separate standard deviations for the apparent resistivity and the phase, respectively. The layered models with underlined site numbers (18, 2, 25, 9 and 14) at bottom right are best-fit models from static-shift corrected sounding curves.

	16 5.5 km	8 6.25 km	15 8.0 km	19 9.5 km	3 11.0 km	21 12.0 km	10 12.8 km	4 15.5 km	11 15.5 km	20 15.8 km	22 16.3 km	7 17.3 km
ρ_3		11			37					14		35
h_3		90			66					97		98
ρ_2		5	124		7	12		13		112	28	14.5
h_2		200	540		98	25		110		271	146	368
ρ_1	10	11	23	22	22	30	30	36	18	26	62	47
h_1	278	520	780	1070	880	935	1100	950	820	1547	1474	955
ρ_{bas}	150	1900	2000	1000	3280	2200	3500	1730	2760	2000	2700	7800
ε_ρ	0.034	0.024	0.048	0.023	0.024	0.025	0.034	0.053	0.064	0.060	0.013	0.035
ε_ϕ	0.073	0.018	0.048	0.023	0.040	0.025	0.045	0.108	0.051	0.084	0.013	0.046

	13 19.2 km	23 20.0 km	5 21.0 km	12 22.5 km	24 25.0 km	26 50.0 km	<u>18</u> 6.0 km	<u>2</u> 6.38 km	<u>25</u> 6.75 km	<u>9</u> 9.25 km	<u>14</u> 13.0 km
ρ_3		9		2465	15						
h_3		3		34	110						
ρ_2	1	202	82	5	28	31	21		15	10	
h_2	2	153	400	68	730	530	300		314	46	
ρ_1	32	36	36	17	10	11	10	10	10	22	36
h_1	1100	1203	1120	1013	941	840	764	585	706	1016	890
ρ_{bas}	1850	5500	4300	2000	800	700	1630	500	650	1100	1500
ε_ρ	0.049	0.061	0.044	0.046	0.021	0.017	0.043	0.046	0.038	0.048	0.017
ε_ϕ	0.066	0.095	0.046	0.053	0.034	0.042	0.042	0.075	0.053	0.067	0.055

eq. (1), to within a constant multiplicative factor D, which is called the static-shift factor.

The MT data from the region of the Araguainha Dome show static distortion at only five of all the soundings performed. To remove the static-shift effects ftom these data, a procedure based on the investigations of Jones (1988) was applied. As mentioned by this author, due to the remaining undetermined multiplicative static-shift factor D, an *a priori* assumption in the form of a constraint must be made to remove the static-shift effect. Jones (1988) proposes a conceptual model of a 3-D thin-sheet over an earth in which the layer parameters vary sufficiently slowly that a 1-D interpretation of the data corrected for static shift is valid down to a certain ftequency. The above assumption consists of at least one layer parameter, e.g. the resistivity, which can be described in a simple parametric manner, such that the estimates of that parameter vary randomly about the true value.

The choice of the constraint was based on the circular, radially symmetric appearance of the Araguainha Dome, which is well illustrated in the geologic map of the area (Fig. 3). A simple way to express a relation between the layer parameters and the spatial distribution of the MT soundings is to represent these parameters as a function of their distance from the centre of the structure, assuming that the resistivity of the sedimentary layer on top of the basement is a function of the radial distance. Indeed, brecciation and fracturing of target rocks indirectly cause large changes in their electrical properties (Pilkington & Grieve 1992). This might well have influenced the rock properties as a function of their distance from the centre of the impact. An excellent example for the radial alteration of physical properties due to an impact process is given by the circular gravity lows, which are the most conspicuous geophysical signature over impact craters, and are due to a lowering of the rock density from impact-induced fracturing (Pilkington & Grieve 1992). Fig. 8 shows the resistivity of the layer just above the basement (layer 1), together with the resistivities of the second and third layer in the cases where they are present, as a function of the radius (the distance from the site to the centre of the structure). The resistivities plotted in Fig. 8 belong exclusively to the

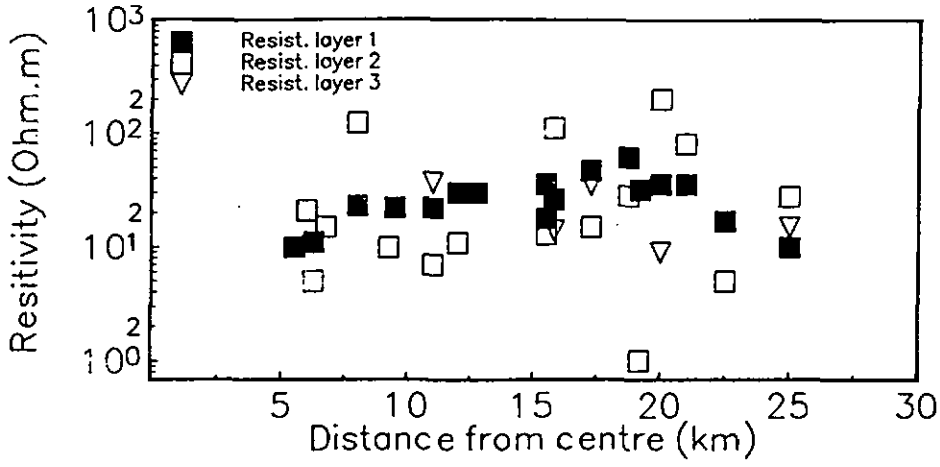

Figure 8. Resistivity of the layers of the best models as a function of the distance from the centre of the structure. Only the results from sounding curves without static-distortion effects are shown.

layered models summarized in Table 1, which were derived from data without static-distortion effects. The plot shown in Fig. 8 illustrates a regular pattern for the resistivity distribution of layer 1, which is the best resolved model parameter (Fig. 6). On the other hand, the corresponding values for layers 2 and 3 give a definitely more scattered picture, due to poor resolution.

Now, according to Fig. 8, the resistivities of layer 1 were divided into three groups, with values of 10 Ωm, 22 Ωm and 36 Ωm, which refer respectively to distances from the centre of the structure smaller than 8 km, 8 to 13 km and 13 to 22 km. Using Jones' (1988) method the resistivities of the layer lying directly above the basement of all sites showing static distortion effects were constrained to one of these three values, depending on the distance from the site to the centre of the structure. A slightly modified version of the 1-D inversion scheme of Fischer *et al.* (1981) made it possible, through the introduction of the constrained-layer resistivity, to calculate a vertical shift factor while minimizing the difference between the model response and the measured resistivity and phase data. The resulting model response is therefore shifted from the measured data by a frequency-independent factor which is the static-shift factor *D*. The response curve is now equivalent to the undistorted resistivity data curve. Since different distortion factors may affect the measured data of each polarization differently and independently, two static-shift factors, one for each polarization, were derived.

The resulting depths to the basement obtained from the 1-D models, including also the sites where static-shift effects had first to be removed, are summarized in Fig. 9(a). The two points in Fig. 9(a) indicating surface values, belong to sites 1 and 17, which are located at 1.6 and 3.7 km from the centre. Site 1 lies directly on the outcropping granites of the basement (Fig. 3) and its MT response is quite similar to the one measured at site 17. The soundings of these two sites are characterized, at the short-period end of the curves, by higher apparent resistivities (200 to 300 Ωm) than at all the

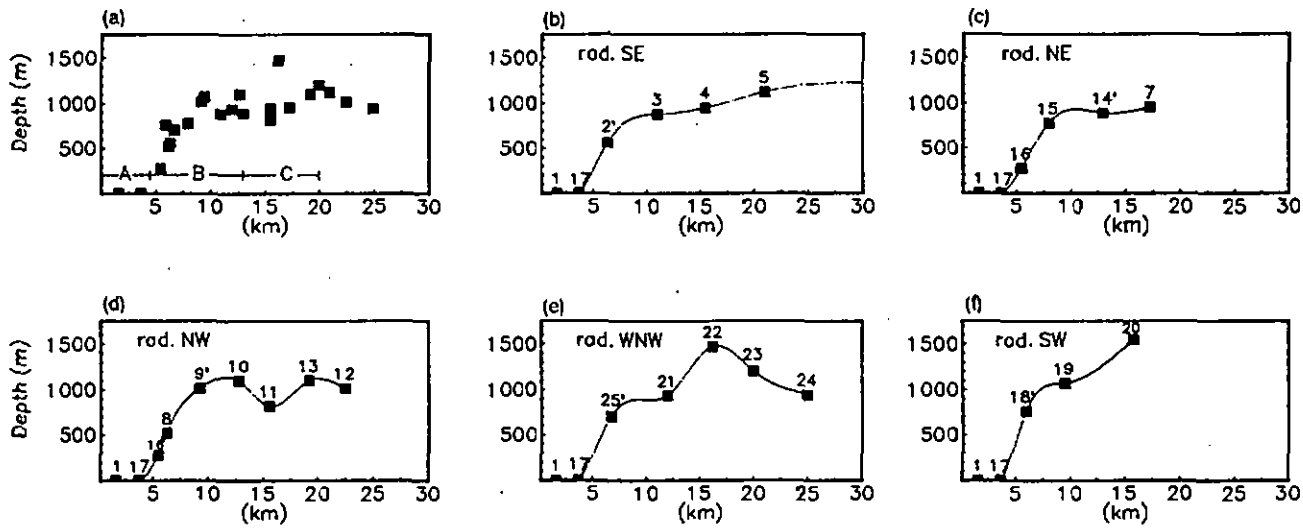

Figure 9. Depth to the crystalline basement based for the layered models shown in Table 1 and for two sites placed in the central area of the structure, where the basement crops out. (a) All depths as a function of distance to the centre with horizontal limits of major structural features (−A− central uplift, −B− flat floor (extension of former transient crater), −C− faulted rim zone) of complex a crater; (b–f) resulting depths for each site along different radial profiles. Primed numbers indicate sites where a static-shift effect was removed.

other sites, where it varies between 10 and 50 Ωm (Figs 4 and 5a). The higher resistivities were attributed to the basement rocks, which outcrop in the central plain and are believed, based on the strong similarity between the MT responses from sites 1 and 17, to lie very close to the surface at radii smaller than 4 km. The depth to the basement at all sites shows a relatively well-defined and uniform distribution when plotted as a function of the radius. A striking feature is the relatively rapid increase of the basement depth inside an area around the centre with a radius of 9 km. This indicates a rise of the basement towards the centre, typical of structures with a central uplift and found in many other impact craters of the size of the Araguainha Dome (Fig. 2).

5 DISCUSSION

The results from the 1-D modelling of soundings performed inside the area of the Araguainha Dome are shown in Table 1. As seen in Fig. 9(a), the depth to the basement increases rapidly within an area extending to a radius of 9 km. Further from the centre, at distances beyond 9 km, the basement lies on the average at a depth of 1000 m.

The depth to the basement diverges significantly, at a few locations, from the mean value mentioned above. At approximately 15 km from the centre, but depending on the exact position inside the structure, the top of the basement lies between 800 and 1500 m below the surface (Fig. 9a). To better understand this variation the resulting depths along each radial profile were plotted separately (Figs 9b–f). At a radius of approximately 15 km, in profiles running SW and WNW (Figs 9e and f), the basement is at a depth of 1500 m, corresponding to the maximum depth obtained in this work, while for the other three profiles (Figs 9b, c and d) the top of the basement lies 800 to 1100 m deep. The horizontal limit of excavation during the impact was only a fraction (50–65 per cent) of the final crater diameter (d) (Melosh 1989, p. 138), which corresponds to the horizontal extension of the transient cavity. For the Aaraguainha Dome this yields a transient crater radius estimated between 10 and 13 km. The sites showing variations in the depth to the basement are placed at a radius of 15 km and lie just beyond the former so-called transient cavity rim. They are believed to reflect the down-faulting of this rim (compare with Fig. 2). Such a process is thought to occur during the modification stage of complex crater formation (Grieve *et al.* 1981; *Melosh* 1989, p. 142). The radial plots shown in Fig. 9 clearly show that there is an asymmetry in the subsurface structure. In the western half of the Araguainha Dome (Figs 9c, d and f) the depth to the basement presents larger variations than in the opposite eastern half (Figs 9a and b). Local deviations of the subsurface structures from a given circular surface symmetry pattern have already been observed in other terrestrial complex craters. At the relatively young and moderately eroded Haughton complex crater on Devon Island in the Canadian Arctic, surface structural studies suggested that faulting is more intense in the northern and eastern sectors, indicating that the Haughton structure is structurally asymmetric (Grieve 1988).

The amount of uplift in a complex impact crater is a measure of the amount of excavation that occurred during the impact. But erosion reduces the observable uplift, as the amount of uplift in the centre of a complex impact structure decreases with depth (Greive *et al.* 1981). According to these authors the stratigraphic uplift in mixed targets, where sedimentary and crystalline rocks are present, is the observed uplift in the sedimentary section, plus an estimated component from the crystalline basement. The presence of granite fragments in the impact breccias found in the central area of the Araguainha Dome (Engelhardt *et al.* 1992) indicates that the excavated transient cavity penetrated the basement. Therefore, the average depth of 1000 m obtained for all sites beyond a radius of 9 km reflects a lower limit for the amount of uplift undergone by the rocks in the central region. Investigations of several complex craters based on best estimates show that the stratigraphic uplift of the central area of complex craters is related to the final crater diameter d by

$$hsu = 0.06d^{1.1} \tag{2}$$

where hsu is defined as the amount of uplift undergone by the deepest horizon now exposed at the surface (Grieve *et al.* 1981). For the Araguainha Dome, with a diameter of 40 km, the stratigraphic uplift hsu given by eq. (2) equals almost 3.5 km. There is now a significant difference of 2.5 km between the calculated value of 3.5 km and the estimated lower limit of 1000 m for the amount of uplift undergone in the core of the structure. This difference could be due to erosion, which has removed the major part of the impact breccias that once covered the bottom of the final crater. According to Engelhardt *et al.* (1992) the breccias preserved in the core region of the structure are sparse remnants of the original mass, which corresponded to the excavated and afterwards redeposited material of the estimated 20 to 26 km wide transient crater. But it is important to keep in mind that dimensional relationships for terrestrial craters, e.g. the amount of stratigraphic uplift hsu (eq. 2), represent only average estimates from several structures and cannot be taken to apply to each individual structure (Grieve 1988).

The 1-D inversion of the main invariant of the MT response at site 26, located 55 km ESE from the centre of the Araguainha Dome, gave a sedimentary thickness of 840 m (Table 1). This is 1000 m less than the thickness measured at a borehole in Alto Garça, located 60 km WSW of the structure and which penetrated 1847 m of Palaeozoic sediments (Engelhardt *et al.* 1992). This difference might well be attributed to the fact that the Alto Carça borehole and the MT site 26 lie 110 km apart on opposite sides of the Araguainha Dome. Sedimentary formation thickness charts of the Paraná basin (Northfleet *et al.* 1969) show that the borehole is situated further inside the basin than site 26 and, therefore, in a region where the top of the basement lies deeper. According to Northfleet *et al.* (1969, Figs 23 and 25), the total thickness of the sedimentary formations is considerably greater at Alto Garça than at location 26, where it is suggested to amount to slightly less than 1000 m. The resulting 840 m of the layered model of site 26 is, therefore, in good agreement with the decrease of the thickness of the sedimentary formations towards the border of the basin and the data of Northfleet *et al.* (1969).

6 CONCLUDING REMARKS

An estimate of the depth to the basement in the region of the Araguainha Dome was obtained by using the MT method. The results from several soundings placed along five radii gave clear evidence of the circular or radial pattern of the subsurface structures. The rise of the crystalline basement from an average depth of 1000 m to the surface, occurs within a circularly shaped area extending to a radius of 9 km from the core of the Araguainha structure. Local deviations from this circular symmetric pattern are observed in the western half of the structure at a radius of approximately 15 km and are probably related to the deep excavation limit of the crater beyond the transient cavity rim. This asymmetry is believed to be associated with the modification stages involving the down-faulting of the transient cavity rim, and had an outer radius that, according to a relationship given in Melosh (1989), is suggested as lying between 10 and 13 km. As we have shown, this is only a fraction of the final and total horizontal extension seen today.

Static shift affected only few of our sounding curves and was successfully removed by means of parametric constraints. The choice of these constraints was based on the radial distribution of the resistivity, believed to be caused by brecciation and fracturing of the target rocks during the impact.

ACKNOWLEDGMENTS

The authors should like to express their gratitude towards their institutions and to the Swiss National Science Foundation and the Brazilian Research Council. They are also grateful to Dr G. Fischer, Dr J. P. Schaer, Dr F. Persoz and Dr M. Marquer for reviewing the manuscript.

REFERENCES

Bahr, K., 1991. Geological noise in magnetotelluric data: a classification of distortion types, *Phys. Earth planet. Inter.*, **66**, 24–38.

Beamish, D. & Travassos, J. M., 1992. A study of static shift removal from magnetotelluric data, *J. appl. Geophys.*, **29**, 1–19.

Crósta, A. P., 1982. Estruturas de impacto no Brasil: uma síntese do conhecimento atual, *Anais XXXII Congr. Bras. Geologia, Salvador, Bahia*, **4**, 1372–1377.

Crósta, A. P., Gaspar, J. C. & Candia, M. A. F., 1981. Feições de metamorfismo de impacto no Domo de Araguainha, *Rev. Bras. Geocênc.*, **11**, 139–146.

Dietz, R. S. & French, B. M., 1973. Two probable astroblemes in Brazil, *Nature*, **244**, 561–562.

DNPM, 1975. *Departamento Nacional da Produção Mineral, Carta geológica do Brasil ao milionésimo*, Folha Goiânia (SE-22), Texto Explicativo, Brasília.

Engelnardt, W. V., Matthäi, S. K. & Walzebruck, J., 1992. Araguainha impact crater, Brazil: I. The interior part of the uplift, *Meteoritics*, 27, 442–457.

Fischer, G., 1982. Magnetotelluric observational techniques on land, *Geophys. Surv.*, **4**, 373–393.

Fischer, G. & Le Quang, B. V., 1981. Topography and minimization of standard deviation in one-dimensional magnetotelluric modelling. *Geophys. J. R. astr. Soc.*, **67**, 279–292.

Fischer, G., Schnegg, P.-A., Peguiron, M. & Le Quang, B. V., 1981. An analytic one-dimensional magnetotelluric inversion scheme. *Geophys. J. R. astr. Soc.*, **67**, 257–278.

Fischer, G. & Le Quang, B. V., 1982. Parameter trade-off in one-dimensional magnetotelluric modelling, *J. Geophys.*, **51**, 206–215.

Grieve, R. A. F., 1988. The Haughton impact structure: summary and synthesis of the results of the HISS project, *Meteoritics*, **23**, 249–254.

Grieve, R. A. F., Robertson, P. B. & Dence, M. R., 1981. Constraints on the formation of ring impact structures, based on terrestrial data, in *Multi-Ring Basins, Proceedings of the Lunar Planet Science*, vol. 12A, pp. 37–57, ed. Schultz, P. H. & Merril, R. B., Pergamon, New York.

Jones, A. G., 1988. Static shift of magnetotelluric data and its removal in a sedimentary basin environment, *Geophysics*, **53**, 967–978.

Larsen, J. C., 1977. Removal of local surface conductivity effects from low frequency mantle response curves, *Acta Geogael., Geophys. Montanist. Acad. Sci. Hung.*, **12**, 183–186.

Mareschal, M. & Choutcau, M., 1990. A magnetotelluric investigation of the structural geology beneath Charlevoix Crater, Quebec, *Phys. Earth. planet. Inter.*, **60**, 120–131.

Masero, W. & Fontes, S. L., 1992. Geolelectrical studies of the Colônia impact structure, Santo Amaro, State of São Paulo—Brazil, *Rev. Bras. Geofis.*, **10**, 25–41.

Melosh, H. J., 1989. *Impact Cratering: A Geologic Process*, Oxford University Press, New York.

Northfleet, A. A., Medeiros, R. A. & Muhlmann, H., 1969. Reavaliação dos dados geológicos da bacia do Paraná, Rio de Janeiro, *Bol. Téc. Petrobrás*, **12**, 291–346.

Park, S. K., 1985. Distortion of magnetotelluric sounding curves by three-dimensional structures, *Geophysics* **50**, 785–797.

Pilkington, M. & Grieve, R. A. F., 1992. The geophysical signature of terrestrial impact craters, *Rev. Geophys.*, **30**, 161–181.

Schnegg, P.-A., Le Quang, B. V., Fischer, G. & Weaver, J. T., 1983. Audiomagnetotelluric study of a structure with a reverse fault, *J. Geomagn. Geolectr.*, **35**, 653–671.

Swift, C. M., Jr., 1967. A magnetotelluric investigation of an electrical conductivity anomaly in the southwestern United States, *PhD thesis*, MIT, Cambridge, MA.

Theilen-Willige, B., 1981. Fernerkundungsverfahren bei geomorphologischen und strukturellen Untersuchungen an Intrusivkörpern und an der Ringstruktur von Araguainha in Goiás/Brasilien, *Diss. TU Clausthal*, Clausthal-Zellerfeld.

Theilen-Willige, B., 1982. The Araguainha astrobleme/Central Brazil, *Geolog. Rundschau*, **71**, 318–327.

Wannamaker, P. E., & Hohmann, G. W. Ward, S. H., 1984. Magnetotelluric responses of three-dimensional bodies in layered earths, *Geophysics*, 49, 1517–1533.

Zhang, P., Rasmussen, T. M. & Pedersen, L. B., 1988. Electric resivity structure of the Siljan impact region, *J. geophys. Res.*, 93, 6485–6501.

II.

Magnetotellurische Untersuchungen eines Meteoritenkraters

Masero, W., and P.-A. Schnegg

Protokoll Kolloquium Elektromagnetische Tiefenforschung,
Höchst im Odenwald, 114-120, 1994

Deutsche
Geophysikalische
Gesellschaft e.V.

Protokoll

über das Kolloquium

"Elektromagnetische Tiefenforschung"

ISSN 0946 - 7467

15. Kolloquium: Höchst im Odenwald, 28.03. - 31.03.1994

herausgegeben von

Karsten Bahr

Geoforschungszentrum Potsdam
Telegrafenberg A45
14473 Potsdam

Andreas Junge

Dept. of Geology and Geophysics
University of Edinburgh
Grant Institute
West Mains Road
Edinburgh EH9 3JW
Scotland

W. Masero, P.-A. Schnegg, Université de Neuchâtel, Schweiz

Magnetotellurische Untersuchungen eines Meteoritenimpaktkraters

Einleitung

Das Ziel der Magnetotellurischen (MT) Untersuchungen am Araguainha Impaktkrater besteht in der Bestimmung der Tiefenstrukturen, die möglicherweise mit dem Impaktereignis zusammenhängen.

Der Araguainha Krater befindet sich im Westen Brasiliens in den paläozoischen Sedimenten des Paraná Beckens (Abb. 1). Die Bestimmung von $^{40}Ar/^{39}Ar$-Isotopenverhältnisse an Impaktschmelzgesteine ergaben für die Kraterbildung ein radiometrisches Alter von 247 Millionen Jahren (Engelhardt et al., 1992). Die Struktur besitzt einen Durchmesser von 40 km und ist durch ein ringähnliches Aussehen gekennzeichnet. Im Zentrum des Kraters sind Granite des Grundgebirges, umgeben von Überresten der Suevitdecke (Impakt-Trümmergesteine), aufgeschlossen. Zunehmend jüngere Sedimente kommen in Richtung des äusseren Randes der Struktur vor (Abb. 1).

Ergebnisse der eindimensionalen Modellierung

Die vorangehenden Resultate der eindimensionalen Modellrechnungen für die Invariante der beobachteten scheinbaren Widerständen und Phasen aller MT Stationen im Periodenbereich zwischen 0.003 und 1 s wiederspiegeln die Abfolge der paläozoischen Sedimente im Paraná Becken und den deutlichen Übergang zum granitischen Grundgebirge. Dieses befindet sich in der Regel in einer Tiefe von 1 km. Die Mächtigkeit der Sedimente nimmt aber deutlich in Richtung der Mitte der Struktur ab, was mit der Hebung des Grundgebirges im Zentrum des Kraters zusammenhängt. Diese zentrale Hebung des Grundgebirges besitzt eine axiale Symmtrie und wird am besten durch einen stumpfen Kegel beschrieben, dessen Basis in einer Tiefe von 1 km liegt und einen Durchmesser von 18 km hat, während die stumpfe Spitze einen Durchmesser von 6 km hat und an der Oberfläche aufgeschlossen ist (Masero et al., 1994).

Zweidimensionale Modellierung und Diskussion

Die Station s007 (Station 7 in Abb. 1) gilt als repräsentativ für die MT Sondierungen in der Region der Araguainha Struktur. Im Bereich der kurzen Perioden (0.003 bis 1 s) zeigen die Messdaten ein eindimensionales Verhalten (Abb. 2) und wurden schon in einer früheren Arbeit behandelt (s. oben). Für Perioden grösser als 1 Sekunde (T>1 s) spalten sich die beiden Polarisationen auf und werden von einer deutlichen Zunahme der Skew-Werte nach Swift (1967) und Bahr (1991) begleitet. Bei ungefähr 20 s ist jedoch eine allmähliche Abnahme des Letzteren feststellbar.

Die Dekomposition des Impedanztensors (Groom und Bahr, 1992) diente zum besseren Verständnis des Aufspalten der scheinbaren Widerstands- und

Abbildung 1: Karte von Brasilien mit der Lage des Araguainha Impaktkraters innerhalb des Paraná Beckens (links). Schematische geologische Karte des Araguainha Kraters: [1] Granite, [2] Suevite - Impakttrümmergesteine, [3-6] Sandsteine des Oberen Devons bis Unteren Perms und [7] Lage der MT Stationen. Die Lage des vorgestellten zweidimensionalen Modelles ist durch die durchgezogene Linie gegeben (unten).

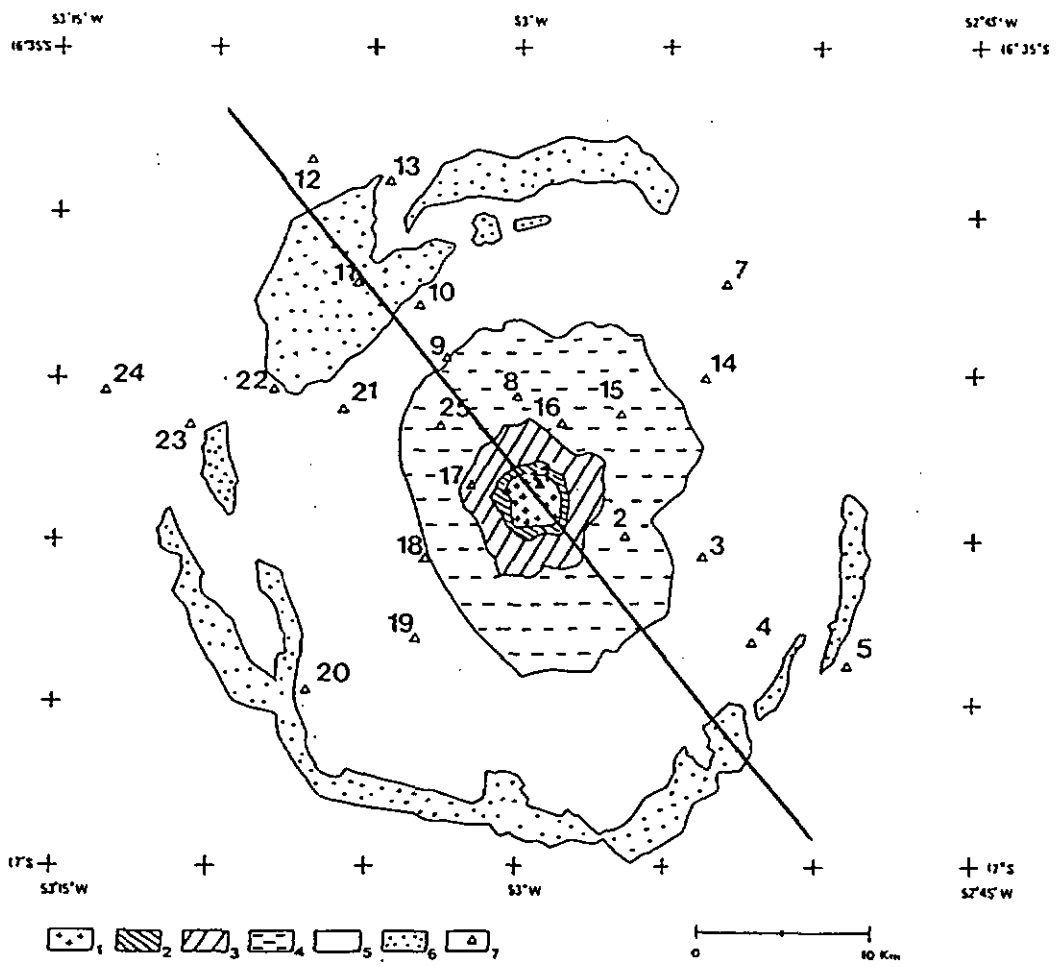

Phasenkurven beider Polarisationsrichtungen im langperiodischen Bereich und der damit eng verbundenen Zunahme beider Skew-Werte. Die dabei resultierenden Winkel *twist und shear* (Groom und Bailey, 1989) stellen ein Mass für die galvanische Verzerrung des Impedanztensors durch *lokale* Leitfähigkeitsanomalien dar. Sie geben die Abweichung der beobachteten Impedanzen vom *regionalen* ein- und zweidimensionalen Fall wieder. Die Bezeichnungen *regional* und *lokal* beziehen sich auf Strukturen, deren horizontale Ausdehnung vergleichbar, bzw. viel kleiner, ist als die Eindringtiefe der beobachteten elektrischen und magnetischen Felder. Die Summe und Differenz zwischen *twist und Shear* entsprechen genau den von Bahr (1991) eingeführten Verzerrungswinkeln - β_1 und β_2 - der beiden tellurischen Vektoren.

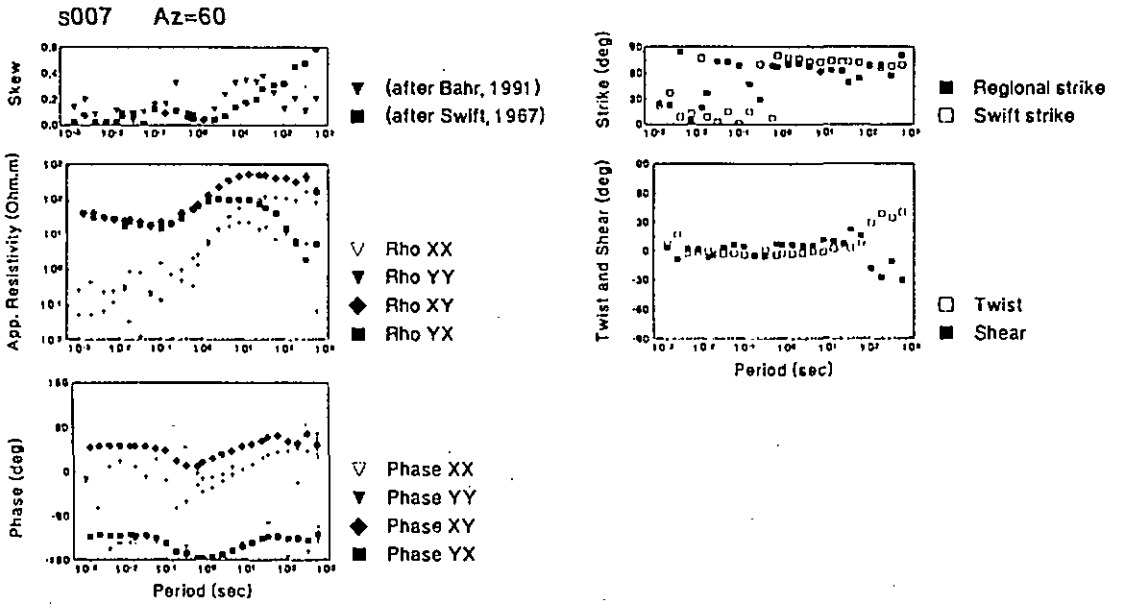

Abbildung 2: Auf der rechten Seite Phase, scheinbarer Widerstand und Skew und auf der linken Seite *shear, twist* und Streichrichtung der MT Station s007 (Station 7 in Abb. 1), die 17 km vom Zentrum der Araguainha Struktur liegt.

Das Ergebnis zeigt, dass, unterhalb von T = 60 s, *twist und shear* um 0° liegen (Abb. 2). Dies weist für den annähernd gesamten Periodenbereich auf verzerrungsfreie Impedanzwerte hin. Aber das deutliche und zugleich starke Eintreten von Verzerrungen für T>60 s wird durch das Vorhandensein einer lokalen Leitfähigkeitsanomalie von kleinem Ausmass, verglichen mit der Eindringtiefe bei dieser langen Perioden (> 75 km), erklärt. Die maximale horizontale Ausdehnung der zentralen Hebung des Grundgebirges beträgt 18 km. Verglichen mit der Eindringtiefe bei langen Perioden, handelt es sich eigentlich um eine lokale Erscheinung. Ein ähnliches Result erhielt Bahr (1991) bei der Interpretation von langperiodischen MT Sondierungen in der Oberpfalz, wo die Erbendorf-Vohenstrauss Zone als lokale Anomalie betrachtet werden musste.

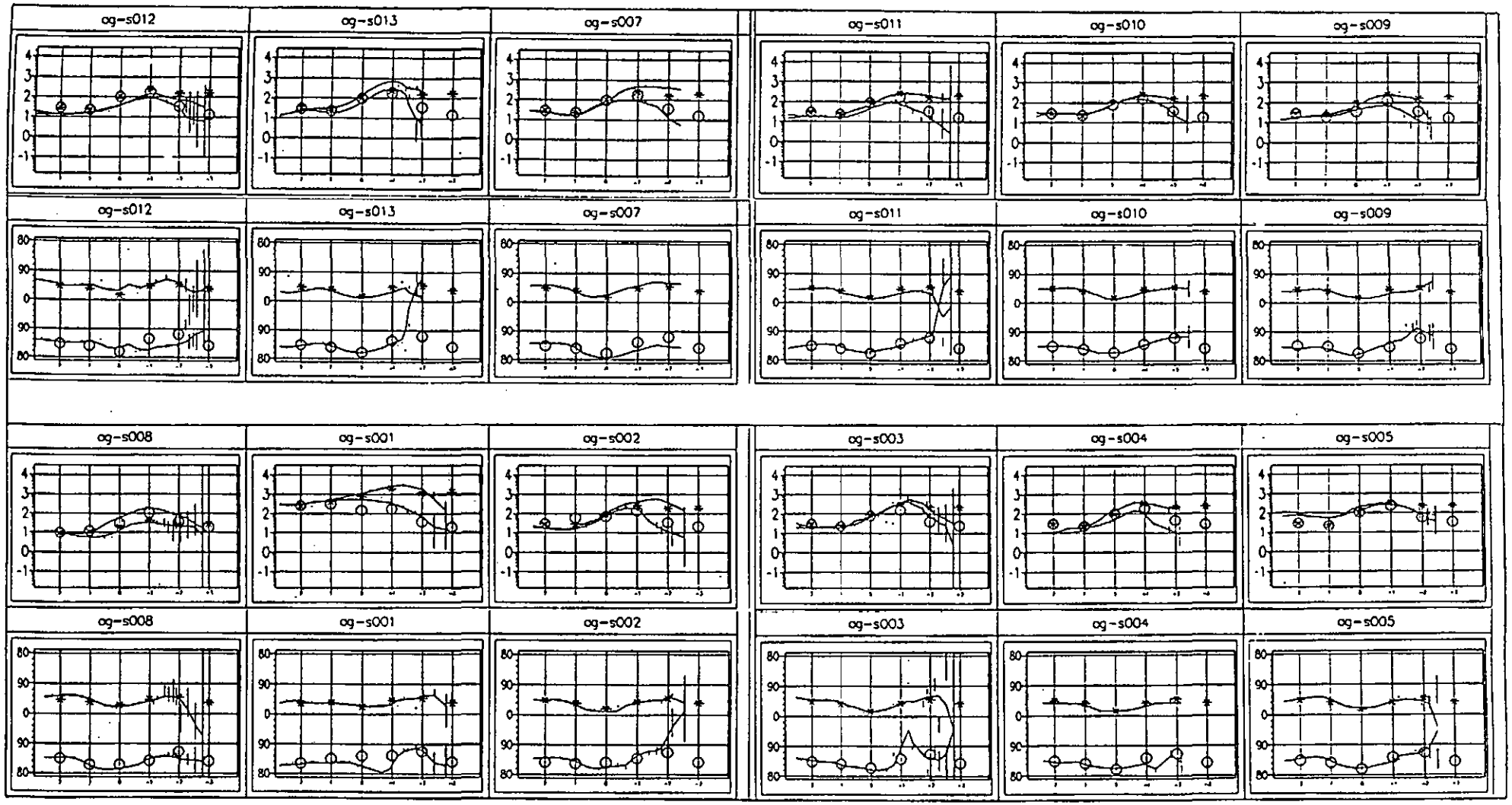

Abbildung 3: Vergleich zwischen den beobachteten und modellierten scheinbaren Widerständen und Phasen der Stationen entlang des zweidimensionalen Modelles. Die durchgezogenen Kurven entsprechen den XY- und YX-Richtungen der gemessenen Daten, während Sternchen und Kreise die Modellantworten der B- und E-Polarisationen sind. Der scheinbare Widerstand (in Ohm.m) entspricht jeweils der ersten und dritten Reihe und die Phase (in Grad) der zweiten und vierten Reihe.

Die berechneten Streichrichtungen nach Swift (1967) und Bahr (1991) sind für T>1 s relativ gleichmässig verteilt und liegen in der Grössenordnung von 60° bis 70° (Abb. 2). Die Streichrichtungen stimmen in der Regel gut mit dem radialen Azimuth der einzelnen Stationen überein. Die MT Daten wurden somit in die radiale Richtung rotiert, welche am geeignetesten für Strukturen mit einer kreissymmetrischen Anordnung zu sein scheint.

Die hohen Skew-Werte für T>1 s deuten auf eine dreidimensionale Verteilung der Leitfähigkeit in Eindringtiefen grösser als 3 km hin. Erwähnenswert sei hier noch, dass das Eintreten der Verzerrungen von einer Abnahme des Skew-Wertes nach Bahr (1991) begleitet wird, während aber der konventionelle Skew nach Swift (1967) weiterhin ansteigt (Abb. 2).

Trotz der deutlichen Anzeichen einer dreidimensionalen Anordnung der Leitfähigkeitsstrukturen wurde vorerst ein zweidimensionales Modell (Abb. 4) als Annäherung in Betracht gezogen. Dennoch ist eine gute Anpassung zwischen den mit finiten Elementen (Wannamaker et al., 1987) berechneten Modellantworten und den beobachteten MT Daten erreicht worden (Abb. 3). Das Modell beruht auf der Interpretation der MT Daten entlang eines radialen, NW-SE verlaufenden Profiles (Abb.1). Der oberflächennahe Abschnitt des Modelles besteht aus einer relativ leitfähigen Schicht (10 und 30 Ωm) von 1 km Mächtigkeit, welche die sedimentäre Bedeckung des Paraná Beckens darstellt.

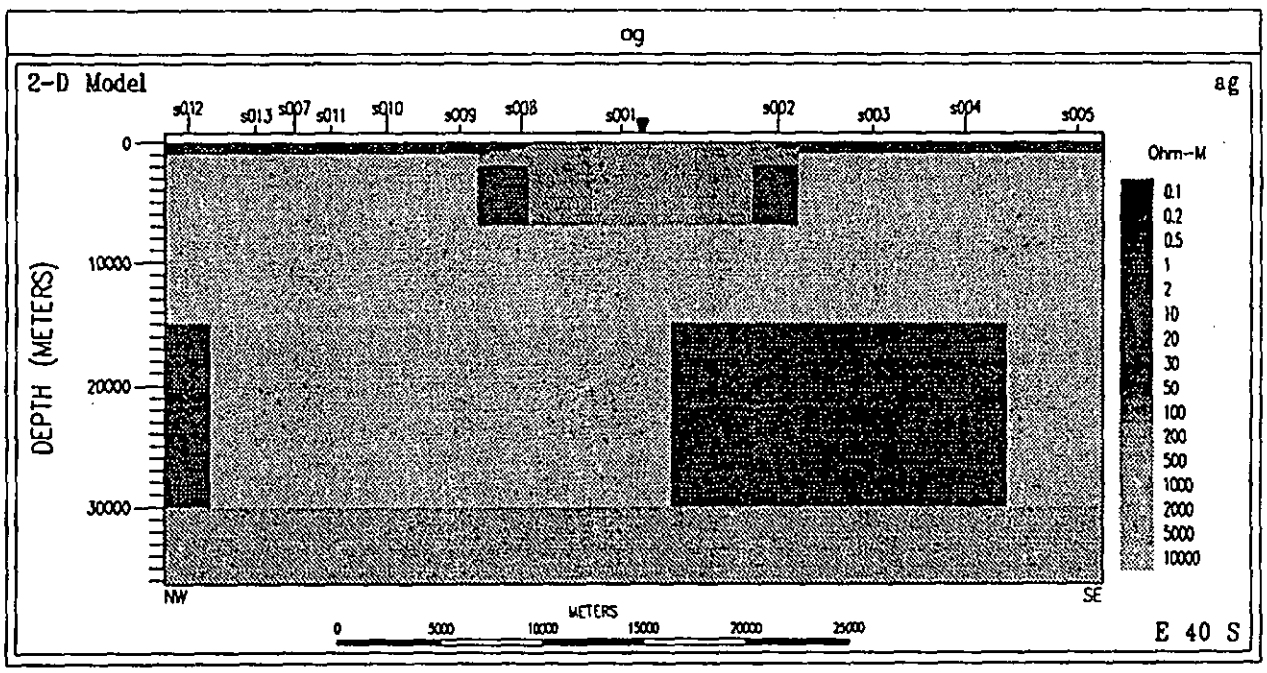

Abbildung 4: Zweidimensionales Modell der Araguainha Struktur beruhend auf der Interpretation der MT Daten entlang eines radialen NW-SE verlaufenden Profiles. Die Lage der Stationen und das Zentrum der Struktur (Dreieck) sind oben auf dem Model angegeben.

Eines der augenfälligsten Merkmale ist ein Block, bestehend aus unterschiedlichen spezifischen Widerständen (20, 200, 500 Ωm), eingebettet in einer oberen Kruste von 5000 Ωm. Seine horizontale Ausdehnung liegt in der

Grössenordnung eines Drittels des gesamten Durchmessers der Struktur. Er ist im Zentrum des Kraters aufgeschlossen und erreicht eine Tiefe von 7 km.

Es wird angenommen, dass der niedrigere elektrische Widerstand dieses Blockes mit einer hohen Anzahl von Brüchen zusammenhängt, die beim Einschlag des Meteoriten erzeugt wurden und durch welche Fluide aus tieferen Krustenbereiche aufsteigen konnten. Zum Vergleich ergaben MT Sondierungen an der Siljan Struktur in Schweden, die mit einem Durchmesser von 55 km den grössten Krater Europas darstellt, eine Leitfähigkeitsanomalie in einer Tiefe zwischen 5 und 20 km (Zhang et al., 1988). Obwohl diese nicht an der Oberfläche beobachtbar ist, besitzt sie ungefähr die horizontale Ausdehnung des Kraters. Sie wird auch dort durch tiefe Brüche erklärt, die beim Einschlag entstanden sind und durch welche Fluide aus der unteren Kruste migrieren konnten.

Ein weiteres Merkmal des vorgeschlagenen Modelles ist eine Schicht in 15 bis 30 km Tiefe, bestehend aus einer Abfolge von sich alternierenden gut und schlecht leitenden Blöcken (2 und 2000 Ωm). Darunter folgt ein gleichmässiger Halbraum von 100 Ωm. Diese Strukturen in der unteren Kruste sind regional und wiederspiegeln sehr wahrscheinlich wichtige strukturelle Elemente im präkambrischen Grundgebirge, die nicht im Zusammenhang mit dem Impaktereignis stehen. Eine frühere MT Untersuchung am NE Rand des Paraná Beckens, einige hundert km von der Araguainha Struktur entfernt, zeigt unterschiedliche Krustenabschnitte unter dem Becken (Padilha et al., 1992). Diese Strukturen in der unteren Kruste könnten mit der Fortsetzung des *Transbrasilianischen Lineamentes*[1] im Grundgebirge unterhalb des Paraná Beckens zusammenhängen (Padilha, mündl. Mitt.).

Bemerkung

[1]Das *Transbrasilianisches Lineament* bezeichnet ein Hauptsystem von Brüchen entlang eines begrenzten Streifens, der in Richtung N30°E streicht und von der Nordküste Brasiliens (Bundesstaat Ceará) bis an den N-NE Rand des Paraná Beckens reicht. Weiter südlich ist dieses Bruchsystem für den geradlinigen Verlauf der NW Grenze des Paraná Beckens verantwortlich. Das Alter dieses Bruchsystems ist Frühpaläozoisch und es wird der Endphase der tektonischen Aktivität im *Ciclo Brasiliano* (800-500 ma) zugeordnet (aus dem Begleittext zur Geologischen Karte von Brasilien 1:2'500'000, 1984).

Literatur

Bahr, K., 1991. Geological noise in magnetotelluric data: a classification of distortion types, Phys. Earth planet. Inter., 66, 24-38.

Engelhardt, W.v., Matthäi, S.K. and Walzebuck, J., 1992. Araguainha impact crater, Brazil: 1. The interior part of the uplift, Meteoritics, 27, 442-457.

Groom, R.W. and Bahr, K., 1992. Corrections for near surface Effects: Decomposition of the magnetotelluric impedance tensor and scaling corrections for regional resistivities: A tutorial, Surv. Geophys., 13, 341-379.

Groom, R.W., Bailey, R.C., 1989. Decomposition of the magnetotelluric impedance tensor in the presence of local three-dimensional galvanic distortion, J. Geophys. Res., 94 (B2), 1913-1925.

Masero, W., Schnegg, P.-A. and Fontes, S.L., 1994. A magnetotelluric investigation of the Araguainha impact structure in Mato Grosso-Goiás, central Brazil, Geophys. J. Int., 116, 377-392.

Padilha, L.A., Trivedi, N.B., Vitorello, I. and Costà, J.M, 1992. Upper crustal structure of the northeast Paraná basin, Brazil, determined from integrated magnetotelluric and gravity measurements, J. Geophys. Res., 97 (B3), 3351-3365.

Swift, C.M., Jr., 1967. A magnetotelluric investigation of an electrical conductivity anomaly in the southwestern United States, PHd thesis, MIT, Cambridge, MA.

Wannamaker, P.E., Stodt, J.A., Rijo, L., 1987. A stable finite element solution for two-dimensional magnetotelluric modelling, J. R. Astr. Soc., 88, 277-296.

Zhang, P., Rasmussen, T.M. and Pedersen, L.B., 1988. Electric resistivity structure of the Siljan impact region, J. Geophys. Res., 93, 6485-6501.

III.

Rotational properties of the magnetotelluric impedance tensor: the example of the Araguainha impact crater, Brazil

Fischer, G. and W. Masero

Geophys. J. Int., **119**, 548-560, 1994

Geophys. J. Int. (1994) 119, 548–560

Rotational properties of the magnetotelluric impedance tensor: the example of the Araguainha impact crater, Brazil

Gaston Fischer and Wilhelm Masero

Institut de Géologie, Université de Neuchâtel, c/o Observatoire Cantonal, CH-2000 Neuchâtel, Switzerland

Accepted 1994 April 19. Received 1994 April 19; in original form 1993 June 29

SUMMARY

The rotational properties of the elements of the magnetotelluric impedance tensor are reviewed in terms of the three identical ellipses that these elements describe in the complex plane. It is shown that graphical representations of these ellipses provide a powerful and simple tool to evaluate MT sounding results. This study required clarification of the characteristics of 2-D structures, where the ellipses reduce to line segments, and of the meanings of such concepts as skew S and anisotropy A. As should be well known, a vanishing skew is not a sufficient condition to guarantee a 2-D structure; all it does is place the middle ellipse over the origin of the complex plane. The additional constraint is to close the ellipses into line segments. It is shown that the orientation of the ellipses in the complex plane is strongly related to the directional properties of the structure. Structures with strong directionality yield ellipses whose major axes point toward the origin. The principal coordinates then are essentially parallel to the directions of maximum anisotropy. For ellipses with their minor axes pointing to the origin, the structure is not very directional and is rather oriented at 45° from the principal coordinates. A given structure can show these two kinds of behaviour simultaneously, though in different period ranges, i.e. in different depths ranges, as is shown with data from the Brazilian Araguainha impact crater. The question of static-shift removal from field data is also addressed.

Key words: anisotropy, Brazilian Araguainha impact crater, rotational properties of MT tensor.

1 ROTATION OF THE IMPEDANCE TENSOR

The rotational properties of the magnetotelluric (MT) impedance tensor Z are reasonably well known (*cf.* e.g. Sims 1969; Vozoff 1972; Fischer 1975; Kaufman & Keller 1981; Rokityansky 1982). Many authors have used them to assess the dimensionality of structures (e.g. Ranganayaki 1984; Beamish 1986; Ingham 1988; Park & Livelybrooks 1989), to find a graphical expression of their characteristics (e.g. Lilley 1976; Eggers 1982), or to describe a complex structure in terms of new basic 'vectors' or 'eigenstates' (Haak 1972; Eggers 1982; Spitz 1985; Counil, Le Mouël & Menvielle 1986; La Torraca, Madden & Korringa 1986; Yee & Paulson 1987). Our purpose is to analyse the most straightforward of the graphical representations as these provide a kind of insight that has not been noted before while giving the MT practitioner a particularly easy tool to interpret his data.

The changes undergone by the tensor elements when the coordinate system (x axis north, y east, and z down) is rotated through a positive angle θ around the vertical axis z can be expressed as follows (*cf.* e.g. Fischer 1975):

$$\begin{aligned} Z_{xx} &= Z_{\mathcal{xx}} \cos^2\theta + Z_{\mathcal{yy}} \sin^2\theta + (Z_{\mathcal{xy}} + Z_{\mathcal{yx}}) \sin\theta\cos\theta \\ Z_{yy} &= Z_{\mathcal{xx}} \sin^2\theta + Z_{\mathcal{yy}} \cos^2\theta - (Z_{\mathcal{xy}} + Z_{\mathcal{yx}}) \sin\theta\cos\theta \\ Z_{xy} &= -(Z_{\mathcal{xx}} - Z_{\mathcal{yy}}) \sin\theta\cos\theta + Z_{\mathcal{xy}} \cos^2\theta - Z_{\mathcal{yx}} \sin^2\theta \\ Z_{yx} &= -(Z_{\mathcal{xx}} - Z_{\mathcal{yy}}) \sin\theta\cos\theta - Z_{\mathcal{xy}} \sin^2\theta + Z_{\mathcal{yx}} \cos^2\theta \end{aligned} \quad (1)$$

In these equations italic script subscripts refer to the tensor elements in the coordinates before rotation, for example those in which the MT soundings were carried out, whereas those with italic times subscripts refer to tensor elements after coordinate rotation.

We now introduce a set of new parameters, with which the rotation can be expressed more concisely:

$$Z_1 = \tfrac{1}{2}(Z_{xy} - Z_{yx}), \tag{2}$$

$$Z_2 = \tfrac{1}{2}(Z_{xx} + Z_{yy}), \tag{3}$$

$$Z_3' = Z_3'(\theta) = \tfrac{1}{2}(Z_{xy} + Z_{yx}), \tag{4}$$

$$Z_4' = Z_4'(\theta) = \tfrac{1}{2}(Z_{xx} - Z_{yy}). \tag{5}$$

As these definitions emphasize, Z_1 and Z_2 are invariant with respect to rotation whereas the primed Z_3' and Z_4' are not (note that similar parameters have been introduced by most of the authors quoted above). In the Appendix several other rotational invariants of the impedance tensor are derived, and it is shown that from their knowledge it is possible to reconstruct the impedance tensor.

With the above definitions it can easily be shown that the rotation of the tensor elements can be expressed as follows:

$$\left.\begin{aligned} Z_{xx} &= +Z_2 \pm Z_3' \frac{T' + t}{\sqrt{1+t^2}} \\ Z_{yy} &= +Z_2 \mp Z_3' \frac{T' + t}{\sqrt{1+t^2}} \\ Z_{xy} &= +Z_1 \pm Z_3' \frac{1 - T't}{\sqrt{1+t^2}} \\ Z_{yx} &= -Z_1 \pm Z_3' \frac{1 - T't}{\sqrt{1+t^2}} \end{aligned}\right\} \tag{6}$$

In these equations

$$T' = Z_4'/Z_3', \tag{7}$$

which is not rotationally invariant,

$$t = \tan 2\theta, \tag{8}$$

and the upper signs on the right hold when $-90° \leq 2\theta \leq +90°$ (i.e. 2θ in quadrants 1 or 4) and the lower ones when $+90° \leq 2\theta \leq 270°$ (i.e. 2θ in quadrants 2 or 3).

2 PRINCIPAL COORDINATES

As is well known, the principal coordinates for the MT impedance tensor are those which maximize

$$|Z_{xy}|^2 + |Z_{yx}|^2, \tag{9}$$

and it is easily seen that the same coordinates also minimize

$$|Z_{xx}|^2 + |Z_{yy}|^2. \tag{10}$$

The search for the extremum of (9) leads to a rotation through an angle θ_p given by

$$\tan 4\theta_p = \frac{T' + T'^*}{T' \cdot T'^* - 1}, \tag{11}$$

where the asterisk means complex conjugation. Slightly different forms of this equation can be found in Sims (1969) and Eggers (1982). It is not surprising that θ_p should be given by an equation of this type, which leads to a set of angles separated by $\pi/4$, since the search gives the minima as well as the maxima. Even the restriction to the maxima involves an ambiguity of $\pi/2$ which can be lifted with the additional requirement that

$$|Z_{xy}| \geq |Z_{yx}|. \tag{12}$$

Note, however, that this does not lift the inherent MT ambiguity of finding the strike direction. As is well known, this can only be done with the help of the vertical magnetic component, or with recourse to several adjoining sounding sites.

For 2-D structures the principal coordinates are also those that maximize $|Z_{xy}|$ and minimize $|Z_{yx}|$. Thus they also maximize the anisotropy A:

$$A = |Z_{xy}|^2/|Z_{yx}|^2 = \rho_{xy}/\rho_{yx}, \tag{13}$$

where ρ_{xy} and ρ_{yx} are the well-known apparent resistivities.

For 3-D structures this is no longer so: in general the angle that maximizes $|Z_{xy}|$ is different from the one which maximizes A and both are different from θ_p. Later on we will give examples of this kind of behaviour. Before doing so, however, it will be useful to turn into the principal coordinates.

In everything that follows we therefore assume that impedance elements given with small italic times subscripts refer to the principal coordinates, whereas those with italic script subscripts are rotated away from θ_p. In other words, beginning with a set of field data we first rotate into the principal coordinates with eq. (11) and condition (12). This yields Z_{xx}, Z_{yy}, Z_{xy}, and Z_{yx}. From these we compute Z_3, Z_4, and T, written unprimed in the principal directions for which they can be considered as constants, and then set up rotational equations similar to eqs (6), but where $\theta = \frac{1}{2}\tan^{-1} t$, as defined in (8), *now directly gives the angle away from the principal axes*:

$$\left.\begin{aligned} Z_{\mathcal{xx}} &= +Z_2 \pm Z_3 \frac{T + t}{\sqrt{1+t^2}} \\ Z_{\mathcal{yy}} &= +Z_2 \mp Z_3 \frac{T + t}{\sqrt{1+t^2}} \\ Z_{\mathcal{xy}} &= +Z_1 \pm Z_3 \frac{1 - Tt}{\sqrt{1+t^2}} \\ Z_{\mathcal{yx}} &= -Z_1 \pm Z_3 \frac{1 - Tt}{\sqrt{1+t^2}} \end{aligned}\right\}, \tag{14}$$

where now, of course, $T = Z_4/Z_3$ is given by unprimed Z_3 and Z_4, and since we are in the principal coordinates we should find that the angle θ_p given by eq. (11) vanishes, i.e. that

$$T + T^* = 0. \tag{15}$$

In the principal coordinates T is therefore purely imaginary and, according to its definition (7), this means that Z_4 lies at right angles to Z_3 (*cf.* Fig. 1). As pointed out by Eggers (1982) the sign of the imaginary T therefore determines the direction of rotation around the ellipses.

If for all the complex impedance elements we write

$$Z_{ij} = R_{ij} + iX_{ij} \tag{16}$$

condition (15) also translates into

$$\frac{R_{xy} + R_{yx}}{X_{xy} + X_{yx}} = -\frac{X_{xx} - X_{yy}}{R_{xx} - R_{yy}}. \tag{17}$$

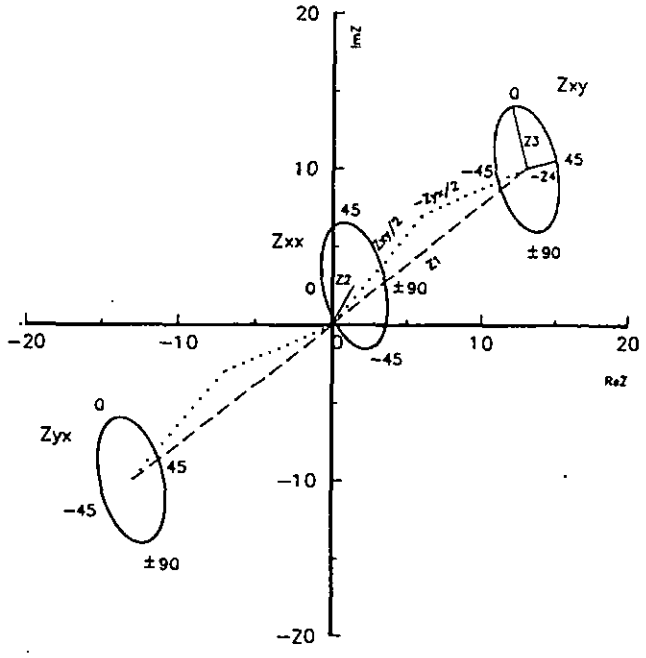

Figure 1. Behaviour of the magnetotelluric impedance elements when the coordinate system is rotated through a positive angle (the z coordinate points downward). In the complex plane these elements describe three identical ellipses. The angle of rotation, indicated around each ellipse, gives the deviation from the principal coordinates. Note that for Z_{xy} and Z_{yx} the principal directions correspond to an endpoint of a major axis, whereas for Z_{xx} and Z_{yy}, which share the middle ellipse, these directions correspond to opposite endpoints of the minor axis (the angle of rotation is given only for Z_{xx}). The centres of the ellipses are given by the invariants Z_1 and Z_2 and their axes by the constants Z_3 and Z_4. The direction of rotation around the ellipses is determined by the signs of Z_3 and Z_4 (see the text for details).

Furthermore, from eqs (14) it also follows that

$$Z_3'(\theta) = \frac{1}{2}(Z_{xy} + Z_{yx}) = \pm Z_3 \frac{1 - Tt}{\sqrt{1+t^2}}$$

$$Z_4'(\theta) = \frac{1}{2}(Z_{xx} - Z_{yy}) = \pm Z_3 \frac{T + t}{\sqrt{1+t^2}} \quad , \tag{18}$$

i.e. $Z_4'(\theta) = \pm Z_3'(\theta \pm 45°)$

and it can be shown that $|Z_3'|$ and $|Z_4'|$ are also extremal in the principal coordinates, and at all multiples of 45°.

2 THE CASE OF 2-D STRUCTURES

For an impedance tensor to represent a 2-D structures it has been shown quite independently by Berdichevsky (1968), Sims (1969) and Fischer (1975) that it is not sufficient for Z_2 to vanish (this is the well-known condition of the vanishing skew S):

$$Z_2 = 0 \Rightarrow S = |Z_2|/|Z_1| = 0. \tag{19}$$

The additional requirement stems from the fact that in eqs (14) [or eqs (1) with the appropriate interpretation of the subscripts] both real and imaginary parts of Z_{xx} and Z_{yy} must become zero at the same rotational angle θ_p corresponding to the principal axes. Because of the linearity of the relations between impedance elements this requirement means that for all angles θ

$$\arg Z_{xx} = \arg Z_{yy} = \arg Z_3', \{\text{i.e.} = \arg (Z_{xy} + Z_{yx})\}. \tag{20}$$

In a certain sense this condition has been rediscovered several times by authors who expressed it in quite different ways (e.g. Word, Smith & Bostick 1971; Lilley 1976, 1993; Eggers 1982; Ranganayaki 1984; Beamish 1986; Bahr 1988), in general not realizing that it had been clearly formulated first by Berdichevsky (1968).

From condition (20) it immediately follows that for 2-D structures

$$T' = Z_4'/Z_3' \quad \text{must be real,} \tag{21}$$

and it can further be shown that θ_p is then given by a relation much simpler than (11):

$$\tan 2\theta_p = -T' = 2Z_{xx}/Z_3'. \tag{22}$$

In the principal coordinates $T' = T$, and vanishes completely for 2-D structures, whereas with (15) we have seen that it becomes purely imaginary in the general case of 3-D structures. It will be shown later that the imaginary part of T never exceeds the limits of $\pm i$.

3 GRAPHIC REPRESENTATIONS OF THE IMPEDANCE ELEMENTS

Sims (1969), in his PhD thesis, has given graphic representations of the variations of the impedance elements when the coordinates are rotated. In the complex-plane eqs (14) describe a set of three ellipses. An example of such a representation is seen in Fig. 1. It can be shown that the centres of the ellipses are at $+Z_1$ and $-Z_1$ for Z_{xy} and Z_{yx} respectively, and at $+Z_2$ for both Z_{xx} and Z_{yy}, which together describe a single ellipse located between the previous two. All three ellipses are identical in shape, but we note that for the middle ellipse the endpoints of the axes correspond to different values of the angle θ, which in such graphs plays the role of a parameter. It can be shown that $|Z_3| \geq |Z_4|$, and the extremities of the major axes of the outer ellipses therefore correspond to $\theta = 0°$ and $\pm 90°$, the $\theta = \pm 45°$ points being at the endpoints of the minor axes. This is exactly reversed for the middle ellipse. The equality $|Z_3| = |Z_4|$ means that the ellipses have become circles. In this limiting situation one finds that $|Z_3'(\theta)|$ and $|Z_4'(\theta)|$, as well as the sums (9) and (10), become rotationally invariant like Z_1 and Z_2. If we were to admit that $|Z_4|$ can become larger than $|Z_3|$ one would observe that conditions (11) and (12) lead to principal axes rotated to the endpoints of the Z_4 axes on the ellipses, these having now become the major ones. What this means is that in the principal coordinates the imaginary part of T cannot exceed the limits of $\pm i$, as announced at the end of the preceding section. In this particular limiting situation we find indeed the expected result that eq. (11) yields an indefinite angle $\theta_p \Rightarrow 0/0$.

As Fig. 1 emphasizes, the sign of $T = Z_4/Z_3 = \pm \beta i$, with $0 < \beta < 1$, determines the sense of rotation around the ellipses for positive θ (Eggers 1982). Here rotation around the ellipses appears to go in the positive sense because this sign is negative.

If the time dependence is expressed as $\exp(+i\omega t)$ the MT

phase ϕ of Z_{xy} over a uniform half-space is 45°, and −135° for Z_{yx}. For 1-D structures in general the impedance remains in the first and third complex quadrants, and this is generally also true for more complicated structures, but a 3-D counter-example will be given toward the end of this Section.

1-D structures

Over a non-magnetic homogeneous half-space of resistivity ρ it is well known that

$$Z_{xx} = Z_{yy} = 0, \tag{23}$$

$$Z_{xy} = -Z_{yx}, \tag{24}$$

and

$$Z_{xy} = \sqrt{i\omega\mu \cdot \rho}. \tag{25}$$

At a given period $\tau = 2\pi/\omega$ the equivalent of the Fig. 1 diagram reduces to three isolated points on the (45°, −135°) quadrant diagonals, at equal distances from the origin, plus the origin itself.

For a layered half-space, conditions (23) and (24) still hold, but not (25), which now must be generalized. This is usually done by introducing the concepts of apparent resistivity $\rho_a(\tau)$ and variable MT phase $\phi(\tau)$:

$$Z_{xy} = \sqrt{\omega\mu \cdot \rho_a(\tau)}\exp i\phi(\tau). \tag{26}$$

At a given period Z_{xy} and Z_{yx} correspond, in the complex plane, to two points equidistant from the origin on a straight line through quadrants 1 and 3.

What we want to stress here, is that coordinate rotations do not correspond to any displacement in these representations: in the 1-D limit every coordinate system is a principal system.

2-D structures

Here the invariant Z_2, given by (3), vanishes and Z_4 is also zero as Z_{xx} and Z_{yy} themselves vanish in the principal coordinates. Because of (7) it then follows that $T = 0$. The graphical representations of the rotational behaviour corresponding to eqs (14) then reduce to straight line segments, as shown in Fig. 2. The principal coordinates, obtained for $\theta = 0$ (i.e. $t = 0$) correspond to the *farthest* point from the origin in the first quadrant and yield Z_{xy}. The corresponding Z_{yx} is *closest* to the origin in the third quadrant. Z_{xx} and Z_{yy} are situated on the line segment through the origin, but the $\theta = 0$ and ±90° points are at the origin itself and the endpoints of the segments correspond to $\theta = \pm 45°$, with Z_{xx} at one end and Z_{yy} at the other. As the coordinates rotate, both move toward the origin, which they reach when $\theta = 0$ or ±90°, and from there they proceed to the opposite endpoints, but their sum always adds to zero.

What Fig. 2 also clearly shows is that in the principal coordinates the four following quantities are all at their maximum:

$$|Z_{xy}|^2 + |Z_{yx}|^2; \quad |Z_{xy}|; \quad A(\theta); \quad Z_3'(\theta); \tag{27}$$

where the anisotropy A is defined as in (13), but for any angle θ. As already mentioned, the principal coordinates are

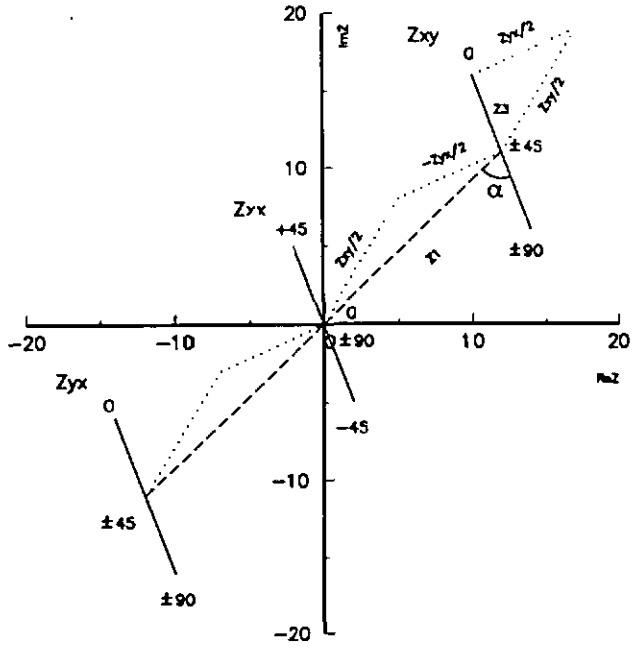

Figure 2. The same as Fig. 1, but for a 2-D structure, or a sounding site located in a plane of vertical reflection symmetry (*cf.* Fischer 1975). The angle α between the directions of Z_1 and Z_3 is the parameter of the curves in Figs 5(a) and 5(b).

obtained by eq. (22) rather than (11), but condition (12) is still required.

The vanishing skew, i.e. $Z_2 = 0$, insures that the middle segment is centred on the origin. But as we have stressed in the preceding section, a vanishing skew is not sufficient to guarantee a 2-D structure. The additional condition (20) means that the rotational behaviour of the impedance elements can be represented by line segments rather than ellipses. As stated before, this has been pointed out by many authors under different forms (e.g. Berdichevsky 1968; Sims 1969; Word *et al.* 1971; Fischer 1975; Lilley 1976, Eggers 1982; Ranganayaki 1984; Beamish 1986; Bahr 1988).

With Fig. 2 it can also be seen that a vanishing skew S does not imply a vanishing anisotropy A. The values and the range of variations of A with θ strongly depend on the relative orientations in the complex plane of $\pm Z_1$, which defines the centres of the Z_{xy} and Z_{yx} segments, and the line segments themselves given by $\pm Z_3$. A will vary the most if Z_1 and Z_3 are parallel, i.e. if

$$Z_3/Z_1 \quad \text{is purely real,} \tag{28}$$

and will remain constant at $A = 1$, i.e. no anisotropy, when

$$Z_3/Z_1 \quad \text{is purely imaginary.} \tag{29}$$

In what follows we look at the implications of conditions such as (28) or (29) as far as the structure is concerned.

An interesting example of strong variation of A is afforded by the two-quarter-space model recently studied in great detail by Fischer *et al.* (1992) and sketched in Fig. 3. This is a structure with a strong axial or directional character; it has a single plane of reflection symmetry with an abrupt discontinuity of resistivity. The model response of Fig. 4 shows that on the interface, but just inside the 10 Ωm medium, the B-polarization apparent resistivity is 1.75 Ωm

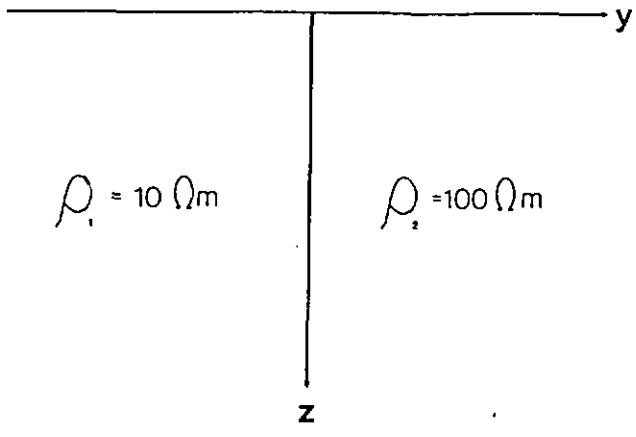

Figure 3. Two-quarter-space model chosen to illustrate a strongly directional structure.

(in the 100 Ωm medium it is, of course, 175 Ωm), whereas for the *E*-polarization it is 24.0 Ωm (identical in both media). For both polarizations the phase ϕ must be exactly 45°, as shown by Fischer & Schnegg (1993). To a common, but period-dependent factor, the various impedance elements can therefore be given in the principal coordinates as

$$\left.\begin{aligned} Z_{xy} &= 3.464(1+i), & Z_{yx} &= -0.935(1+i) \\ Z_{xx} &= 0, & Z_{yy} &= 0 \end{aligned}\right\}, \tag{30}$$

i.e.

$$\left.\begin{aligned} Z_1 &= 2.200(1+i), & Z_2 &= 0 \\ Z_3 &= 1.264(1+i), & Z_4 &= 0 \\ A_{max} &= 13.7, & S &= 0 \end{aligned}\right\}. \tag{31}$$

Structures for which condition (29) is realized are quite different. If there is no anisotropy in any direction the structure must possess four-fold symmetry: the principal axes are located in vertical planes of reflection symmetry. If this happens the sounding site is an isolated point in a 3-D structure with these properties (Fischer 1975), and the axial bisectors at 45° also lie in vertical planes of reflection symmetry. In these 45° directions $|Z_{xy}|$ and $|Z_{yx}|$ will be at their common minimum. Such highly symmetrical features are certainly not very frequent; moving away from the special symmetry point sees the MT response at once becoming 3-D, except if one moves along some of the symmetry axes which are found every 45° (*cf.* the example of the next §), where it will mimic 2-D behaviour without being 2-D, since moving sideways, along what would be the direction of a profile of the 2-D structure, it immediately

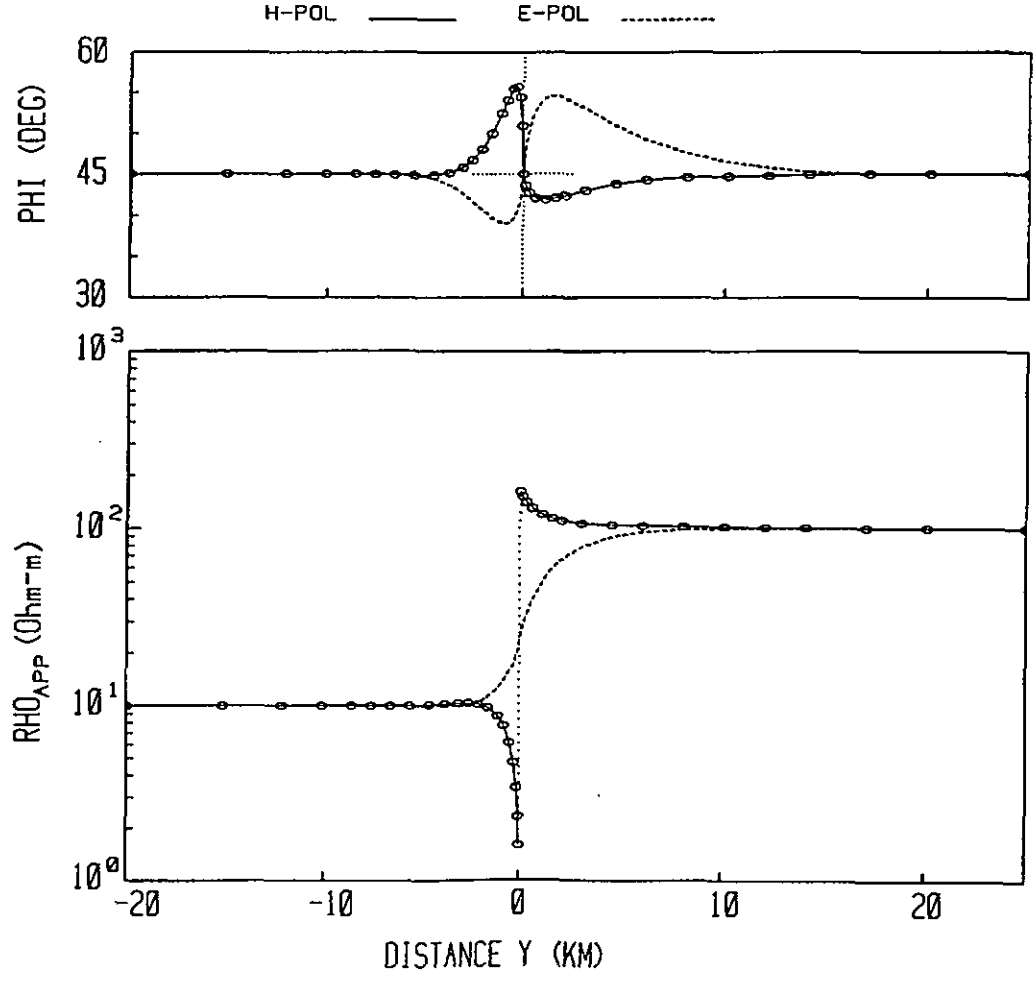

Figure 4. Response of the two-quarter-space model of Fig. 3 at the period of one second.

becomes 3-D. Along the many symmetry directions the Z_3 vector will, therefore, not remain perpendicular to Z_1 and condition (29) will no longer be fulfilled. In spite of the fact that the sounding site seems to possess 2-D properties it is effeetively a highly particular point of a 3-D structure; but the response will also reveal that this special site has no strong directionality, even if the apparent resistivity has no perfectly rotational symmetry.

3-D structures with features of symmetry like those we have just described can be constructed along the lines of Groom & Bailey (1991) in their Fig. 4. In that structure site 01 is on a plane of reflection symmetry. It behaves as a 2-D site but is not 2-D. Somewhere along the perpendicular from the centre of the hemispherical inclusion to the interface a site can probably be found where the anisotropy $A \equiv 1$ in all directions. This particular structure illustrates the statement made in the previous § that away from the singular point, 2-D behaviour will continue to be observed only if one moves along some specific directions, here toward or away from site 01.

To illustrate the importance of the relative orientations of Z_1 and Z_3 on the directionality of a structure, we make a plot in Fig. 5 of the apparent resistivity $\rho_a(\theta)$ for the (Z_1, Z_3) couple of vectors given in (31), rotating Z_3 away from its parallel orientation (for example, $\alpha = 0$ in Fig. 2, corresponding to the quarter-space structure of Fig. 3), until it becomes perpendicular ($\alpha = 90°$) to Z_1. The progressive loss of directionality as the angle α increases from 0 to 90° is striking. Also noteworthy are the minima of resistivity at 45° from the principal directions.

3-D structures

In this most general situation the four complex impedance elements can take arbitrary values, which means that there are eight degrees of freedom. Rotation into principal coordinates imposes condition (15) and only removes one degree of freedom. The three parallel line segments of Fig. 2, characteristic of a 2-D structure, now become three identical ellipses, as seen in Fig. 1. The two outer ellipses are located symmetrically with respect to the origin of the complex plane, whereas the centre of the middle ellipse is shifted away from the origin by an amount Z_2.

The principal coordinates correspond, in Fig. 1, to the endpoint of the major axis of the $Z_{xy}(\theta)$ ellipse which is furthest from the origin of the complex plane.

Several other interesting features are worth mentioning with regard to Fig. 1.

(1) The skew S is given by the ratio of distances to the centres of the middle and external ellipses. A small skew means that the centre of the middle ellipse is close to the origin.

(2) Quite obviously, of the four quantities (27), only

$$|Z_{xy}|^2 + |Z_{yx}|^2 \quad \text{and} \quad |Z_3'(\theta)| \tag{32}$$

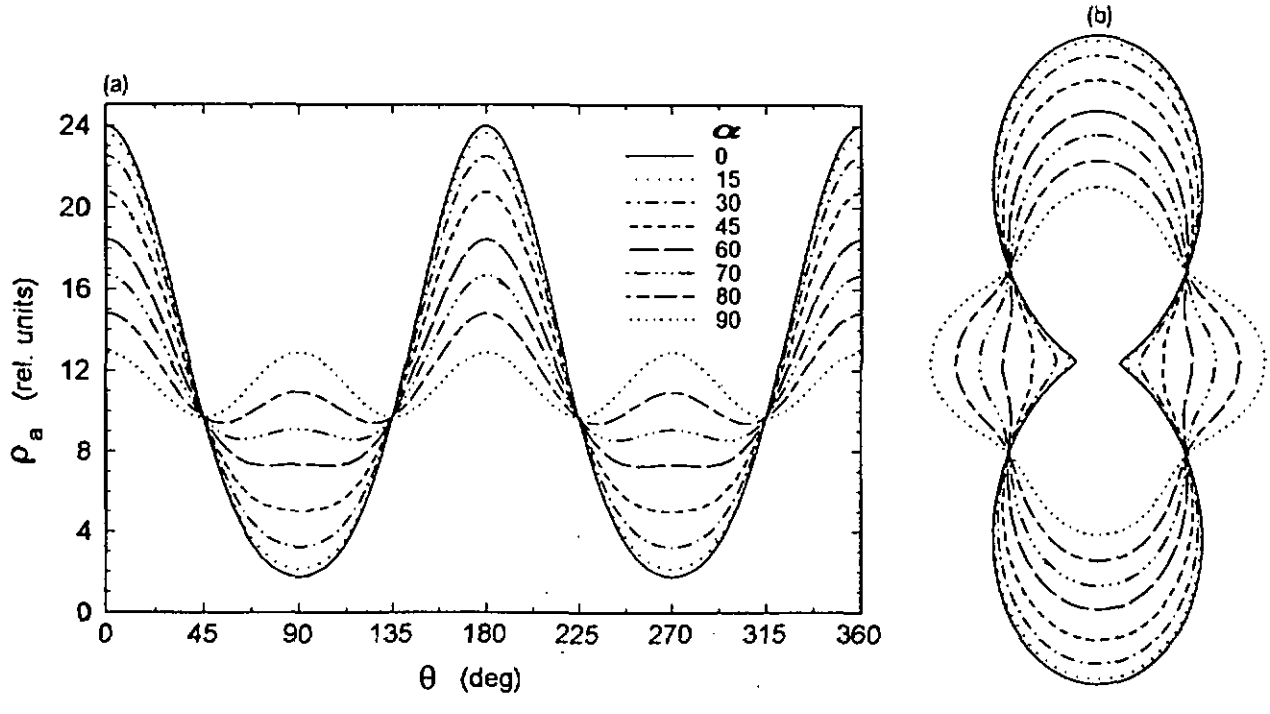

Figure 5. (a) Variation of the apparent resistivity $\rho_a = \rho_{xy}(\theta)$ as a function of the polar angle θ for a hypothetical model whose impedance parameters are those of the two-quarter-space model of Fig. 3, given under (30), but where the vector Z_3 is rotated away from its direction parallel to Z_1 (i.e. $\alpha = 0$ in Fig. 2) when the response is highly directional. (b) Polar diagram representation of the same data. Near the perpendicular orientation (i.e. $\alpha = 90°$) the response has lost its strong directionality: the structure has an axis of symmetry every 45° (i.e. four-fold symmetry!), the anisotropy $A = 1$, the resistivity is at a maximum in both principal directions, and the highest conductivity occurs along the 45° diagonals. Note how the directions of minimum $\rho_{xy}(\theta)$ shift gradually from $\theta = 45°$ toward $\theta = 90°$. In this particular example the Z_1 vector is along the 45° diagonal of the complex plane, but exactly the same results is obtained for any orientation of Z_1.

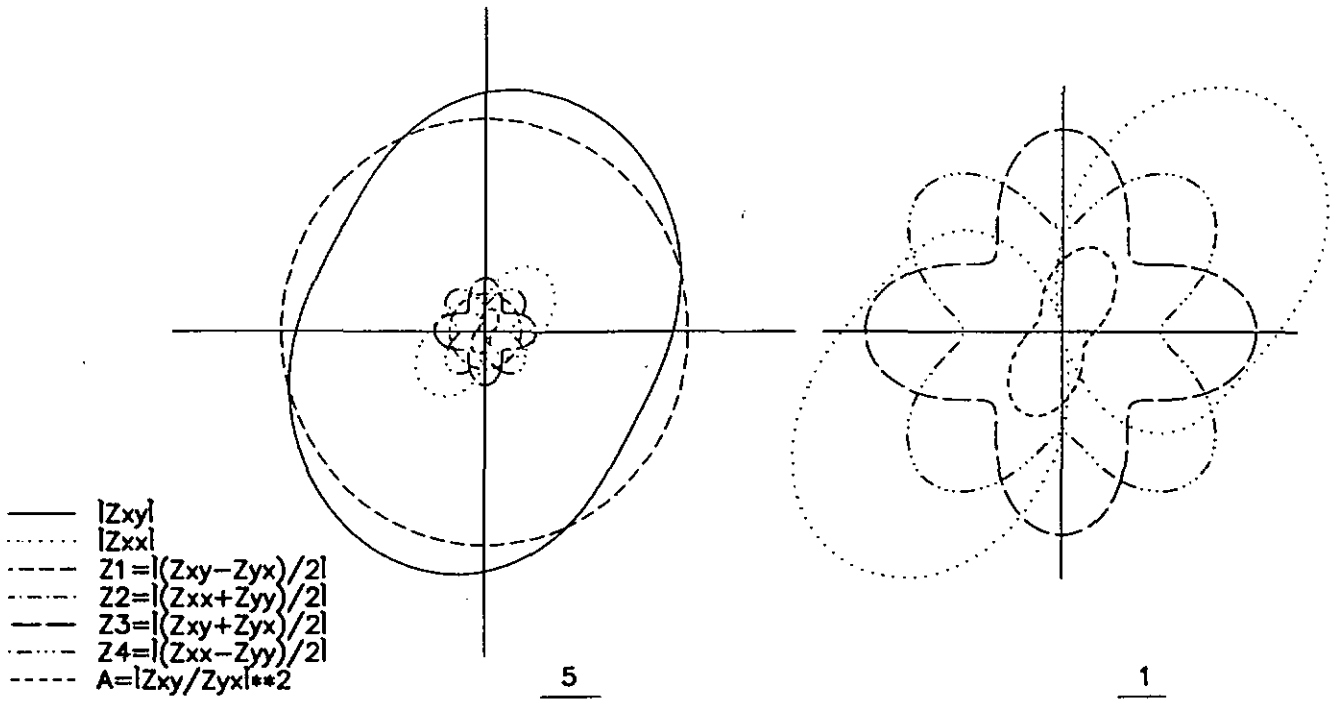

Figure 6. Polar diagram of various parameters derived from the impedance elements represented in Fig. 1. The axes correspond to the principal coordinates, with $\theta = 0$ at the top and positive rotation to the east. The right side is an enlargement of the central left part. Note that $|Z_{xy}|$ and the anisotropy A are not at a maximum in the principal directions, nor $|Z_{xx}|$ at a minimum.

reach a maximum in the principal coordinates. $|Z_{xy}(\theta)|$ and $A(\theta)$ are not at a maximum for the angle of rotation corresponding to the principal coordinates. This is clear in Fig. 1, but a still better demonstration of this is given in Fig. 6.

(3) The variation of the anisotropy with respect to the angle of rotation, $A(\theta)$, depends on the opening, or ellipticity, of the ellipses and on their orientation. In particular, if the outer ellipses lie with their Z_3 axis perpendicular to Z_1, the anisotropy disappears in the principal coordinates: $A = 1$. If the ellipses are wide, i.e. have only a small ellipticity, then $|Z_4| \approx |Z_3|$ and the anisotropy may vary quite substantially with the angle θ, but it will go through unity for every multiple of $\theta = 90°$. An example is shown in Figs 7 and 8 where the ellipticity is quite important and Z_3 is almost perpendicular to Z_1: $A(\theta)$ there remains close to unity for all orientations, even though for these particular data the skew can be considered as rather large with $S = 0.28$.

(4) The variations of A with θ will be strongest when an elongated ellipse is almost aligned with Z_1, i.e. points to and away from the origin.

(5) A further interesting situation is depicted in Figs 9 and 10, where we see a $Z_{xy}(\theta)$ that wanders out of the first quadrant (and concomitantly a $Z_{yx}(\theta)$ that moves out of the third quadrant). For these data $Z_{xy}(\theta)$ describes a very elongated ellipse, and $|Z_{xy}(\theta)|$ is maximum at $\theta = 0.5°$, i.e. almost exactly along the principal axes, but the maximum of $A(\theta)$, on the other hand, occurs at $\theta = 9°$.

Let us assume that we have a structure with a skew which is not very large. If, in addition, it yields ellipses which are closely aligned with Z_1, thus nearly fulfilling condition (28),

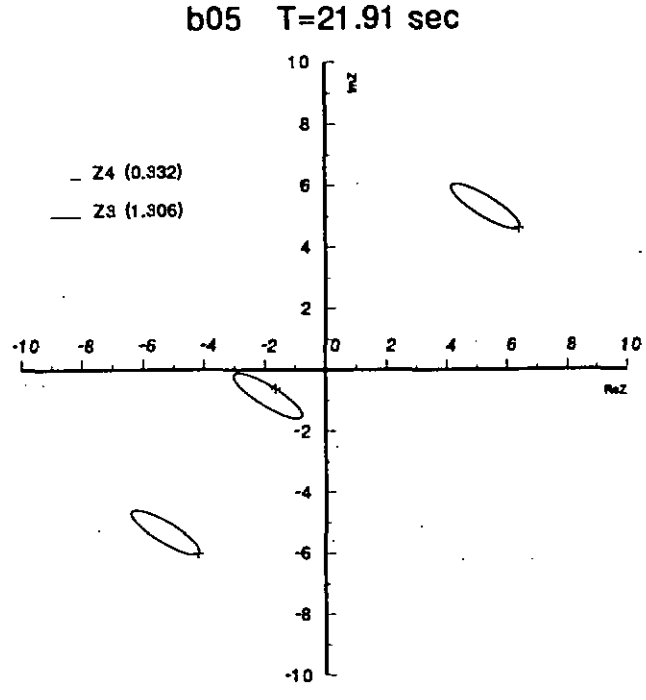

Figure 7. Magnetotelluric impedance elements at $\tau = 21.91$ s for sounding site b05 at the Araguainha impact crater (Masero *et al.* 1994). For these data the skew $S = |Z_2/Z_1| = 0.28$ is fairly large, but because the ellipses are oriented nearly at right angles to Z_1 the anisotropy remains small ($A \cong 1$) for all coordinate directions, as shown in Fig. 8. The crosses on the ellipses signal the original measured field data. For the central ellipse only the position of Z_{xx} is given (Z_{yy} is on the opposite radius). With this information one sees what one is rotating away from. Here, and in all the data presented in this paper, the crosses rotate clockwise on the ellipses when the field angle θ increases.

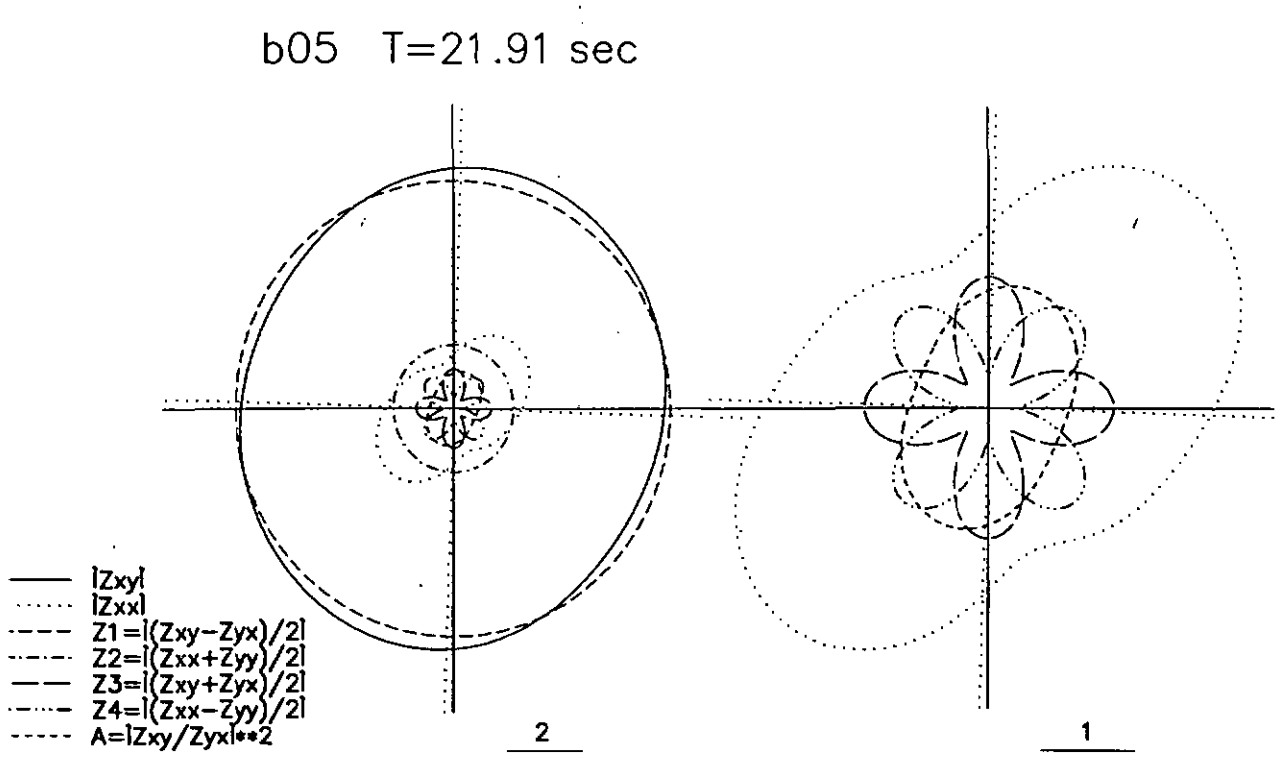

Figure 8. Polar diagrams for the impedance data of Fig. 7. The original sounding directions are indicated with dotted lines whereas the solid lines are the principal coordinates. Note the small variations of the anisotropy A.

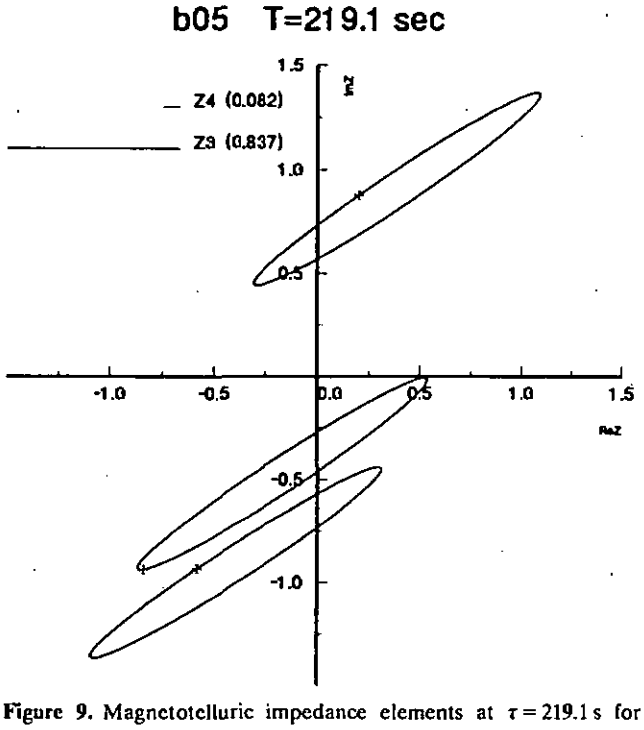

Figure 9. Magnetotelluric impedance elements at $\tau = 219.1$ s for sounding site b05 at the Araguainha impact crater (Masero *et al.* 1994). Note for these data the rather unusual observation of Z_{xy} and Z_{yx} impedance ellipses that extend beyond the first and third complex quadrants. Whether this is a genuine feature or rather an artefact caused by external perturbations is uncertain, but for this remote site cultural noise was very weak. The crosses on the ellipses refer to the field data and have the same properties as in Fig. 7.

the structure will have a marked directional character, in this case even an axial character, and lie close to one of the principal axes. This will remain true even if the ellipses are wide, but if the ellipses are not very wide the structure will almost be 2-D. When the skew becomes large the strong directional character will be retained, but the larger sum of the diagonal tensor elements then means that the structure deviates more from pure 2-D symmetry.

When the skew is small and the ellipses are oriented at right angles to Z_1, and if they are not much open, the sounding site will be close to having four-fold reflection symmetry. As we have seen in the preceding discussion of 2-D responses, the principal coordinates then yield similar apparent resistivities close to their maximum, and the 45° axes lead to minimum resistivities. The principal directions, as well as those at 45°, then exhibit some directional but not axial character, and the sounding site is an isolated point with features of high symmetry. If, on the contrary, the ellipses are very wide, $|Z_{xy}|$ and $|Z_{yx}|$ may achieve extremal values on the 45° axes, one being at a minimum there, the other at a maximum. These 45° axes, rather than the principal coordinates, may then indicate the gross directional features of the structure. But the sounding site could still be an isolated special point.

To strengthen the interpretations of features like those that we have just described, it will be necessary to investigate the responses of several adjacent sites in various directions. And, as we shall see below, a single site is likely to exhibit responses which change in character in different period ranges.

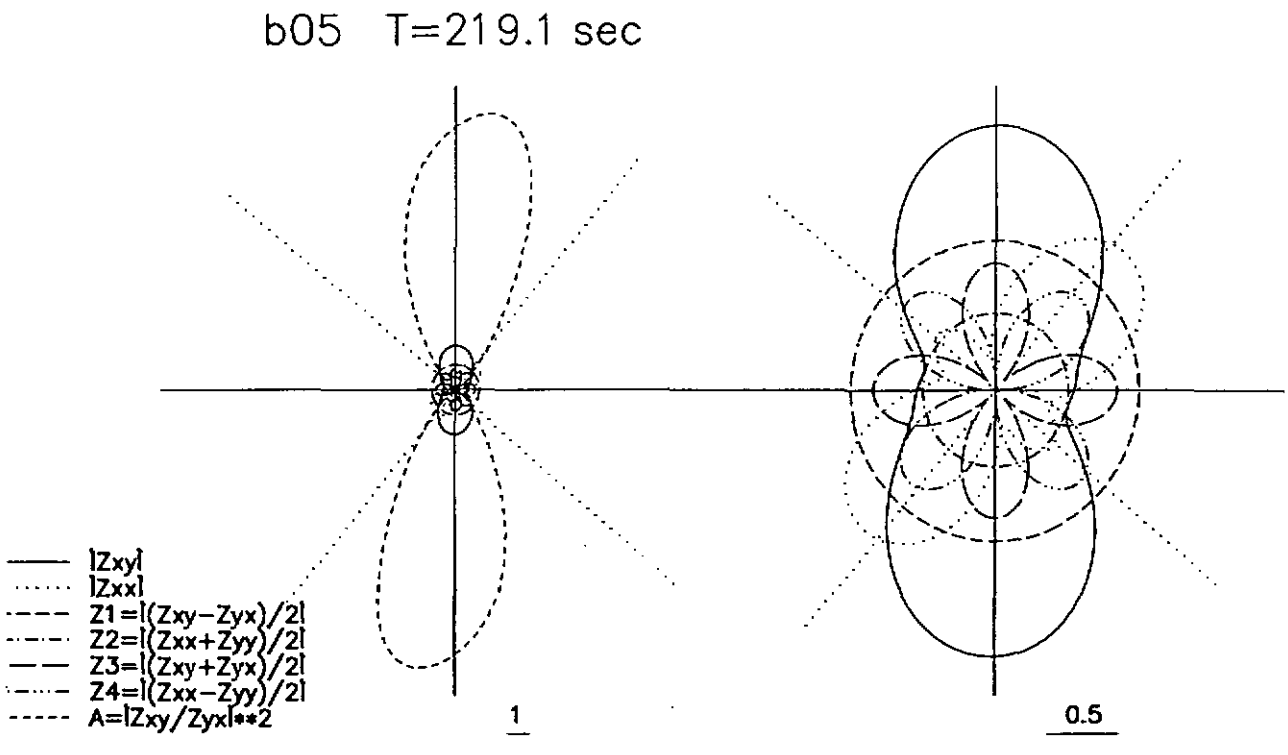

Figure 10. Polar diagrams for the impedance data in Fig. 9. The original sounding directions are indicated with dotted lines whereas the solid lines are the principal coordinates. The anisotropy A is fairly large in directions close to the principal coordinates. The feature worth noting is the double kink in $|Z_{xy}|$. This arises because the length of Z_{xy} undergoes rather peculiar variations in the area where its ellipse crosses into the second quadrant of the complex plane in Fig. 9.

4 CORRECTION OF DISTORTION

In Section 5 we propose to demonstrate the usefulness of our scheme of analysis with a set of MT field data. Before this can be done it is sometimes necessary to remove the effects of static shifts in the data. As is well known, MT soundings are a skin-effect experiment and therefore return a depth-dependent information, where the high frequencies are influenced by near-surface features, whereas the long periods are also sensitive to the deeper structure. Our scheme should therefore give us information about structural features at various depths.

In recent years several groups have proposed methods of analysing MT data which separate a distorting local or short-range 3-D structure from a regional or longer range 2-D matrix (*cf.* e.g. Larsen 1977; Cox *et al.* 1980; Zhang, Roberts & Pedersen 1987; Bahr 1988, 1991; Groom & Bailey 1989, 1991; Groom & Bahr 1992). Local features can distort the MT response at all frequencies and are of two kinds.

Static shift (*cf.* e.g. Jones & Savage 1986; Kurtz, Delaurier & Gupta 1986; Sternberg *et al.* 1988; Jones 1988) multiplies apparent resistivities by a constant factor, up or down, without affecting the phase. Such effects occur when the ground at the sounding site, in a very small area, has a resistivity different from the formations sampled at the shortest periods. For example, continuity of the current crossing a very resistive narrow dike produces a very high electric field over the dike and suggests a very high resistivity everywhere. This effect is particularly strong because MT apparent resistivities are derived from the square of the electric-field amplitude. We have experienced such effects over what seemed the most homogeneous alluvial plain in Sardinia (Peruzza *et al.* 1990) where it sufficed to move the sounding site a few hundred metres to recover 1-D conditions at 1000 Hz, i.e. a homogeneous short-range environment.

Locally the ground can also be strongly inhomogeneous, as in mountain areas when sounding over surfaces of rubble or scree. Here it is the direction of the electric field which may be strongly affected, again at all frequencies, and this will distort the impedance tensor. However, because of the continuity of the current it is generally accepted that the electric field is far more sensitive to such effects than the magnetic field (*cf.* e.g. Groom & Bailey 1989).

When discussing MT results the implicit assumption is generally made that the data are derived from measurements of the electric and magnetic fields, respectively E and B. However, it is well known that in MT practice, instead of E what is measured is a potential difference over a certain distance (*cf.* e.g. Fischer, LeQuang & Müller 1983; Poll, Weaver & Jones 1989). For both types of MT distortions it is evident that this practice tends to reduce their perturbing effect, and our own observations suggest that the effect is strongest in reducing the directional disturbances. A large electrode separation is also beneficial to insure a large ratio of signal-to-electronic noise (we generally work with electrode separations of 50 m).

To obtain a valid analysis of our data with the scheme we have described in the preceding sections it is imperative to remove static shift when it is present, since such shifts directly affect the anisotropies we derive from our data. This

can be done following the authors quoted above, or according to a method specially adapted to the Araguainha impact crater data by Masero *et al.* 1994. On the other hand, we shall not correct the data for any rotational distortions, since our scheme is designed precisely to reveal the changing structural properties as a function of depth at each sounding site. It turned out, however, that most of the data collected at the Araguainha impact crater did not require any static-shift corrections. At nearly all the sites the data were almost ideally 1-D at periods below a few tenths of a second, suggesting that to depths of the order of one kilometre there were no distorting structures. This is especially true for site b05, which will be used to demonstrate the usefulness of the scheme of data analysis presented in this paper.

5 APPLICATION TO A FIELD EXAMPLE

In Figs 7 to 10 we have already considered field examples from site b05 on the Brazilian Araguainha impact crater (Masero *et al.* 1994), but shall now discuss this data set in greater detail. In Fig. 11 we see why these data drew our attention: the skew starts to rise markedly at periods above about 5 s, but the maximum anisotropy A_{max}, which in general does not obtain in the principal coordinates, only begins to rise at periods above 100 s. This was at first surprising because at the shortest periods we had practically 1-D responses. With increasing periods we assumed that the structure would gradually exhibit 2-D and then 3-D behaviour, and therefore expected to see the anisotropy rise *before* the skew. We wanted to understand whether the unexpected behaviour could be explained and what it means.

To compare sounding data obtained at various periods it is advisable, according to (26), to multiply the impedances by $\sqrt{\tau}$. This removes the direct effect of the period and the impedance variations are then entirely controlled by the apparent resistivities. Since impedances are proportional to the root of resistivities large resistivity variations turn out

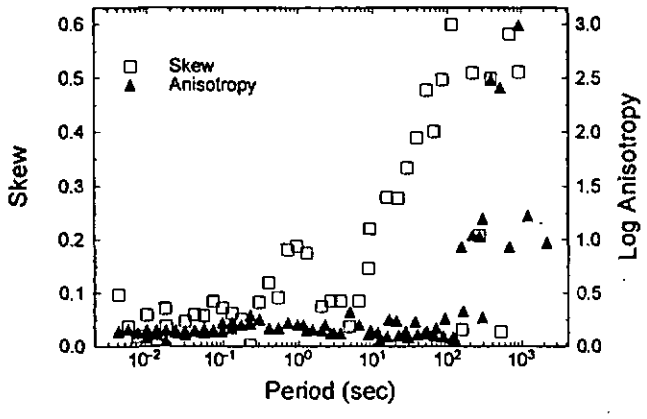

Figure 11. Variations with the period τ of skew S and maximum anisotropy A_{max} at sounding site b05 over the Araguainha impact crater (Masero *et al.* 1994). As we have seen, A_{max} generally does not occur in the principal coordinates. Note that S rises rapidly above periods of 5 s whereas A_{max} remains low until τ exceeds 100 s. This can be understood in terms of impedance elements which vary according to Fig. 12.

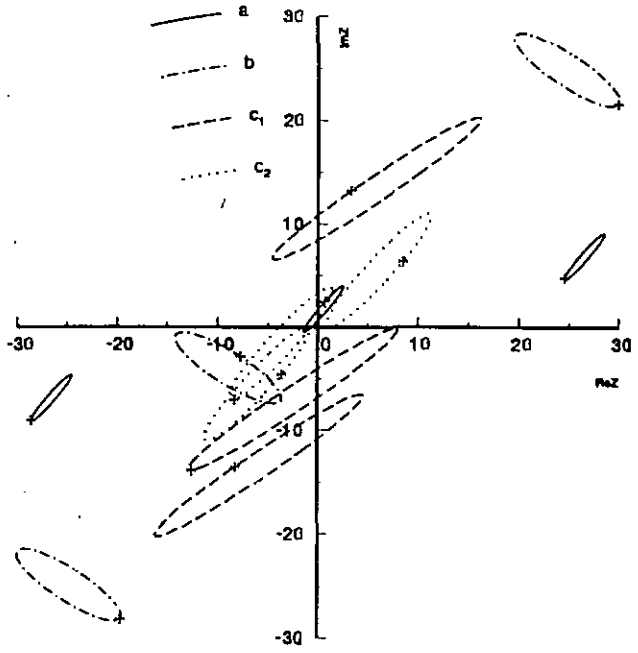

Figure 12. Magnetotelluric impedance elements, multiplied by $\sqrt{\tau}$, at site b05 over the Araguainha impact crater (Masero *et al.* 1994) for periods in the three characteristic ranges (a) below 5 s ($\tau = 1.54$ s), (b) from 5 to 100 s ($\tau = 21.91$ s), (c) above 100 s ($\tau = 219.1$ and 389.6 s). The ellipses are small, far from the origin, but close to the real axis in the short period range (a); they increase in size turning their major axis Z_3 at right angles to the radial vector Z_1 in range (b); and finally they increase further in size while moving closer to the origin and turning their major axis Z_3 parallel to Z_1 in (c). Here the skew is large not so much because $|Z_2|$ is large, but also because $|Z_1|$ has become small. The behaviour of the impedance ellipses with the period τ explains the observations of Fig. 11. The crosses on the ellipses always refer to the measured field data and have everywhere the same properties as in Fig. 7.

attenuated in plots of $\sqrt{\tau} \cdot Z_{ij}$ and linear scales can generally still be used.

In the Fig. 11 plot we consider three distinct regions: (a) periods shorter than $\tau = 5$ s, (b) periods between 5 and 100 s, and (c) periods longer than 100 s. For each region Fig. 12 displays the impedance ellipses in the complex plane for one or two data sets characteristic of that period range in a diagram where the scales correspond to $\sqrt{\tau} \cdot Z_{ij}$.

In region (a) we have a middle ellipse centred close to the origin, which means a small skew, and very small ellipses, i.e. almost a 1-D response. At only $15 \pm 5°$ the phase is quite low and suggests that the deeper formations of the structure are more resistive than the subsurface ones (*cf.* Fischer *et al.* 1992).

In region (b) the middle ellipse is far from the origin so the skew is large (0.28) and the ellipses have become somewhat larger: we have 3-D conditions. But the ellipses are oriented with their Z_3 axes essentially at right angles to Z_1. In the principal coordinates the anisotropy is therefore very close to $A = 1$. The ellipses are reasonably wide, but the outer ones are rather far from the origin so that the anisotropy A remains close to unity for all orientations, as seen in Figs 8 and 11. Even though the skew is already important the data are not too different from a 2-D set with Z_3 almost perpendicular to Z_1, as in the example of Fig. 2. At these periods the structure, therefore, does not exhibit

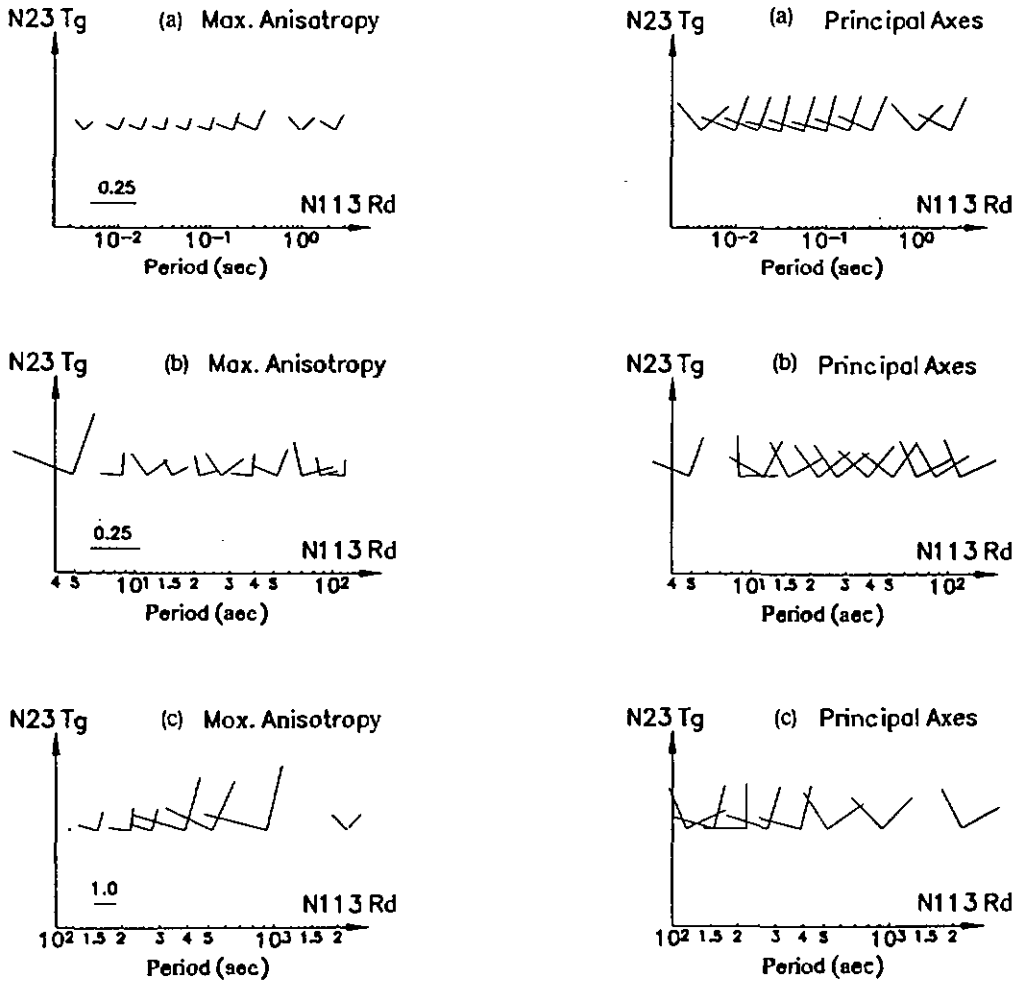

Figure 13. Plot in three period ranges of the directions of maximum anisotropy A_{max} and principal coordinates of MT data from site b05 at the Brazilian Araguainha impact crater (Masero *et al.* 1994). (a) Periods shorter than 5 s. (b) Periods between 5 and 100 s. (c) Periods longer than 100 s. The abscissa is along the crater radius, the ordinate along its rim. Note in range (b) that the axes of maximum anisotropy are aligned fairly well with the symmetry features of the structure, whereas the principal coordinates rather point at 45° to these directions. In range (c) both systems of axes are closely aligned with the structure, especially at the shorter periods where its influence is important, but there is more consistency for those of maximum anisotropy.

strong directionality, especially not along the principal coordinates, but as seen in Fig. 13, these features, i.e. the directions of the crater radius and rim, are rather oriented with the axis of maximum anisotropy.

Finally, in region (c) the 3-D character has become very pronounced: the centres of the middle ellipses have moved quite far from the origin, i.e. the skews are large (0.51 and 0.50 for the two periods considered), and the ellipses are fairly wide, so that condition (20) is clearly violated. But the ellipses have also changed their orientation, with Z_3 rather closely parallel to Z_1. In one case it has also become almost identical to it and the anisotropy then attains extremely high values. The particular data set c_2 chosen to illustrate region (c) is in fact fairly extreme with $A_{max} \cong 300$. The less extreme set c_1 displayed in Figs 9 and 10 has a smaller anisotropy A_{max} of about 11. As shown in Fig. 13, at these long periods there is a marked directional character to the data, in agreement with the location of this site on the outer rim of the Araguainha impact crater (Masero *et al.* 1994), one direction pointing to the centre of the impact crater and the other being along its tangent, and we notice that the directions of maximum anisotropy give these directions with greater consistency than the principal coordinates.

6 CONCLUSIONS

The graphic display in the complex plane of the rotational properties of a given MT data set provides a simple but powerful method for deriving information on the directional properties of the site under investigation. This information is essentially contained in the orientation of the ellipses described by the tensor elements in the complex plane when the coordinate system is rotated. If the major axes of the ellipses are orientated approximately toward the origin of the complex plane the structure is highly directional and probably axial along directions which are essentially those given by the principal coordinates. When the ellipses are rather at right angles to the previous orientation, i.e. when it is their minor axes which point toward the origin, the structure is generally much less directional, and whatever directionality remains may be oricnted at 45° to the principal coordinates given by the major axes of the ellipses.

Data from the Araguainha impact crater in Brazil have provided an interesting illustration of these findings. In particular, it was found that a given site can exhibit different directional properties in different period ranges. While this is often interpreted as different depth ranges it also means different lateral ranges. This is certainly true with a circular formation like an impact crater. The true shape of the structure can only be perceived at periods that are sufficiently long for the skin depth to become approximately of the same order as the radius of the crater.

In a very recent paper Lilley (1993) has extended his method of MT data analysis in terms of Mohr circles (Lilley 1976). In this method the real and imaginary parts of the impedance tensor are treated separately. In some instances the two data sets could lead toward different interpretations. By treating the real and imaginary information simultaneously the present method attempts to avoid any possible ambiguity.

ACKNOWLEDGMENTS

This research was supported by a grant from the Swiss National Science Foundation. One of the authors (W.M.) also received a grant from the Brazilian Research Council.

REFERENCES

Bahr, K., 1988. Interpretation of the magnetotelluric impedance tensor: regional induction and local telluric distortion, *J. Geophys.*, 62, 1219–127.

Bahr, K., 1991. Geological noise in magnetotelluric data: a classification of distortion types, *Phys. Earth planet. Inter.*, **66**, 24–38.

Beamish, D., 1986. Geoelectrical structural dimensions from magnetotelluric data: methods of estimation, old and new, *Geophysics*, **51**, 1298–1309.

Berdichevsky, M.N., 1968. *Electrical prospecting by the magnetotelluric profiling method*, (in Russian), Nedra, Moscow. (If not available see: Rokityansky, I.I., 1982. *Geoelectromagnetic Investigation of the Earth's Crust and Mantle*, pp. 191–193, Springer Verlag, Berlin.)

Counil, J.L., Le Mouël, J.L. & Menvielle, M., 1986. Associate and conjugate directions concepts in magnetotellurics, *Ann. Geophys.*, **4**, B, 115–130.

Cox, C.S., Filloux, J.H., Gough, D.I., Larsen, J.C., Von Herzen, R.P. & Winter, R., 1980. Atlantic lithosphere sounding, *J. Geomagn. Geoelect.*, 32, SI13–SI32.

Eggers, D.E., 1982. An eigenstate formulation on the magnetotelluric impedance tensor, *Geophysics*, **47**, 1204–1214.

Fischer, G., 1975. Symmetry properties of the magnetotelluric impedance tensor for structures with a vertical plane of reflection symmetry, *Geophysics*, **40**, 1046–1050. (Contrary to its claims this paper gives formulae for a *negative* rotation of the coordinates.)

Fischer, G. & Schnegg, P.-A., 1993. The magentotelluric dispersion relations over 2-D structures, *Geophys. J. Int.*, **115**, 1119–1123.

Fischer, G., Le Quang, B.V. & Müller, I., 1983. VLF ground surveys, a powerful tool for the study of shallow two-dimensional structures, *Geophys. Prospect.*, **31**, 977–991.

Fischer, G., Szarka, L., Adam, A. & Weaver, J.T., 1992. The magnetotelluric phase over 2-D structures, *Geophys. J. Int.*, 108, 778–786.

Groom, R.W. & Bahr, K., 1992. Correction for near surface effects: decomposition of the magnetotelluric impedance tensor and scaling corrections for regional resistivities: a tutorial, *Surv. Geophys.*, **13**, 341–379.

Groom, R.W. & Bailey, R.C., 1989. Decomposition of magnetotelluric impedance tensor in the presence of local three-dimensional galvanic distortion, *J. geophys. Res.*, **94**, 1913–1925.

Groom, R.W. & Bailey, R.C., 1991. Analytic investigation of the effect of near-surface three-dimensional galvanic scatters on MT tensor decomposition, *Geophysics*, **56**, 496–518.

Haak, V., 1972. Magnetotellurik: Bestimmung der Übertragungsfunktionen in Gebieten mit Lateraler Änderung der Elektrischen Leitfähigkeit, *Z. für Geophys.*, **38**, 85–102.

Ingham, M.R., 1988. The use of invariant impedances in magnetotelluric interpretation, *Geophys. J.*, **92**, 165–169.

Jones, A.G., 1988. Static shift of magnetotelluric data and its removal in a sedimentary basin environment, *Geophysics*, **53**, 967–978.

Jones, A.G. & Savage, P.J., 1986. North American central plains conductivity anomaly goes east, *Geophys. Res. Lett.*, **13**, 685–688.

Kaufman, A.A. & Keller, G.V., 1981. *The magnetotelluric sounding method*, Elseiver, Amsterdam.

Kurtz, R.D., DeLaurier, J.M. & Grupta, J.C., 1986. A magnetotelluric sounding across Vancouver Island detects the subducting Juan de Fuca plate, *Nature*, **321**, 596–599.

Larsen, J.C., 1977. Removal of local surface conductivity effects from low frequency mantle response curves, *Acta Geodaet., Geophys. Montanist. Acad. Sci. Hung.*, **12**, 183–186.

La Torraca, G.A., Madden, T.R. & Korringa, J., 1986. An analysis of the magnetotelluric impedance for three-dimensional conductivity structures, *Geophysics*, **51**, 1819–1829.

Lilley, F.E.M., 1976. Diagrams for magnetotelluric data, *Geophysics*, **41**, 766–770.

Lilley, F.E.M., 1993. Magnetotelluric Analysis Using Mohr Circles, *Geophysics*, **58**, 1498–1506.

Masero, W., Schnegg, P.-A. & Fontes, S.L., 1994. A magnetotelluric investigation of the Araguainha impact structure in Mato Grosso–Goiás, central Brazil, *Geophys. J. Int.*, **116**, 366–376.

Park, S.K. & Livelybrooks, D.W., 1989. Quantitative interpretation of rotationally invariant parameters in magnetotellurics, *Geophysics*, **54**, 1483–1490.

Peruzza, L., Fischer, G., Schnegg, P.-A. & Ranieri, G., 1990. Analysis of the Sardinian N–S magnetotelluric profile, in *The European Geotraverse: integrative studies*, pp. 329–346, eds Freeman, R., Giese, P. & Mueller, St., European Science Foundation, Strasbourg.

Poll, H.E., Weaver, J.T. & Jones, A.G., 1989. Calculations of voltages for magnetotelluric modelling of a region with near-surface inhomogenities, *Phys. Earth planet. Inter.*, **53**, 287–297.

Ranganayaki, R.P., 1984. An interpretive analysis of magnetotelluric data, *Geophysics*, **49**, 1730–1748.

Rokityansky, I.I., 1982. *Geoelectromagnetic Investigation of the Earth's Crust and Mantle*, Springer Verlag, Berlin.

Sims, W.E., 1969. Methods of magnetotelluric analysis, *PhD thesis*, University of Texas, Austin, TX.

Spitz, S., 1985. The magnetotelluric impedance tensor properties with respect to rotation, *Geophysics*, **50**, 1610–1617.

Stemberg, B.K., Washburne, J.C. & Pellerin, L., 1988. Corrections for the static shift in magnetotellurics using transient electromagnetic soundings, *Geophysics*, **53**, 1459–1468.

Vozoff, K., 1972. The magnetotelluric method in the exploration of sedimentary basins, *Geophysics*, **37**, 98–141.

Word, D.R., Smith, H.W. & Bostick, F.X., Jr., 1971. Crustal investigations by the magnetotelluric tensor impedance method. *Am. geophys. Un. Monogr.*, **14**, 397–416, (or in *Magnetotelluric Methods, Geophysics reprint series* No. 5. pp. 626–648, ed. Vozoff, Soc. Explor. Geophys., Tulsa, OK (1985).)

Yee, E. & Paulson, K.V., 1987. Canonical decomposition of a telluric transfer function tensor, *J. geophys.*, **61**, 190–199.
Zhang, P., Roberts, R.G. & Pedersen, L.B., 1987. Magnetotelluric strike rules, *Geophysics*, **52**, 267–278.

APPENDIX: THE ROTATIONAL INVARIANTS OF THE IMPEDANCE TENSOR

In a general 3-D situation the four complex elements of the impedance tensor $\mathbb{Z}$ represent a set of eight independent variables:

$$\mathbb{Z} = \begin{pmatrix} Z_{xx} & Z_{xy} \\ Z_{yx} & Z_{yy} \end{pmatrix}. \tag{33}$$

Under rotation some combinations of the tensor elements are known to yield rotational invariants. The two best known of these are $Z_{xy} - Z_{yx}$ and the trace $Z_{xx} + Z_{yy}$; these can be expressed in terms of Z_1 and Z_2 which were defined with eqs (2) and (3).

A slightly less well known rotational invariant is the determinant $D = \det(\mathbf{Z})$. It is possible to show that D can be represented in terms of the set of basic parameters (2–5), i.e. Z_1 to Z_4, *with or without primes*:

$$D = (Z_1)^2 + (Z_2)^2 - (Z_3')^2 - (Z_4')^2. \tag{34}$$

Indeed, with the set of eqs (18) it is easy to see that the last two terms of (34) alone form a rotational invariant:

$$(Z_3')^2 + (Z_4')^2 = (Z_3)^2 + (Z_4)^2 = (Z_3)^2 \cdot (1 - \gamma^2), \tag{35}$$

where the second equality will become evident with condition (36) below. Relation (35) says that the sum of the squared radii from the centres of the impedance ellipses always equals the sum of the squared elliptical semi-axes.

But this fourth invariant (35) is not independent of the first three we have listed, and so far we have only six separate quantities for a tensor with eight independent parameters. We therefore believe that there must be further invariants, of which two, or a single complex one, must be independent of those already quoted. We have found two of these. The first expresses that the Z_i refer to the prinicpal coordinates and in these the unprimed T defined by (7) is purely imaginary, as expressed by (15), and we have seen in Section 3 that its amplitude cannot exceed unity:

$$Z_4 = i \cdot \gamma \cdot Z_3, \qquad |\gamma| \leq 1, \tag{36}$$

where a positive sign for γ means a positive rotation around all the ellipses for an increasing field angle θ. Note that (36) simply gives the ratio of minor to major axes of the impedance ellipses.

The second new invariant we found is the sum Σ of the squared absolute values of the four tensor elements Z_{ij} of (33). This sum amounts to:

$$\Sigma = 2[|Z_1|^2 + |Z_2|^2 + |Z_3|^2 + |Z_4|^2]. \tag{37}$$

Again, the first two terms are invariant under rotation, the sum of the last two is therefore also rotationally invariant, i.e.:

$$|Z_3|^2 + |Z_4|^2 = |Z_3'|^2 + |Z_4'|^2 = |Z_3|^2 \cdot (1 + \gamma^2). \tag{38}$$

Furthermore, eq. (37) cannot be entirely independent of the invariants already found. Since real and imaginary parts of the impedance elements transform independently, i.e. do not get mixed—as seen most easily with eqs (1)—Σ can be separated in two independent real numbers: the summed squares of the real parts and the summed squares of the imaginary parts. Not surprisingly the difference between these two numbers is related to the real part of D.

If four independent rotational invariants are known one should be able to recover all the elements of the impedance tensor. This can easily be verified for the case when Z_1, Z_2, D, and γ are known, where the knowledge that a real γ refers to $\theta = 0$, i.e. principal coordinates, constitutes the eighth independent parameter. The impedance elements can therefore be computed for the principal coordinates, and then for any rotated coordinates via eqs (6). The only things that cannot always be recovered are the signs of γ and Z_4, or the sense of rotation around the ellipses when θ is varied, i.e. when the measurement coordinate system is rotated. The sign of Z_3, however, is determined by condition (12).

The properties found for the magnetotelluric impedance tensor are, of course, equally valid for any tensor subject to the same rotational properties.

IV.

Magnetotelluric investigation of the Serra da Cangalha impact crater, Northeast Brazil

Masero, W., P.-A. Schnegg, and S. L. Fontes

1995

J. Geomag. Geoelectr., 00, 000–000, 1995

Magnetotelluric investigation of the Serra da Cangalha impact crater, Northeast Brazil

W. MASERO[1], P.-A. SCHNEGG[1], S.L.FONTES[2]

[1] *Institut de Géologie, Université de Neuchâtel, CH-2007 Neuchâtel, Switzerland*
[2] *CNPq-Observatório Nacional, CEP 20291 Rio de Janeiro, Brazil*

(October 27, 1995)

In order to know more about the structural characteristics underneath impact craters a series of magnetotelluric (MT) soundings were carried out in the Serra da Cangalha in the Northeast of Brazil. The investigated crater has a diameter of 13 km and its prominent feature is a central ring of mountains with a diameter of 3 to 4 km. The MT data is generally of isotropic nature, indicating a one-dimensional conductivity distribution of the subsurface. Nevertheless, anisotropic MT responses in the period range between 0.01 and 0.1 s are observed at a few sites, all located in the vicinity of the centre. They reflect a fractured zone, which reaches a depth of a few hundred metres and has an horizontal extension smaller than the total diameter of the structure. In spite of the crater-like appearance, the outcropping structure is belived to represent the root of a deeply eroded complex crater. The identification in the data of only shallow impact favours this point of view. Besides, the recognition at all MT sites of a good conducting layer at a depth around 1100 m provides an accurate maximum depth for the observed disturbances related to the impact event.

1. Introduction

The Serra da Cangalha impact crater is located in a remote area in the Northeast of Brazil at the border of the intracratonic Parnaíba Basin (Fig. 1). The sediments of the Parnaíba Basin are mainly of Palaeozoic age and reach a thickness of about 2700 m. They are predominantly constituted of clastics of continental origin, namely sandstones, siltstones and shales. Mesozoic and Cenozoic deposits are poorly represented in the basin, their thickness not exceeding 500 m (Schobbenhaus et al., 1984). The relatively thin sedimentary cover is in contrast to the large horizontal dimensions of the basin, which exhibits NE-SW and NW-SE extensions of around 1000 km and 800 km, respectively, thus indicating a very slow subsidence during the Palaeozoic. In the region of the investigation the crystalline basement is found at a depth of about 1400 m.

Worth mentioning is a nearby additional ring structure, lying only 40 km to the North of the Serra da Cangalha crater. The structure is called the Riachão Ring and has a diameter of 4 km. The structure is not emphasised on topographic maps, but clearly illustrated in aerial and satellite images. Riachão Ring is like the Serra da Cangalha classified as a probable meteoritic impact structure (Santos and McHone, 1979).

The Serra da Cangalha structure is a remarkably impressive feature in the soutwestern part of the Parnaíba Basin (Fig. 2). The given name for the structure comes from a breach in the northern segment of the central mountain ring, which gives it the form of a mule pack-saddle (cangalha: portuguese for pack-saddle). The crater has a total diameter of 13 km and the prominent aspect is the central ring of mountains with a diameter of 3-4 km which reaches an altitude of 650 m. This is 200 m above the surrounding annular trough and also higher than the level of flat-lying sediments beyond the limits of the structure. Due to the steep dip-angles ($> 60°$) of the rock bedding inside the Serra da Cangalha there are Permian to Upper Devonian sediments cropping out within the 6-7 km between the outer border and the centre of the structure (Fig. 3).

These sediments correspond to 650 m of the sequence found in a borehole located 70 km south of the area of investigation (Fig. 13). In a later section we shall discuss some stratigraphic aspects of the sedimentary column in the region of the Serra da Cangalha and establish a correlation between the lithologies and the electric resistivity log of a borehole.

The rocks bordering the outskirt of the Serra da Cangalha belong to the Permian Pedra de Fogo Formation, which consist almost entirely of fine-grained sandstones, and siltstones (Bruni et al., 1974). The annular trough defines the outer part of the structure (Fig. 3) and mainly consists of undulating beds of thick sand and soil, and some outcrops of Upper Carbon Piauí Formation, which appear in the field as two distinct forms: small hills and mounds of thin and nearly vertical sheets of chert breccias and solitary sheets of sandstones, both linear and concentric with the circular patterns of the main structure (Santos and McHone, 1979).

Near the central part there is a ring, 3-4 km in diameter, of very steeply dipping sandstones of the Poti Formation (Lower Carbon). On the inside wall of this ring mountain, and at a breach in the northern wall (Fig. 3) where a small river cuts the structure, a quartzite conglomerate crops out which corresponds to the base of the Poti Formation (Santos and McHone, 1979).

The ring of mountains surrounds a central plain which is in the form of a depressed bowl. The plain is believed to be formed of Upper Devonian Longá shales (Fig. 3). Veins of a soft and moist breccia, with clastics of 2-3 cm angular blocks of green micaceous shales, belonging most probably to the Upper Devonian Longá Formation, are found in the small river beds that drain to the North (Santos and McHone, 1979). In 1971 the Brazilian government owned Company for Research on Mineral Resources (CPRM) realised three drill holes in the centre of the Serra da Cangalha, each 200 m deep, to test the possibility that the structure might be a kimberlitic intrusion. No evidences for any kind of igneous intrusion was found. The drilling encountered only highly deformed and steeply dipping Longá shales (Dietz and French, 1973). The central part of the structure has a crater-like appearance resulting from the preferential erosion of the Longá shales by streams which flow through the breach in the Poti conglomerate and sandstone wall (Dietz and French, 1973).

Strong evidence in favour of a meteoritic origin of the Serra da Cangalha structure was obtained through the discovery of shatter cones in the quartzite boulders of the Poti Formation by Santos and McHone, 1979. Some of these quartzite boulders show an unusual and intense micro-fracturing of the quartz grains. Electronic microscope pictures exhibit spheres of melted material in these micro fractures, which were also found in association with shatter cones from other known impact structures. Nevertheless, the sites which produced shatter cones failed to reveal further evidences of an impact, such as high pressure polymorphism of quartz and shock lamellae in the quartz grains. The highly circular shape and the presence of a central uplift in the Serra da Cangalha are considered as indirect evidences of the meteoritic origin. The intensively disturbed sediments found in the central area, the near vertical beds of the inner mountain ring (see above), and the ratio of central uplift diameter and total diameter are consistent with the structural features found in impact sites (Dietz and French 1973). An endogenic origin - igneous intrusion or salt diapir - is almost out of the question, because igneous rocks are entirely absent in the region of the Serra da Cangalha and the sediments underlying the structure do not contain significant carbonate or salt units.

Magnetotellurics (MT) is a geophysical technique which provides information about the electrical conductivity distribution of the Earth's underground (e.g. FISCHER, 1982; VOZOFF, 1972). The method is based on the relationship between transient electric and magnetic fields, which are measured at the Earth's surface. The main source of the fields are natural fluctuations of the Earth's magnetic field, which occur over a wide spectrum of frequencies. The magnetic field variations diffuse into the Earth and induce electric currents, the so-called telluric currents, which in turn are the origin for secondary magnetic fields. The first task when carrying out a MT sounding is to record the time-varying geoelectromagnetic fields. The recordings are then

processed into frequency-dependent responses, which are then used for the interpretation of the Earth's electrical conductivity σ. In MT we will mostly speak in terms of the resistivity $\rho = 1/\sigma$. The depth of penetration of the method is controlled by the skin-effect, i.e., the recorded variations of the geoelectromagnetic fields give information concerning increasing depths as the period of the signal becomes larger.

The amplitude and phase relationship at a particular frequency, between the horizontal electric $\mathbf{E}(\omega)$ and magnetic $\mathbf{H}(\omega)$ fields are indicative of the conductivity distribution of the subsurface. In the general case of a 3-D structure both horizontal fields are linearly related to each other:

$$\mathbf{E}(\omega) = \underline{\mathbf{Z}}(\omega)\mathbf{H}(\omega), \tag{1}$$

with

$$\underline{\mathbf{Z}} = \begin{pmatrix} Z_{xx}(\omega) & Z_{xy}(\omega) \\ Z_{yx}(\omega) & Z_{yy}(\omega) \end{pmatrix}, \tag{2}$$

where ω is the angular frequency $\omega = 2\pi/T$ and T being the period in seconds.

MT results are commonly presented in terms of apparent resistivity ρ_a and phase ϕ, which are derived quantities from the ratio between the electric and magnetic field intensities, known as the surface impedance $\underline{\mathbf{Z}}$ of the medium. The complex elements of the impedance tensor (Eq. 2) are converted to apparent resistivities ρ_a and phases ϕ,

$$\rho_{a,ij}(\omega) = 1/\omega\mu_0 \, |Z_{ij}(\omega)|^2, \tag{3}$$

$$\phi_{a,ij}(\omega) = \arg(Z_{ij}) = \arctan[\Im Z_{ij}/\Re Z_{ij}], \tag{4}$$

where $\mu_0 = 4\pi 10^{-7} H/m$ is the free space permeability and $i, j = x, y$. In field practice Z_{ij} is computed in terms of E_i expressed in mV/km and $B_j = \mu_0 H_j$ with B_j expressed in nT. This yields Z_{ij} in ohms and the following simple expression is then used to derive an apparent resistivity at the particular sounding site:

$$\rho_{a,ij}(\omega) = 0.2T|Z_{ij}(\omega)|^2. \tag{5}$$

The SI unit of the apparent resistivity is Ωm. In MT practice it is from this apparent resistivity as a function of period, and from the corresponding phase given by Eq. 4, that one attempts to construct a model of the structure under study, rather than from the surface impedance Z_{ij}. With its corresponding phase the MT apparent resistivity thus represents the conductivity distribution in the Earth at a given frequency.

For the simplest case of a uniform half-space the impedance tensor reduces to a scalar of fix argument and the apparent resistivity is then identical with the true resistivity of the half-space. If the time dependence is expressed as $\exp(+i\omega t)$ the phase obtains a constant value of 45°. For 1-D structures in general the tensor remains scalar, but now apparent resistivity and phase both depend on the period. In this case a phase value $\phi_{xy} > 45°$ is indicative of a lower layer of high conductivity, whereas $\phi_{xy} < 45°$ suggests a poorer conductor at depth. A truly tensorial response for the impedance is obtained with 2-D and 3-D structures only.

The Serra da Cangalha structure is one of six impact craters known in Brazil (Crostá, 1987). MT surveys have been already carried out in two of the six Brazilian structures. In the Araguainha Dome (diameter 40 km) MT studies were able to determine the depth to the crystalline basement and to give an estimate of the amount of uplift in the central region of the structure (Masero,

Schnegg and Fontes, 1994). High-frequency MT data in the Colônia crater (3.6 km) revealed a bowl shaped depression filled with 440 m of Quaternary sediments (Masero and Fontes, 1992). The objective of the present work is, based on MT data, the determination of the deep electrical structures associated with the Serra da Cangalha impact event.

2. The magnetotelluric data

MT soundings were performed at a total of 25 different sites. The locations of the sites were mainly determined by the roads inside the structure. They were placed along three profiles crossing the structure radially, and are oriented in the NW-SE, NNE-SSW and ENE-WSW directions. The locations are shown on the schematic geologic map of the Serra da Cangalha (Fig. 3). Measurement of the electric and magnetic field variations were performed in the direction of magnetic North and in the corresponding E-W direction. Magnetic North during fieldwork was about 20° West of geographic North in the region of the Serra da Cangalha.

The presence of near-surface and local structural inhomogeneities, which are often not the primary targets of investigation, can be the source of severe distortions of the electric fields, causing a phase mixing and also a frequency-independent shift of the apparent resistivities, better known as static-shift effect. The analysis of electric distortion effects is performed by decomposing the impedance tensor $\underline{Z}$. Theoretical aspects and the application of decomposition methods are reviewed by Groom and Bahr (1992). All methods generally assume a model, where small-scale, near-surface structures are treated as scatters of galvanic currents overlying a one-dimensional (1-D) or two-dimensional (2-D) regional Earth.

For most of the sites in the Serra da Cangalha a tensor decomposition following Groom and Bailey (1989) indicates that the data are not severely affected by distortion effects. Nevertheless, two distortion parameters remain unknown. These are the frequency-independent amplifications of the electric fields in the direction of the principal co-ordinates, which are referred to as static-shift factors. The term "static" refers to the fact that it is a frequency-independent effect. It takes the form of a multiplicative constant applied to the apparent resistivity, i.e., a vertical shifting of the log-apparent resistivity versus frequency curves relative to the regional values, without any effect on the phases. This factor cannot be determined from the MT data alone. A method of static-shift removal will be treated in a next section. The static-shift problem has been treated in different numerical modelling studies (e.g. Park, 1985; Wannamaker et al., 1984) and in a series of regional MT investigations (e.g. Beamish and Travassos, 1992; Jones, 1988; Berdichevsky, Vanyan and Dmitriev, 1989; Sternberg, Washburne and Pellerin, 1988; Masero et al., 1994).

Most of the MT responses observed in the Serra da Cangalha show no significant galvanic distortion effects. They belong in general to stations located beyond the limits of the outer ring of crater. A representative example of distortion-free data is station 25. Fig. 4 presents the MT data and the parameters of the tensor decomposition according to Groom and Bailey (1989). Twist and shear angles, representing a measure of the angular deviations of the electric fields, are of the order of 0° for the whole range of periods, clearly indicating the lack of the so-called galvanic distortion.

Two differently defined skew parameters, the conventional one after Swift (1967) and the regional one after Bahr (1991), are used as structural dimension indicator. The regional skew is based on the phases of the impedance tensor and is sensitive to local distortion effects on the measured impedances. In the co-ordinate system of a regional 2-D structure and in the presence of local distortion the impedance element Z_{xx} has the same phase as Z_{yx}, and Z_{yy} the same phase as Z_{xy}. Therefore, the phases in each column of the impedance tensor are identical (see Eq. 2). Any departure from these conditions yields a regional skew larger than zero (Bahr, 1991). The conventional skew after Swift (1967) is defined as the ratio of the magnitudes of the rotationally invariant sum and difference of the diagonal elements Z_{xx} and Z_{yy}, and the off-

diagonal elements Z_{xy} and Z_{yx}, respectively. It would, in the presence of a local heterogeneity, only give the skew of the distortion tensor. Both skews are for most of the period range of the order of zero and rarely exceed 0.2 (Fig. 4), which can be considered a strong indication for the absence of three-dimensional (3-D) distortion.

In addition the 1-D character of the data is well illustrated in Fig. 5, where a stepwise rotation of the impedances shows practically identical apparent resistivities and phases for both polarizations, XY and YX, thus indicating no anisotropic MT response. It is also evident that there is no static-shift factor influencing the data. The conventional strike corresponds to an azimuth of approximately 30° (Fig. 4), reflecting the direction which gives the minimum of the diagonal elements (exactly speaking, the minimum of the sum of the squared absolute values of the impedance elements Z_{xx} and Z_{yy}) when rotating the impedance tensor to 30° (see second frame of the bottom row in Fig. 5). The regional strike, resulting from the Groom and Bailey (1989) tensor decomposition does not succeed in suggesting a systematic direction (Fig. 4). This behaviour rather confirms the absence of a strike direction, in accordance with the assumed 1-D nature of the sounding. The few values between 10 and 100 s of the phase-sensitive regional skew that are larger than 0.2 most probably reflect the lower quality of the observed data for these periods.

Anisotropic MT responses were observed only at a few sites located inside the Serra da Cangalha structure, and their data sets are usually moderately affected by galvanic distortion. In fact, several stations inside the structure continue to show an evident 1-D character, but are often affected by static-shift. As emphasised by Chakridi, Chouteau and Mareschal (1992), the removal of galvanic distortion effects on a 1-D structure does not yield more information than the simpler representation by any kind of invariant of the impedance tensor. The phases extracted from the tensor decomposition correspond to the true regional phases, while the apparent resistivities are shifted from the regional values. This is a consequence of the fact that the static-shift factor always remains unknown after a tensor decomposition. Station 1 is a good example a of 1-D sounding affected by galvanic distortion effects (Figs 6 and 7). It is located just on the border of the structure. The distortion parameters twist and shear obtained for the data of site 1 are of the order of +15° and −15°, respectively, indicating a rather moderate distortion, and exhibiting a larger variability with increasing periods (Fig. 6). Both skews in general do not exceed 0.2 for periods smaller than 10 s, but increase for periods between 10 and 100 s, and in this latter range also have less well defined shear, twist and strike parameters. This is due to somewhat more scattered impedances, reflecting the lack of good data in this period range (Fig. 7). Nevertheless, the general 1-D nature of the data is well illustrated by the stepwise rotation of the impedances. The calculated strike directions yield, for both definitions of regional and Swift strike, a fairly period-independent azimuth of the order of 60° (Fig. 6). It is evident from Fig. 7 (see 60° frame of the top half) that this azimuth corresponds to a rotation angle that minimises the sum of the squared absolutes of the diagonal elements of the observed impedance tensor. In the case of 1-D impedances this is equivalent to the strikes of the distortion tensor. The 60° direction of this calculated strike agrees very well with the azimuth of site 1 with regard to the centre of the structure (radial azimuth), which is N37 and in the region of the Serra da Cangalha equivalent to 57° in geomagnetic co-ordinates. This radial direction is believed to be related to the preferential strike direction of the near-surface and local structures, which are the source of possible static and galvanic distortion effects. The correspondence between the radial azimuth of site 1 and the calculated strike direction correctly reflects at least the near-surface circular symmetry of the Serra da Cangalha.

As mentioned above, there are a few stations, all located inside the Serra da Cangalha structure, that present data with evident anisotropic MT responses for periods between 0.01 and 0.1 s. Site 7 is an example of such a sounding. Fig. 8 shows the anisotropic MT response of this site, which is characterised by different apparent resistivities and phases for both polarizations.

The representation of the impedance in terms of four apparent resistivities and phases helps to identify the presence of local and galvanic distortion effects superposed on a regional structure. The galvanic distortion is characterised, in this example, by fairly period-independent twist and shear parameters, which are of the order of 25° and 5°, respectively.

The decomposition of the impedance tensor yields a regional strike of 30°, while the regional skew is 0.2 (Fig. 8). The phases of the impedance elements Z_{xx} and Z_{yx}, and Z_{yy} and Z_{xy}, respectively, are identical for impedances rotated to 30°. Therefore, the principal axes of the regional structure are defined by the regional strike, which is given by an azimuth of 30°. After the removal of the galvanic distortion effects the phase corresponds to the true regional phase, while the apparent resistivity remains affected by a static-shift that the tensor decomposition cannot resolve. The direction of the regional strike is approximately the same as the radial azimuth of site 7, which is N90 or equivalent to 110° in geomagnetic co-ordinates. In analogy with the results obtained for site 1, the calculated strike direction reflects the circular symmetry of the Serra da Cangalha. The strike and skew according to Swift (1967) diverge from the values above. The skew is of the order of 0.4 and the strike is around 60°. They give the skew of the distortion tensor and the rotation angle which minimises the sum of the squared absolutes of the diagonal elements of the observed impedances.

An outstanding feature present in all data sets is a well defined apparent resistivity minimum associated with a sharp decrease of the phases at periods around 0.1 to 1 s. This is an evidence throughout the whole area investigated of a good conducting layer on top of a significantly more resistive basal formation. The major characteristics of the data can be summarised as follow: (a) 1-D nature of all soundings realised beyond the limits of the outer ring, and of some soundings inside the structure, (b) soundings with evident anisotropic MT responses are restricted to a few sites located inside the structure, in general in the vicinity of the inner ring, (c) anisotropic MT responses are confined to short periods, i.e. periods between 0.01 and 0.1 s, and (d) the correspondence between the radial azimuths of the MT sites and the calculated strike directions reflects the circular symmetry of the structure.

3. The vertical magnetic transfer function - induction arrows

Lateral conductivity gradients are the cause of a vertical magnetic field H_z. Recordings of H_z are therefore sensitive to lateral changes of the electric conductivity. They are especially well-suited to identify zones of enhanced current and to map 2-D and 3-D anomalies. The ratios of the vertical to both horizontal magnetic field variations are caused essentially by induced currents in the Earth. They define the vertical magnetic transfer function, which is described by a pair of complex coefficients in the frequency domain. The vertical field component H_z and the two horizontal components H_x (North) and H_y (East) are coupled through a linear relationship of the form

$$H_z(\omega) = A(\omega)H_x(\omega) + B(\omega)H_y(\omega). \tag{6}$$

The coefficients A and B are complex and referred to as *tipper*, since they describe a vertical tipping of the horizontal magnetic field. For a purely 1-D Earth no tipping occurs and thus $A = B = 0$.

However, the transfer function responses are more frequently displayed in the form of vectors, the induction arrows, which were first introduced by Parkinson (1962) and Wiese (1962), and later were extended to the complex domain (Everett and Hyndman, 1967; Schmucker, 1970). The complex amplitude of the induction arrows is proportional to the local effects of induction on H_z at a particular field location and the orientation is perpendicular to the electric current flow. As the coefficients are in general complex, there are directions associated with both the real

and the imaginary parts. The induction arrows can be expressed as a pair of real (in-phase) and imaginary (quadrature) vectors or arrows (Chen and Fung, 1985).

$$P = \Re(A)\mathbf{x} + \Re(B)\mathbf{y}, \tag{7}$$

$$Q = \Im(A)\mathbf{x} + \Im(B)\mathbf{y}, \tag{8}$$

where $\mathbf{x}$ and $\mathbf{y}$ are the unit vectors in the North and East direction. For a 2-D structure the in-phase and quadrature arrows are parallel or anti-parallel, but for 3-D situations they generally diverge.

Depending on which definition is used for the induction arrows, the real part points either towards or away from regions of current concentration (Jones, 1986). However, it is not possible to establish a consistent sign convention for the imaginary induction vector since this arrow reverses direction at a certain period of the inducing field, depending on the nature of the model (Agarwal and Dosso, 1990; Chen and Fung, 1985). The real induction arrows though small in amplitude are found to reverse direction at periods for which the depth of burial of a conductive body in a less conductive host is more than one skin-depth (Jones, 1986). In this work we opted for the convention where the real parts of induction arrows point towards zones of low electrical conductivity.

The vertical magnetic field observations in the Serra da Cangalha usually yield induction arrows of very low amplitude, therefore reflecting the general 1-D nature of that structure. Examples of real and imaginary parts of the induction arrows are shown for two selected sites in Fig 9. As seen in this figure, the small vertical magnetic fields are probably the result of relevant induction effects in the subsurface. However, as emphasised by Zhang et al. (1993), vertical fields could also be the result of galvanic effects, when local inhomogeneities are thinner than the inductive scale length. This effect is better known under current channelling (Jones, 1983) by local electrical heterogeneities. It is not surprising that significant vertical fields occur at the same sounding sites in the Serra da Cangalha where anisotropic MT responses were observed. Fig. 3 gives the location of the anisotropic MT responses which were already mentioned in a previous section.

Fig. 9 shows induction arrows at sites where an anisotropic MT response was detected at short periods. Direction and magnitude of the real parts of the induction arrows are generally constant for a given data set and periods smaller than 1 s. Unfortunately, for most of the soundings the data for periods longer than 10 s is of poor quality. The magnitude of the imaginary parts of the corresponding arrows are distinctly smaller, though generally oriented in the same direction. At site 2 the imaginary parts of the induction are evidently antiparallel with respect to their corresponding real parts, i.e., both real and imaginary arrows point in opposite directions. Parallel or antiparallel orientations of the real and imaginary induction arrows occur near 2-D structures, implying that the ratio between the transfer function coefficients are real quantities.

At site 6 there is in addition a change from parallel to antiparallel direction of the imaginary induction arrow. The sign reversal in the imaginary part takes place at 0.1 s. For a conductive plate embedded in a resistive host the characteristic period, defined as the period at which the imaginary arrow changes sign and the magnitude of the real arrow is maximum, was found to depend on the conductivities, on the layer depths, and on the horizontal dimension of the conductive plate (Agarwal and Dosso, 1990). The same authors emphasise that the sign reversal of the induction arrow is helpful to identify the location of the interface of a conductivity anomaly. In the case of site 6 the amplitude of the real part is fairly constant at periods ranging from 0.01 to 10 s (Fig. 3.3.2), and therefore no proper association could be established between the imaginary minimum and a real maximum. We note that for site 6 the imaginary arrows are clearly smaller than the real arrows. The apparent resistivity at site 6 for a period of 0.1 s is of the order of 10

Ωm and the corresponding skin-depth is of the order of 500 m, which implies that the interface of the conductivity anomaly lies no deeper than a few hundred meters.

4. One-dimensional modelling

It was shown above that it seems well justified to use a 1-D scheme to analyse the data from the Serra da Cangalha. The determination of the layered models was achieved with the 1-D modelling program of Fischer and Le Quang (1981). The main invariant of the MT response $[\frac{1}{2}(Z_{xy} - Z_{yx})]$ was used to construct the layered 1-D models.

An example of a representative model is illustrated in Fig. 10, together with the model responses for apparent resistivity and phase, and the main invariant of the data. The final layered models of all 1-D inversions are summarised in the Tabs 1-3, together with their standard deviations ε, defined according to Fischer et al. 1981. The tables also contain the static-shift corrected layered models (site numbers with heavy type) of sites where static distortion effects are present (see below). The model responses fit the observed data very well, as shown by the in general small ε values, which are an average of the separate standard deviations for the apparent resistivity and the phase. For instance, ε is equal 0.031 for the model of site 14 (Fig. 10). This means that the calculated apparent resistivity is uncertain by a factor of 1.064, i.e. the calculated apparent resistivity is either 6.4 per cent too large or 6.0 per cent too small. The deviation of the calculated phases are 1.8°.

The ensemble of the resulting 1-D models show some common features (Tabs 1-3). The number of layers varies between 4 and 5, including the half-space. The models sometimes present a relatively thin and often very resistive uppermost layer. In every model the half-space is resistive, of the order of some thousands of Ωm. Nonetheless, the prominent feature seen in almost all of the 1-D results is a good conducting layer lying on top of the significantly more resistive half-space. In most cases the bottom of this conducting layer lies at a depth of approximately 1100 m, and its resistivity is around 10 to 20 Ωm. The depth to the top of this layer shows a much larger variation than the depth to the base, with values scattered between the extreme of 100 and 1000 m. However, in most of the models this depth is restricted to values between 400 and 600 m. This large variation among the calculated models is to some extent due to the different resolutions of the model parameters (see below).

The resolution of the model parameters was determined by way of a parameter trade-off analysis according to Fischer and Le Quang (1982), where the family of models is determined for which the standard deviation ε remains within 10 percent of the minimum value ε_0. This is achieved by varying each of the model parameters (resistivity ρ and layer thickness d) to larger or smaller values. Under the constraint of the imposed variation all the other parameters are adjusted to minimise ε. The set of limiting parameters is obtained when $\varepsilon = 1.10\varepsilon_0$. They can be expressed in terms of those of the best-fitting model. Fig. 11 show some trade-off diagrams which give the resolution limits of every model parameter. The relatively high resolution of the good conducting layer above the half-space is evident from these diagrams, in particular the depth to the bottom of this layer, which has an upper and lower resolution given by factors of 1.3 and 1.4, respectively. This corresponds to a variation range of the order of 30 per cent around the best-fitting value. The two other model parameters - the resistivity and the depth to the top of this layer - are less well constrained. The upper and lower resolution of the resistivity are given by factors of 2.25 and 2.5, respectively, whereas the depth can be multiplied or divided by factors of 1.9 and 2.0, respectively. The other layers are clearly less well resolved.

5. Removal of static-shift effects

In order to correct for static distortion effects a constant multiplicative factor, called *static-shift factor*, must be determined. This static-shift factor can be derived by imposing a constraint on the layered models, based on additional information, independent of MT data. A very similar procedure was very successful in eliminating the static distortion effects in the Araguainha impact structure in central Brazil (Masero et al., 1994).

Before proposing a constraint on the layered models, it is useful to have a brief look at some aspects of the stratigraphic column of the Parnaíba Basin. It should be noted that, unless specified otherwise, this paragraph is based entirely on a study of the Palaeozoic evolution of the Parnaíba Basin by Cunha (1986). Fig. 12 represents the detailed lithostratigraphic column of the Palaeozoic sediments of this basin. The column is divided into three groups, the Silurian Serra Grande, the Devonian Canindé group, and a third group of mainly Permo-Carboniferous formations. These Palaeozoic sediments are underlain by metamorphic rocks of the Precambrian crystalline basement. It was possible to derive the total and partial thicknesses of the Palaeozoic sediments in the region of the Serra da Cangalha from a series of isopachyte maps (map of lines joining points of equal stratigraphic thickness of a formation or group of strata) in Cunha's work.

The top of the basement in the region of the Serra da Cangalha is at an estimated depth of 1400 m. Above the basement is the Silurian Serra Grande group, a rather inhomogeneous sequence of three distinct sedimentary formations, which are made of sandstones and conglomerate (Ipu), shales and siltstones (Tianguá), and coarse grained sandstones with abundant intercalations of quartz pebbles (Jaicós). In the region of the Serra da Cangalha the thickness of the Casa Grande group was estimated to be of the order of 300 m.

Lying discordantly on top of the Jaicós formation are the fine sandstones of the Lower Devonian Itaim formation, which is the base of the Canindé group. This group contains significant amounts of shales. The total thickness of the Canindé group in the Serra da Cangalha is approximately of the order of 700 m. The group comprises the mentioned Itaim formation, the Middle Devonian Pimenteiras formation, a sequence of 350 m of shales and siltstones, the Upper Devonian sandstones from the Cabeças formation, and the Upper Devonian - Lower Carboniferous shales and siltstones of the Longá formation.

On top of the Canindé group follow a series of Permo-Carboniferous formations: the Lower Carbon Poti, the Upper Carbon Piauí, the Lower Permian Pedra de Fogo and the Permo-Triassic Motuca and Sambaíba. The Motuca and Sambaíba formations, are absent. They are only found 150 km north of the Serra da Cangalha, in the direction of the centre of the Parnaíba Basin. The Poti formation and the Piauí formation are predominantly made of fine sandstones with occasional zones of conglomerates and intercalated sheets of chert. There is a sedimentary discordance between both formations. In the region of the Serra da Cangalha the estimated thickness of each formation is of the order of 200 m. The Permian Pedra de Fogo formation is mainly found just beyond the limits of the Serra da Cangalha structure (Fig. 3). It is basically made of sandstones and siltstones with intercalated sheets of chert, and its thickness in the area of investigation is estimated to be only a few tens of metres.

From the calculated 1-D models it can be deduced that a good conductor lies approximately between 600 and 1100 m depth (Fig. 10 and Tabs 1-3). As shown above, the depth to the bottom of this layer is especially very well resolved. This layer can be correlated with the above-mentioned Canindé group. The thick sequences of shales and the depth to the top and to the bottom of the Canindé group, estimated in the region of the Serra da Cangalha to lie between 700 and 1100 m, are strong evidence for this correlation. The Canindé group is believed to be responsible for the good conductor observed in the MT data of the Serra da Cangalha.

Fig. 13 shows the electric resistivity log, together with the stratigraphic column of a borehole located 70 km south of the Serra da Cangalha. The high bulk conductivity of the Longá, Cabeças,

Pimenteiras and Itaim sediments is well illustrated in Fig. 13, and gives strong support for the interpretation attributing the good conductivity to the large amount of shale found in the Canindé group. Of particular interest is the evident and sharp increase of electrical resistivity between the Lower Devonian Itaim formation and the Upper Silurian Jaicós formation, which agrees very well with the high resolution of the transition between the good conductor and the more resistive half-space in the calculated 1-D models. The transition between the top of the Canindé group and the Permo-Carboniferous formations is characterised in the electric log by an oscillation of low and high resistivity values, due probably to the change from the Upper Devonian Longá shales to the Lower Carbon sandstones and conglomerates.

It should be noted that the depths and thicknesses of the Palaeozoic formations given in the borehole profile of Fig. 13 are different from the thicknesses and depths estimated above in the region of the Serra da Cangalha. For instance, the base of the Canindé group in the borehole is given at 1312 m and in the Serra da Cangalha at 1100 m. This difference is due to the location of this borehole which, according to the isopachyte and borehole location maps (Cunha 1986), lies in a region of the Parnaíba Basin where the total thickness of the sediments is larger than in the Serra da Cangalha. In the borehole the basement was reached at a depth of 1685 m, whereas the depth to the basement in the Serra da Cangalha is estimated to be at 1400 m.

The agreement between the thicknesses of the sediments derived in region of the Serra da Cangalha and the calculated 1-D results from data not affected by static-shift, and also the correlation between the 1-D models and the electric resistivity log of a series of boreholes, all located 70 to 100 km away from the centre of the structure, made it possible to relate the good conductor observed in all MT soundings to the Devonian sediments of the Canindé group, which comprise a few hundred metres of good conducting shales. The identification and the high resolution of the base of this good conductor will be used in the following paragraphs to constrain the layered models in order to remove static-shift effects from the MT data.

In the layered models in Tabs 1-3 it was not possible to differentiate between the Devonian Longá, Cabeças, Pimenteiras and Itaim formations (Fig. 13). However, the models resolve the lower base of the good conducting layer quite well. This interface lies on top of the considerably more resistive Silurian sediments (sandstones and conglomerates) and the metamorphic rocks of the Precambrian basement. It is believed that the major contribution to the bulk conductivity of this good conducting layer comes from the Middle Devonian Pimenteiras formation, a 400 m sequence of shales, whereas the Upper and Lower Devonian units, respectively on top and below, consist both of an alternating sequence of shales and sandstones. Geological information on the stratigraphic column of the Parnaíba Basin places the base of the Devonian formations in the region of the Serra da Cangalha at a depth of the order of 1100 m, which corresponds rather well to the depth of the good conductor in the calculated layered 1-D models.

The 1-D inversion of data with static distortion effects was thus accomplished by constraining the base of the good conductor to a depth of 1100 m in the resulting layered models (Tabs 1-3). The justification for this constraint lies in the good correlation with the results of the models which are free of static distortion effects (see above) and the geological information in the stratigraphic column. Additionally, the high resolution of the depth to this conducting layer gives extra support to this correction procedure.

As mentioned in a previous section, the observed data for some of the sites located inside the limits of the outer ring of the Serra da Cangalha exhibit an anisotropic MT response, i.e., a difference between the apparent resistivities and phases of both polarizations. Site 7 is a good example of this behaviour (see also Fig. 8). According to Groom and Bahr (1992), after the determination of the telluric distortion parameters a single parameter remains unknown, the static-shift factor. To remove this factor the base of the good conductor was constrained to a depth of 1100m in the resulting layered models. This procedure seems quite justified, because for periods $T > 0.2s$ the phase values of both polarizations are identical and the apparent resistivity

curves are parallel, indicating a 1-D response at the longer periods. The corrected apparent resistivities are shown in Fig. 14, together with the 1-D models for both polarizations. The two models show an anisotropic picture for the first layer. However, the results of this first layer have little meaning. For both polarizations the good conducting layer lies between 500 and 1100 m, which agrees quite well with the results obtained so far. Because of the constraint imposed on the model, the variation ranges were only determined for the depth to the top and for the resistivity of this layer. The upper and lower limits for the resistivity are set by multiplying and dividing the best-fitting value by factors of 1.16 and 2.5, respectively. The depth is far less well constrained. The best-fitting value for the depth is uncertain by factors of 2.5 for the upper and 0.4 for the lower limit.

6. Summary of the one-dimensional results and conclusions

The MT measurements at the Serra da Cangalha are located roughly along three profiles crossing the structure radially (Fig. 3). These profiles are oriented in the NW-SE, NNE-SSW and ENE-WSW direction. Most of the MT data are characterised by a perfect isotropy of both polarizations, indicating a 1-D distribution of the subsurface conductivity. These soundings are generally located close to or beyond the border of the structure. Some MT observations inside the circular structure show an anisotropic MT response for periods shorter than 0.1 s. However, a common feature of all data sets is a well defined resistivity minimum for periods between 0.1 and 1 s. This suggests, for all sites free of static-shift, the presence of a good conducting layer with a base somewhere between depths of 1000 and 1200 m.

A schematic view summarising the major MT results is given in an assemblage of the 1-D models along each of the three profiles (Fig. 15). Especially outlined is the good conducting layer present in all of the 1-D inversion results. It is believed that this layer corresponds to a series of 600 to 700 m of Devonian sediments, which consist mainly of shales. The identification in all the undistorted data sets of this good conductor down to the uniform depth of about 1100 m, i. e. through the entire Devonian sedimentary sequence of the Parnaíba Basin, provided a reliable constraint with which to remove the effects of static-shift at the few sites where it occurred by constraining the base of the good conductor to that depth. This gives the impression that the base of the Devonian sediments lies almost at a constant depth in Fig. 15. However, it was shown in the 1-D modelling results that this base is not only well established for sites free of static distortion effects, but also well resolved at a relatively constant depth of the order of 1100 m.

Also outlined in Fig. 15 are the localities where the data show anisotropic MT responses for periods smaller than 0.1 s. These sites are all located inside the circular structure and are relatively close to the inner ring of the Serra da Cangalha. The induction arrows at these MT sites generally point toward the centre of the structure at a period of 0.1 s (Fig. 16), confirming the expected radial and circular symmetry of the subsurface structures. Both the MT responses and the magnetic transfer functions reveal a possible zone of structural disturbance, which may have been generated by impact-induced shock waves. However, the depth of penetration for these short periods ($T < 0.1s$) does not exceed 500 m. This zone is therefore restricted to a depth of only a few hundred metres as pointed out in Fig. 15 and its horizontal extension is smaller than the total diameter of the Serra da Cangalha structure. The deformation is confined to relatively shallow units, occurring all above 1100 m, which is the undisturbed base of the Devonian sedimentary formation. An accurate maximum depth for the actual observable effects of the Serra da Cangalha impact event is therefore at a depth of about 1100 m.

The interior bowl-shaped basin of the Serra da Cangalha structure can easily be misinterpreted as a recent crater. The crater-like appearance is caused by the preferential erosion of the Devonian Longá shales found in the centre of the structure. The MT measurements showed that

there was no structural evidence found below a depth of 1100 m of a central uplift for the Serra da Cangalha and should, therefore, be considered as a further argument in favour of the meteoritic impact origin, excluding the possibilty of an igneous intrusion or a salt diapir. Additionally, the unperturbed 1-D distribution of the subsurface confirms the opinion that the Serra da Cangalha represents the root of a deeply eroded impact structure.

The authors would like to express their gratitude towards their institutions and to the Swiss National Science Foundation (grant 21 - 30911.91) and the Brazilian Research Council. They are grateful to Prof. G. Fischer for his advice during the course of this investigation and for his various helpful suggestions.

REFERENCES

Agarwal, A. K. and H. W. Dosso, On the behaviour of the induction arrows over a buried conductive plate - a numerical model study, *Phys. Earth. planet. Inter.*, **60**, 265-277, 1990.

Bahr, K., Geological noise in magnetotelluric data: a classification of distortion types, *Phys. Earth. planet. Inter.*, **66**, 24-38, 1991.

Beamish, D. and J. M. Travassos, A study of static shift removal from magnetotelluric data, *J. appl. Geophys.*, **29**, 1-21, 1992.

Berdichevsky, M. N., L. L. Vanyan and V. I. Dimitriev, Methods used in the U.S.S.R. to reduce near-surface inhomogeneitiy effects on deep magnetotelluric sounding, *Phys. Earth planet. Inter.*, bf 53, 194-206, 1989.

Bruni, M. A. L., J. T. Almeida and E. C. Bruni, Carta geológica do Brasil ao milionésimo, Folha Rio São Fransisco (SC.23), Texto Explicativo, DNPM, Brasilia, pp. 85, 1974.

Chakridi, R., M. Chouteau and M. Mareschal, A simple technique for analysing and partly removing galvanic distortion from the magnetotelluric impedance tensor: application to Abitibi and Kapuskasing data (Canada), *Geophys. J. Int.*, **108**, 917-929, 1992.

Chen, P. F. and P. C. W. Fung, Significance of the sign changing of the imaginary arrows in geomagnetic induction investigation, *Geophys. J. R. astr. Soc.*, **80**, 257-263, 1985.

Crósta, A. P., Impact structures in Brazil, in: Research in Terrestrial Impact Structures, ed. J. Pohl, Vieweg and Sohn, Braunschweig, 30-37, 1987.

Cunha, F. M. B., Evolução Paleozóica da Bacia do Parnaíba e seu Arcabouo Tectônico. Tese de Mestrado, Universidade Federal do Rio de Janeiro, Rio de Janeiro, Brasil, pp. 107.

Dietz, R. S. and B. M. French, Two probable astroblemes in Brazil, *Nature*, **244**, 561-562, 1973.

Everett, J. E. and R. D. Hyndman, Geomagnetic variations and electrical conductivity structure in south-western Australia, *Phys. Earth planet. Inter.*, **1**, 24-34, 1967.

Fischer, G., Magnetotelluric observational techniques on land, *Geophys. Surv.*, **4**, 373-393, 1982.

Fischer, G., P.-A. Schnegg, M. Peguiron, and B.V. Le Quang, An analytic one-dimensional magnetotelluric inversion scheme, *Geophys. J. R. astr. Soc.*, **67**, 257-276, 1981.

Fischer, G. and B. V. Le Quang, Topography and minimization of standard deviation in one-dimensional magnetotelluric modelling, *Geophys. J. R. astr. Soc.*, **67**, 279-292, 1981.

Fischer, G. and B. V. Le Quang, Parameter trade-off in one-dimensional magnetotelluric modelling, *J. Geophys.*, **51**, 206-215, 1982.

Groom, R. W. and R. C. Bailey, Decomposition of magnetotelluric impedance tensor in the presence of local three-dimensional galvanic distortion, *J. Geophys. Res.*, **93**, 1913-1925, 1989.

Groom, R. W. and K. Bahr, Corrections for near-surface efects: decomposition of magnetotelluric impedance tensors and scalling corrections for regional resistivities, *Surv. Geophys.*, **13**, 341-380, 1992.

Jones, A. G., The problem of 'current channelling': a critical review, *Geophys. Surv.*, **6**, 79-122, 1983.

Jones, A. G., Parkinson's pointers' potential perfidy!, *Geophys. J. R. astr. Soc.*, **87**, 1215-1224, 1986.

Jones, A. G., Static shift of magnetotelluric data and its removal in a sedimentary basin environment, *Geophysics*, **53**, 967-978, 1988.

Masero, W. and S. L. Fontes, Geoelectrical studies of the Colônia impact structure, Santo Amaro, State of São Paulo - Brazil, *Rev. Bras. Geofís.*, **10**, 25-41, 1992.

Masero, W., P.-A. Schnegg and S. L. Fontes, A magnetotelluric investigation of the Araguainha impact structure in Mato Grosso-Goiás, central Brazil, *Geophys. J. Int.*, **116**, 366-376, 1994.

Park, S. K., Distortion of magnetotelluric sounding curves by three-dimensional structures, *Geophysics*, **50**, 785-797, 1985.

Parkinson, W. D., The influence of continents and oceans on geomagnetic variations, *Geophys. J. astr. Soc.*, **24**, 3-30, 1962.

Projcto Radambrasil, Radar Image 1:250'000, sheet SC.23-V-A, DNPM, 1981.

Santos, U. P. and J.F. McHone, Field report on Serra da Cangalha and Riachão circular features, INPE, Report No. INPE-1548-NTE/153, pp. 13, 1979.

Schmucker, U., Anomalies of geomagnetic variations in the southwestern United States, Bull. 13, Scripps Inst. of Oceanogr., La Jolla, Univ. of California, 1-165, 1970.

Schobbenhaus, F. C., D.A. Campos, G.R. Derze and H.E. Asmus, Geologia do Brasil. Texto explicativo do mapa geológico do Brasil e da área oceânica adjacente incluindo depósitos minerais, escala 1:250000, DNPM, Brasilia, pp. 501, 1984.

Sternberg, B. K., J. C. Washburne, and L. Pellerin, Correction for static shift in magnetotellurics using transient electromagnetic soundings, *Geophysics*, **53**, 1549-1468, 1988.

Swift, C. M., A magnetotelluric investigation of an electrical conductivity anomaly in the southwestern United States, Phd. Thesis, Geophys. Lab. MIT, Cambridge, Massachusetts, 1967.

Vozoff, K., The magnetotelluric method in the exploration of sedimentary basins, *Geophysics*, **37**, 98-141, 1972.

Wannamaker, P. E., G. W. Hohmann and S. H. Ward, Magnetotelluric responses of three-dimensional bodies in layered earths, *Geophysics*, **49**, 1517-1533, 1984.

Wiese, H., Geomagnetische *Tiefentellurik Teil II: Die* Streichrichtung der Untergrungstrukturen des elektrischen Widerstandes, erschlossen aus geomagnetischen Variationen, *PAGEOPH*, **52**, 83-102, 1962.

Zhang, P., L. B. Pedersen, M. Mareschal and M. Chouteau, Channelling contribution to tipper vectors: a magnetic equivalent to electrical distortion, *Geophys. J. Int.*, **113**, 693-700, 1993.

Figure captions:

Table 1. Resistivities and depths of the layered models for sites located along the NNE-SSW striking profile. ρ_4 is the resistivity in Ωm and d_4 the depth in m to the base of this layer, whereas the indices 3, 2 and 1 refer to the layers above. The bottom resistivity value - ρ_5 or ρ_4 - is the half-space resistivity. The distance to the centre of the structure is given underneath the site number. The columns containing two parameters are layered models from data with an anisotropic response for periods smaller than 0.1 s. The resistivities and depths on the left correspond to pol 1, with the electric line parallel to the direction of the calculated regional strike, and the ones on the right (in brackets) to pol 2, with the electric line perpendicular to strike. ϵ is the standard deviation for apparent resistivity and phase. The sites with heavy type numbers refer to best-fit models from static-shift corrected sounding curves.

Table 2. Same as table 1. Resistivities and depths of the layered models for sites located along the NW-SE striking profile. Table 3. Same as table 1. Resistivities and depths of the layered models for sites located along the WSW-ENE striking profile.

Figure 1. Parnaíba Basin, shaded on map of South America. The location of the Serra da Cangalha crater is indicated by the small rectangle (not to scale). The centre of the structure is located at $8°05'S$ and $46°52'W$.

Figure 2. Radar image of the Serra da Cangalha crater. The image displays both the central plain and the mountains forming the inner ring. This part of the structure corresponds to the central uplifted area of a complex impact crater. Also easily identified is the annular trough surrounding the inner structure (Projeto Radambrasil, 1981).

Figure 3. Schematic map of the geologic units cropping out in the Serra da Cangalha, indicating the outer and inner ring of the structure. The limit of the inner ring is marked by the dashed line. The location of the MT stations is given along with the site number. Circled numbers represent sites that show effects of static and galvanic distortion. Soundings showing anisotropic MT responses are indicated with underlined site numbers. The lack of soundings in the southern part is due to the impossibility of reaching these areas.

Figure 4. MT responses (phase, apparent resistivity and skew) and tensor decomposition parameters (twist, shear and strike) for site 25. The apparent resistivities and phases are for the impedances rotated to 0°.

Figure 5. Apparent resitivities (above) and phases (below) of the measured impedances rotated stepwise to 0°, 15°, 30°, 45°, 60° and 75° at site 25. Empty squares and empty downward pointing triangles represent Z_{xy} and Z_{yx}, whereas full squares and full triangles represent Z_{xx} and Z_{yy}, respectively.

Figure 6. MT responses (phase, apparent resistivity and skew) and tensor decomposition parameters (twist, shear and strike) for site 1. The apparent resistivities and phases are for the impedances rotated to 60°.

Figure 7. Apparent resistivities (above) and phases (below) of the measured impedances rotated stepwise to 0°, 15°, 30°, 45°, 60° and 75° at site 1. Empty squares and empty downward pointing triangles represent Z_{xy} and Z_{yx}, whereas full squares and full triangles represent Z_{xx} and Z_{yy}, respectively.

Figure 8. MT responses (phase, apparent resistivity and skew) and tensor decomposition parameters (twist, shear and strike) for site 7. The apparent resistivities and phases are for the impedances rotated to 30°.

Figure 9. Real (below) and imaginary (above) part of the induction arrows for site 2 (left) and site 6 (right). Geographic North is in the direction of the ordinate for both real and imaginary parts.

Figure 10. Best model and data fit (continuous lines) for the main invariant of the observed MT response (left side) for site 14.

Figure 11. Trade-off diagram for the data and model of sites 14, 19 and 25. Vertical lines give the trade-off limits for each model parameter, i.e. the range within which it is possible to achieve $\epsilon = 1.1\epsilon_0$.

Figure 12. Lithostratigraphic column of the Palaeozoic sediments of the Parnaíba Basin. The values correspond to the maximum thicknesses of the sedimentary formations (after Cunha, 1986).

Figure 13. Schematic profile and electric resistivity log of a borehole located 70 km south of the centre of the Serra da Cangalha structure.

Figure 14. Best models and data fits (continuous lines) for the static distortion corrected polarizations 1 (a) and 2 (b) of the observed MT response (left side) for site 7.

Figure 15. Assemblage of 1-D models along three profiles crossing the Serra da Cangalha radially and showing the distribution of the good conducting layer (vertically hatched). The punctuated small rectangles indicate the localities where the data show anisotropic MT responses for periods smaller than 0.1 s. Sites showing static distortion effects are in italics. The triangles indicate the outer rim of the structure.

Figure 16. Map of induction arrows (real and imaginary part) for a period of 0.1 s. The dashed circle represents the inner rim of the Serra da Cangalha structure.

Table 1

site	19	17	16	14	5	
	18.4 km	15.8 km	14.2 km	11.2 km	8.9km	6.7 km
ρ_1	1000000	24	20.4	58	10482	33215
d_1	67	72	195	131	55	87
ρ_2	8	14	26	29	28	42
d_2	105	250	629	396	729	694
ρ_3	23	11832	10	626	8	17
d_3	1269	394	1002	710	1058	1258
ρ_4	2089	12	3263	9	2377	22904
d_4		996		1030		
ρ_5		3725		3265		
ε	0.030	0.047	0.034	0.036	0.031	0.027

Table 1 *(cont.)*

site	**1**		2		**3**	6		10
	5.5 km		4.9 km		2.8 km	2.4 km		2.9 km
ρ_1	219	(74)	410	(19)	51	24	(26)	174
d_1	16	(115)	37	(93)	325	117	(16)	86
ρ_2	20	(10)	3	(4)	125	147	(38)	39
d_2	36	(159)	69	(172)	648	557	(407)	556
ρ_3	8	(42)	9	(1781)	11	13	(14)	12
d_3	1100	(763)	746	(535)	1100	1100	(1100)	941
ρ_4	998	(6)	634	(12)		5872	(773)	2080
d_4	1100	(1100)	1100	(1100)				
ρ_5		(7167)	21000	(15510)				
ε	0.054	(0.045)	0.093	(0.038)	0.029	0.036	(0.055)	0.047

Table 2

site	**23**	**22**	21	**20**	9		8	
	12.6 km	7.7 km	5.5 km	4.2 km	2.5 km		1.8 km	
ρ_1	23	808	73	23	57	(238)	5	(4)
d_1	116	89	142	39	141	(96)	22	(61)
ρ_2	61	35	11	9	13	(25)	2	(1)
d_2	506	402	201	192	249	(493)	88	(245)
ρ_3	13	14	150	18	432	(11)	1	(37)
d_3	1100	1100	497	1100	556	(1005)	222	222
ρ_4	13291	1681	16	2900	12	(5278)	70	70
d_4		1198		1074				
ρ_5		3005		4977				
ε	0.055	0.043	0.021	0.055	0.038	(0.038)	0.035	(0.063)

Table 3

site	**12**	**11**		**15**	**7**		**24**	25
	4.2 km	2.7 km		0.4 km	2.6 km		4.2 km	14.7 km
ρ_1	1130	47	(32)	52	12	(1619)	482	71
d_1	69	201	(19)	270	105	(75)	182	160
ρ_2	9	21	(920)	22	26	(34)	20	11
d_2	368	1100	(349)	615	442	(416)	510	234
ρ_3	26	8477	(21)	9	12	(13)	8	57
d_3	1100		(1100)	1100	1100	(1100)	1100	695
ρ_4	5663		(1541)	1137	5064	(1237)	1147	11
d_4								1101
ρ_5								1436
ε	0.035	0.065	(0.044)	0.028	0.052	(0.064)	0.045	0.042

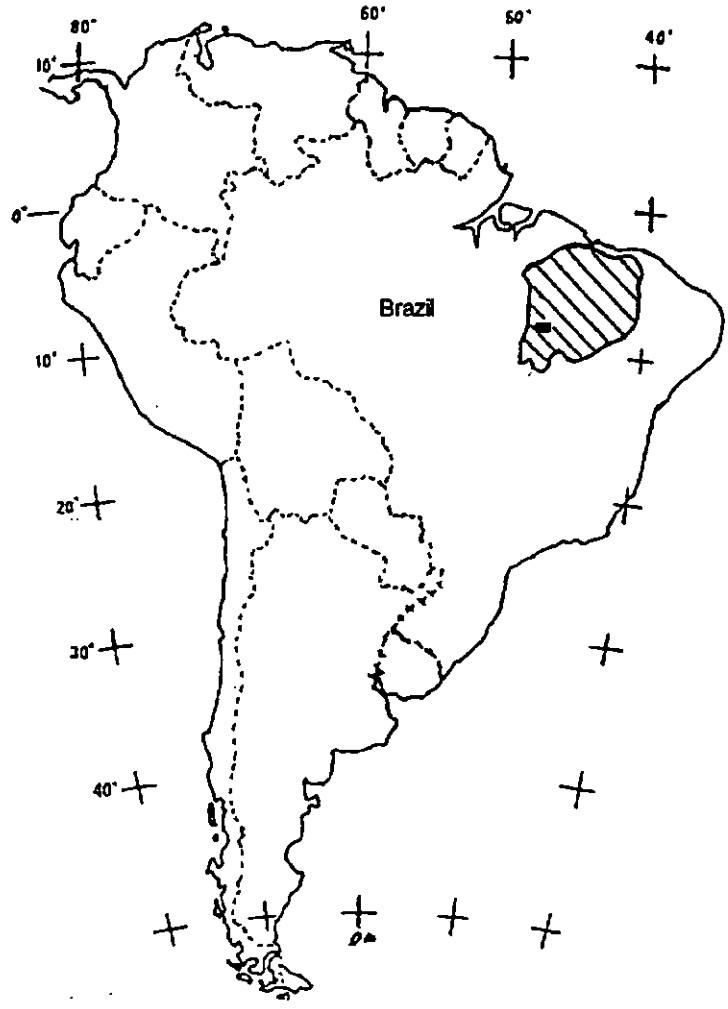

Figure 1.

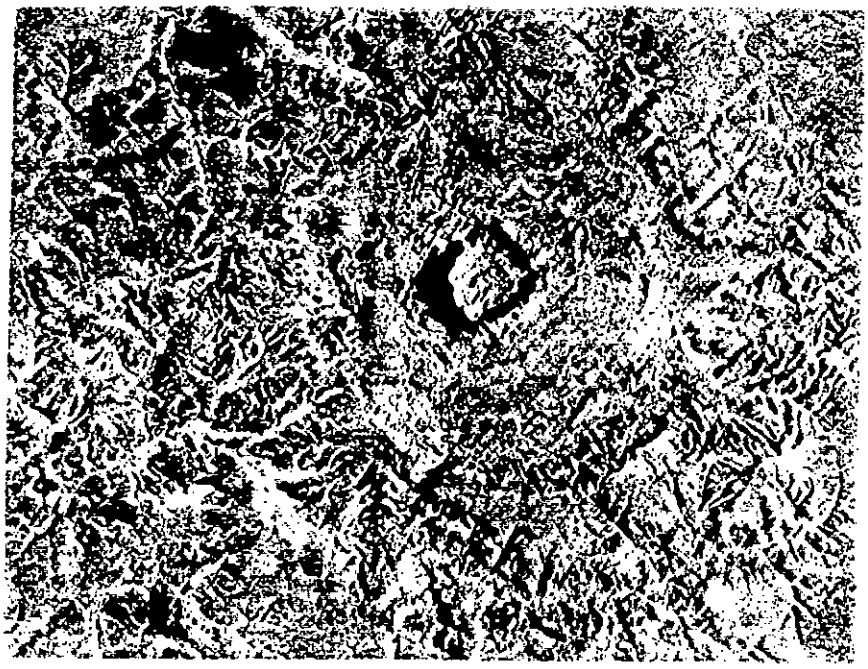

Figure 2.

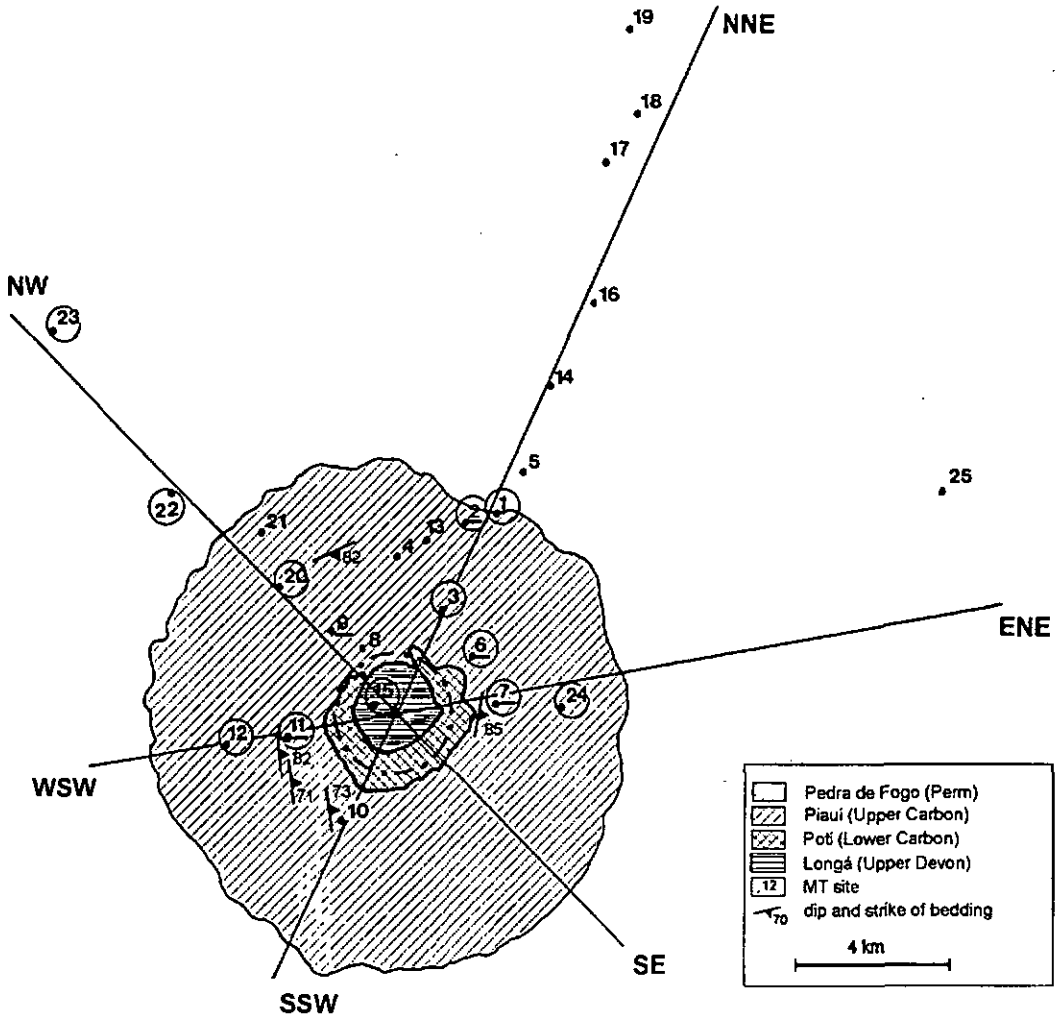
NNE
ENE
SE
SSW
WSW
NW
Pedra de Fogo (Perm)
Piauí (Upper Carbon)
Poti (Lower Carbon)
Longá (Upper Devon)
MT site
dip and strike of bedding
4 km

Figure 3.

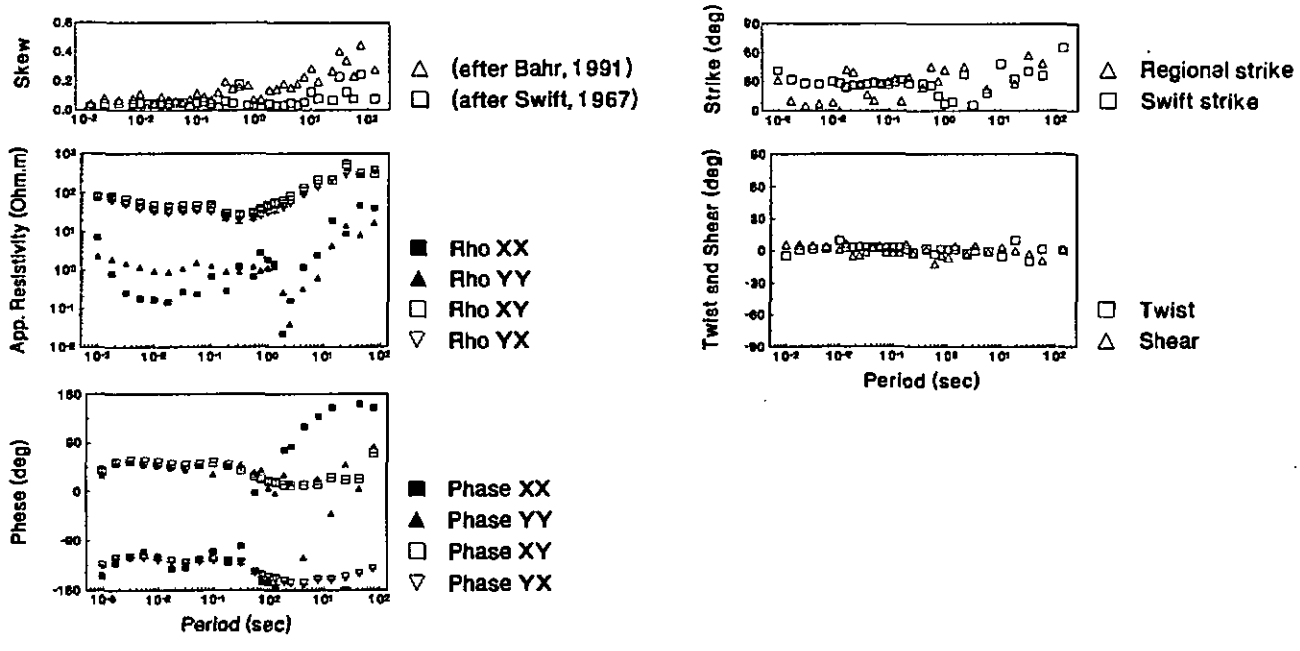
Skew
(after Bahr, 1991)
(after Swift, 1967)
App. Resistivity (Ohm.m)
Rho XX
Rho YY
Rho XY
Rho YX
Phase (deg)
Phase XX
Phase YY
Phase XY
Phase YX
Period (sec)
Strike (deg)
Regional strike
Swift strike
Twist and Shear (deg)
Twist
Shear
Period (sec)

Figure 4.

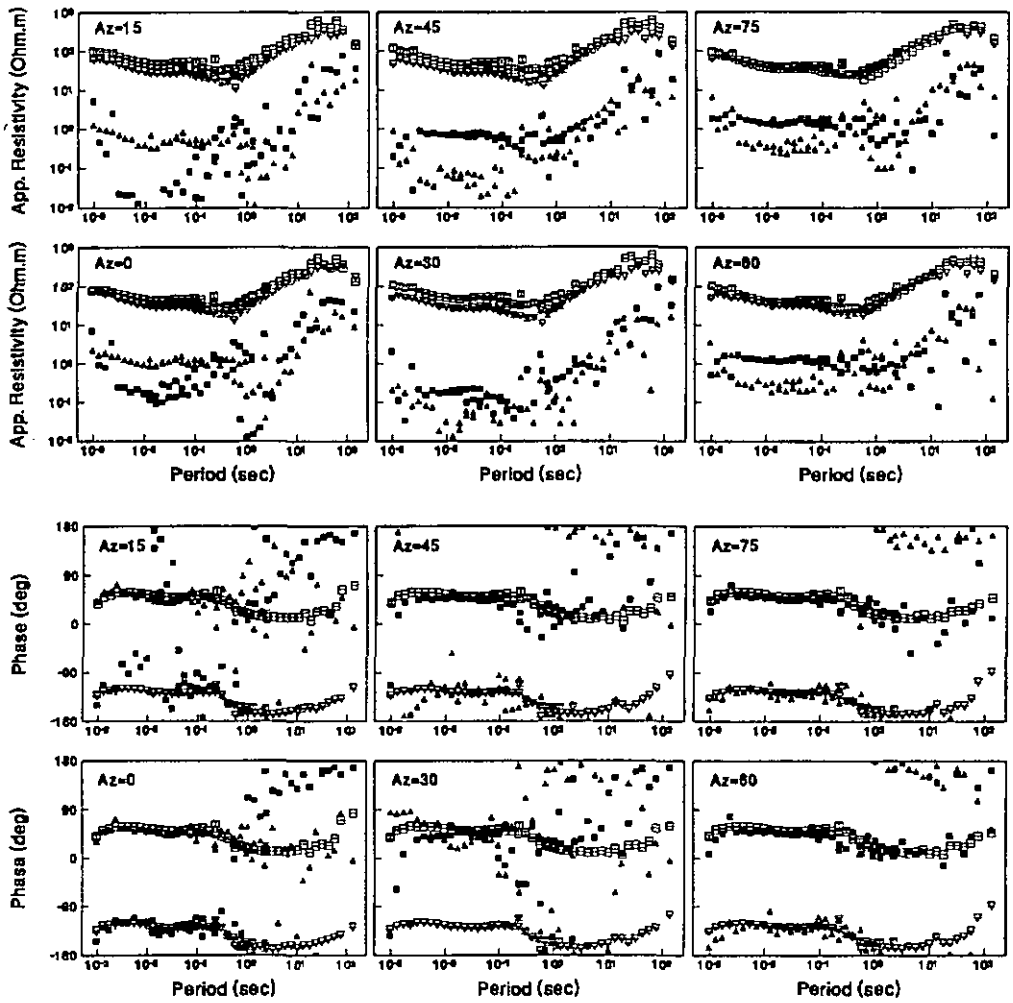
App. Resistivity (Ohm.m)
Az=15
Az=45
Az=75
App. Resistivity (Ohm.m)
Az=0
Az=30
Az=60
Period (sec)
Period (sec)
Period (sec)
Phase (deg)
Az=15
Az=45
Az=75
Phase (deg)
Az=0
Az=30
Az=60
Period (sec)
Period (sec)
Period (sec)

Figure 5.

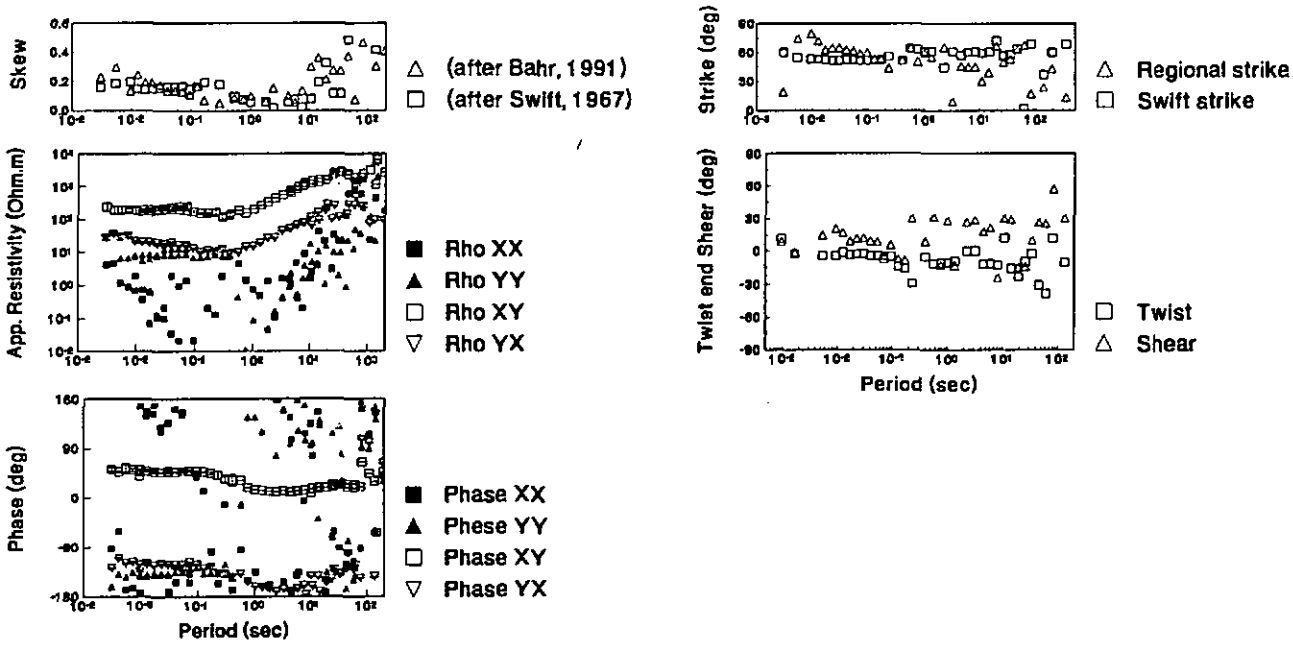
Skew
△ (after Bahr, 1991)
□ (after Swift, 1967)
App. Resistivity (Ohm.m)
■ Rho XX
▲ Rho YY
□ Rho XY
▽ Rho YX
Phase (deg)
■ Phase XX
▲ Phese YY
□ Phase XY
▽ Phase YX
Period (sec)
Strike (deg)
△ Regional strike
□ Swift strike
Twist and Shear (deg)
□ Twist
△ Shear
Period (sec)

Figure 6.

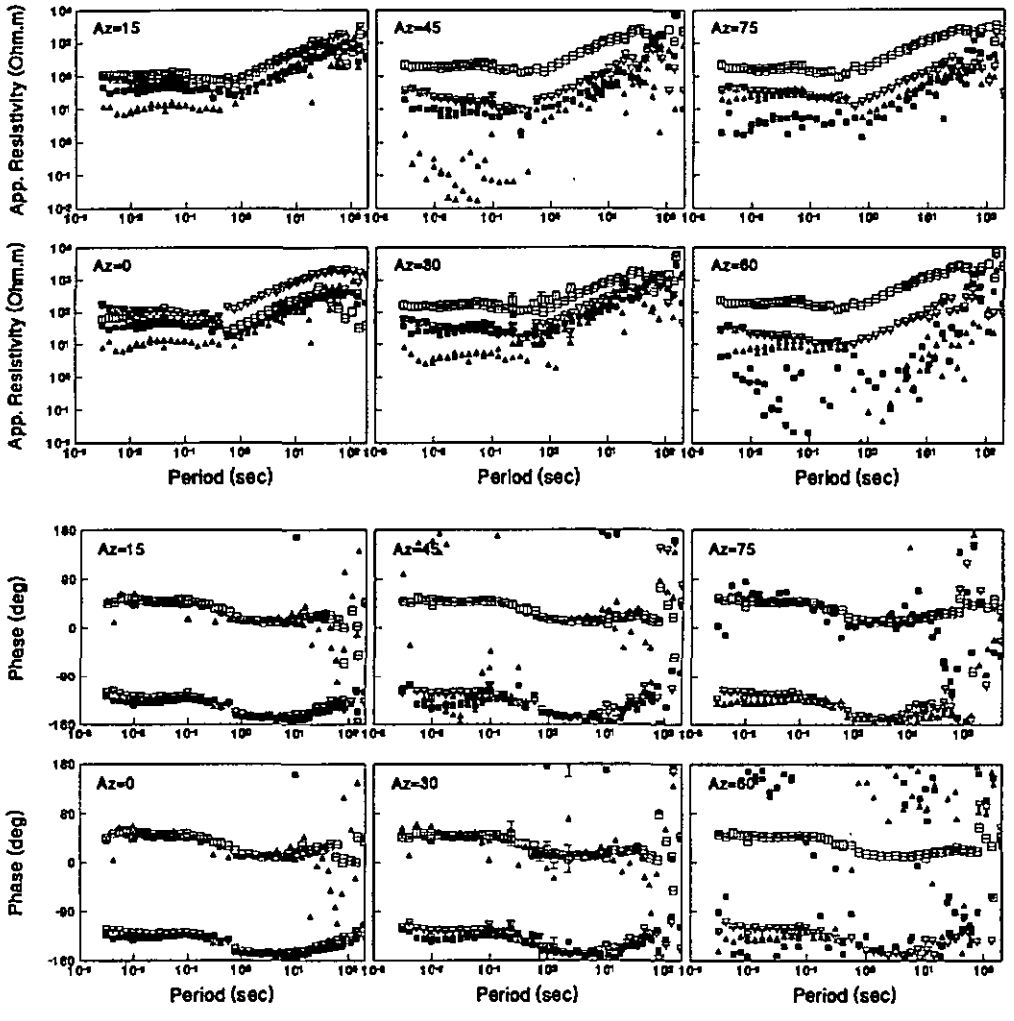
App. Resistivity (Ohm.m)
Az=15
Az=45
Az=75
Az=0
Az=30
Az=60
Period (sec)
Phase (deg)

Figure 7.

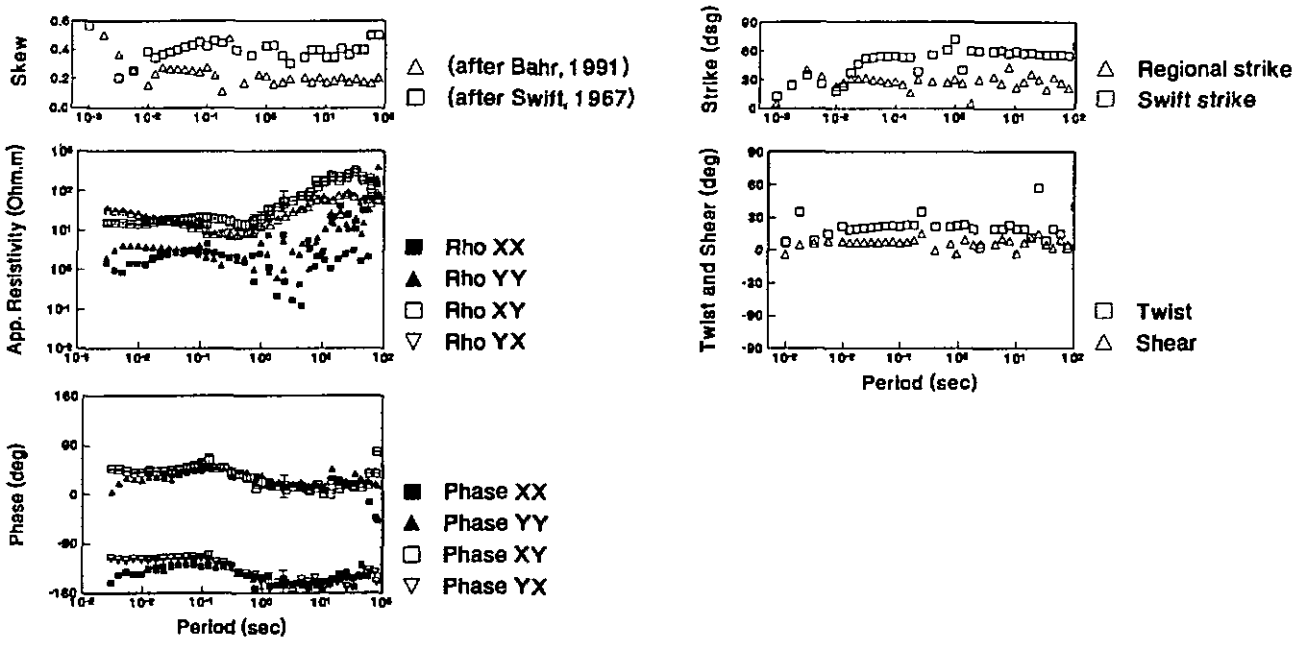
Skew
(after Bahr, 1991)
(after Swift, 1967)
App. Resistivity (Ohm.m)
Rho XX
Rho YY
Rho XY
Rho YX
Phase (deg)
Phase XX
Phase YY
Phase XY
Phase YX
Period (sec)
Strike (deg)
Regional strike
Swift strike
Twist and Shear (deg)
Twist
Shear
Period (sec)

Figure 8.

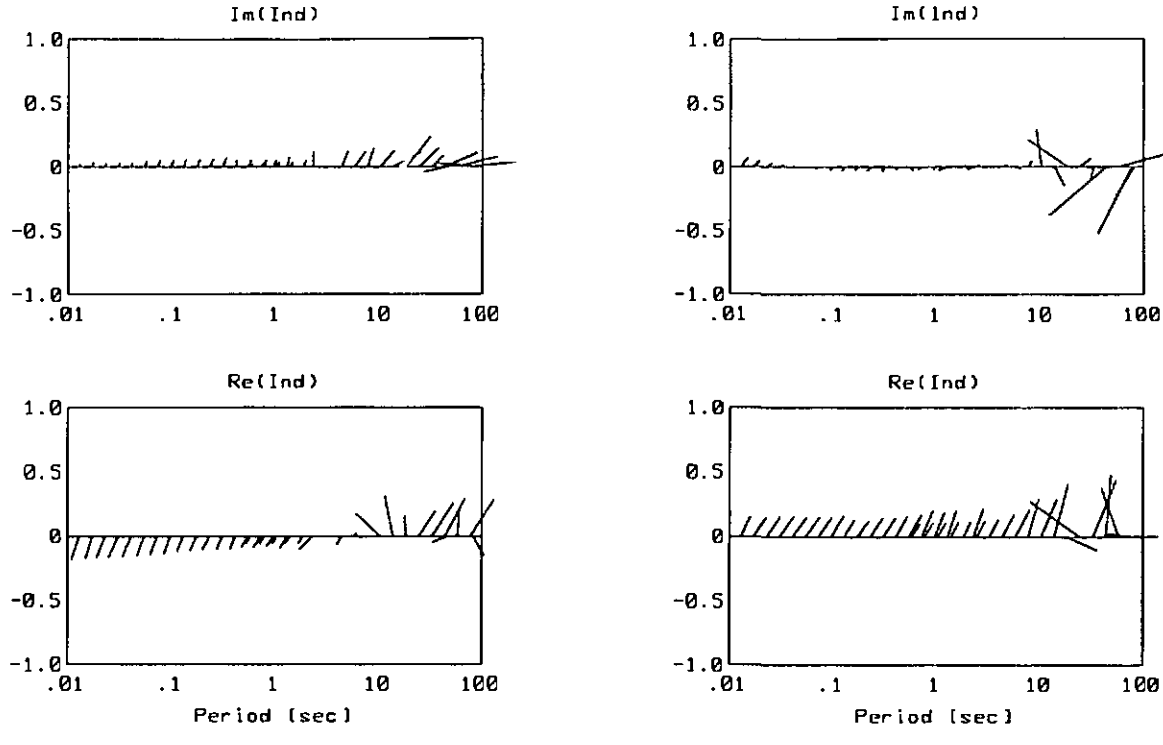
Im(Ind)
1.0
0.5
0
-0.5
-1.0
.01
.1
1
10
100
Im(Ind)
Re(Ind)
Re(Ind)
Period [sec]
Period [sec]

Figure 9.

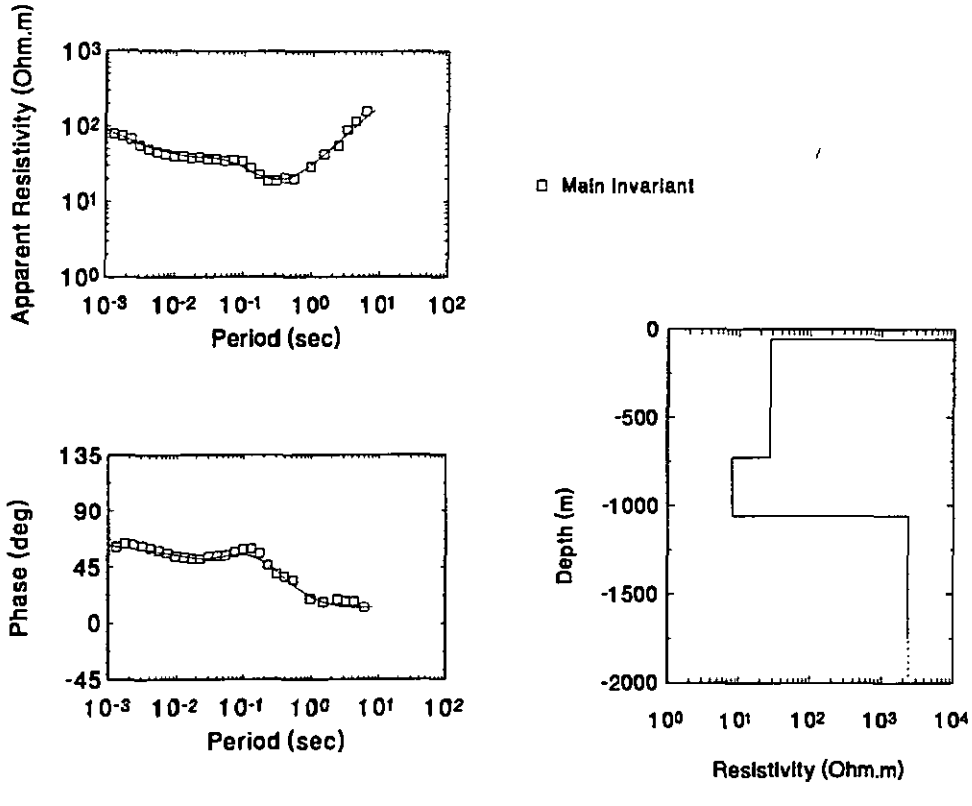
Apparent Resistivity (Ohm.m)
10^3
10^2
10^1
10^0
10^-3 10^-2 10^-1 10^0 10^1 10^2
Period (sec)
Main Invariant
Phase (deg)
135
90
45
0
-45
10^-3 10^-2 10^-1 10^0 10^1 10^2
Period (sec)
Depth (m)
0
-500
-1000
-1500
-2000
10^0 10^1 10^2 10^3 10^4
Resistivity (Ohm.m)

Figure 10.

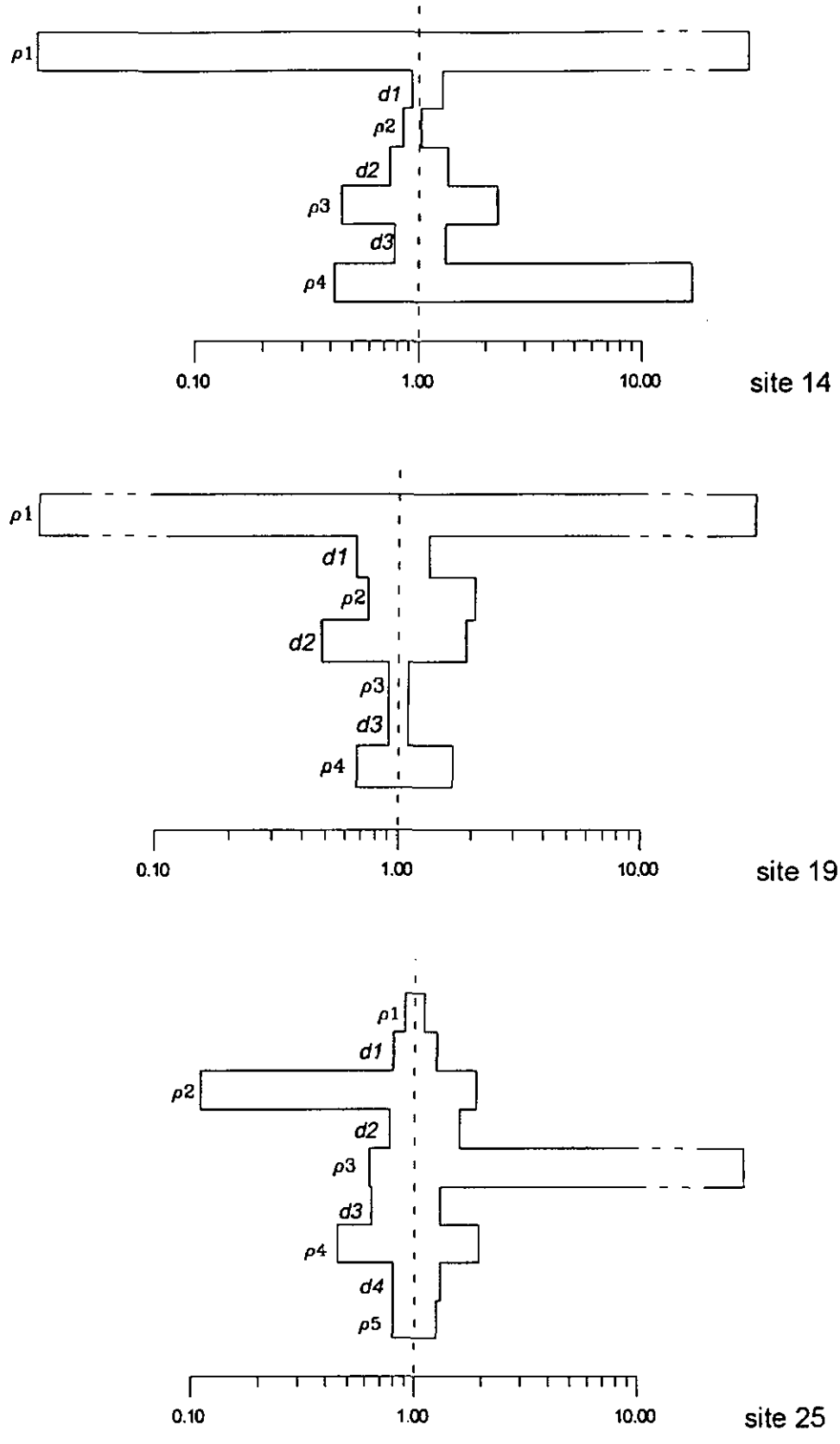
ρ1
d1
ρ2
d2
ρ3
d3
ρ4
0.10
1.00
10.00
site 14
ρ1
d1
ρ2
d2
ρ3
d3
ρ4
0.10
1.00
10.00
site 19
ρ1
d1
ρ2
d2
ρ3
d3
ρ4
d4
ρ5
0.10
1.00
10.00
site 25

Figure 11.

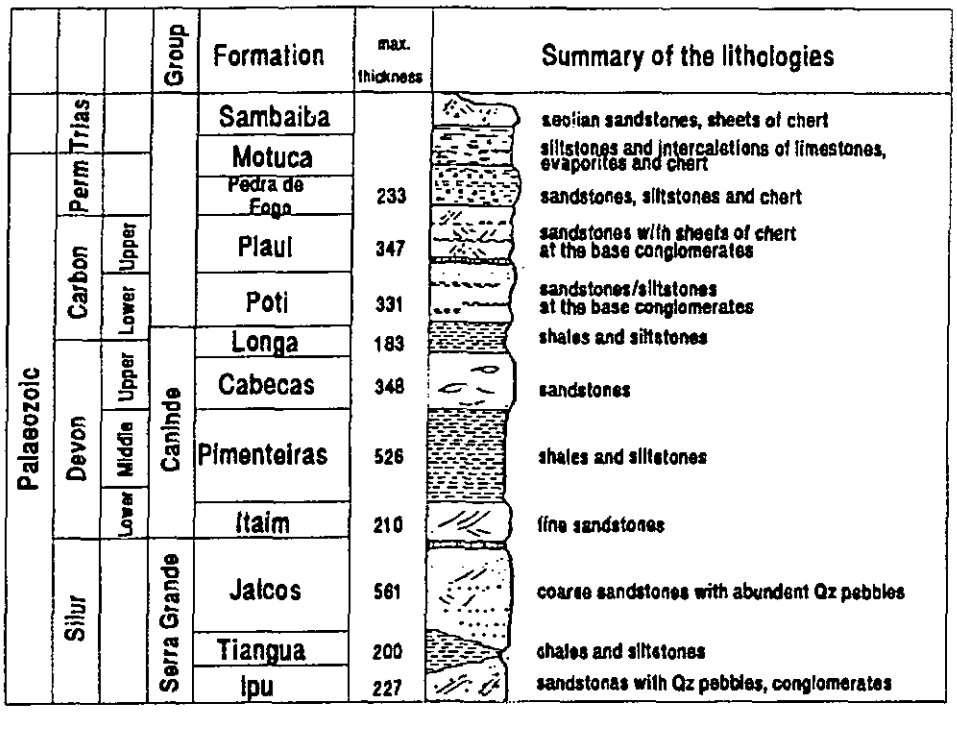
Palaeozoic
Silur
Devon
Lower
Middle
Upper
Carbon
Lower
Upper
Perm
Trias
Group
Serra Grande
Canindé
Formation
max. thickness
Ipu
Tiangua
Jaicos
Itaim
Pimenteiras
Cabecas
Longa
Poti
Piauí
Pedra de Fogo
Motuca
Sambaiba
227
200
561
210
526
348
183
331
347
233
Summary of the lithologies
sandstones with Qz pebbles, conglomerates
shales and siltstones
coarse sandstones with abundant Qz pebbles
fine sandstones
shales and siltstones
sandstones
shales and siltstones
sandstones/siltstones at the base conglomerates
sandstones with sheets of chert at the base conglomerates
sandstones, siltstones and chert
siltstones and intercalations of limestones, evaporites and chert
aeolian sandstones, sheets of chert

Figure 12.

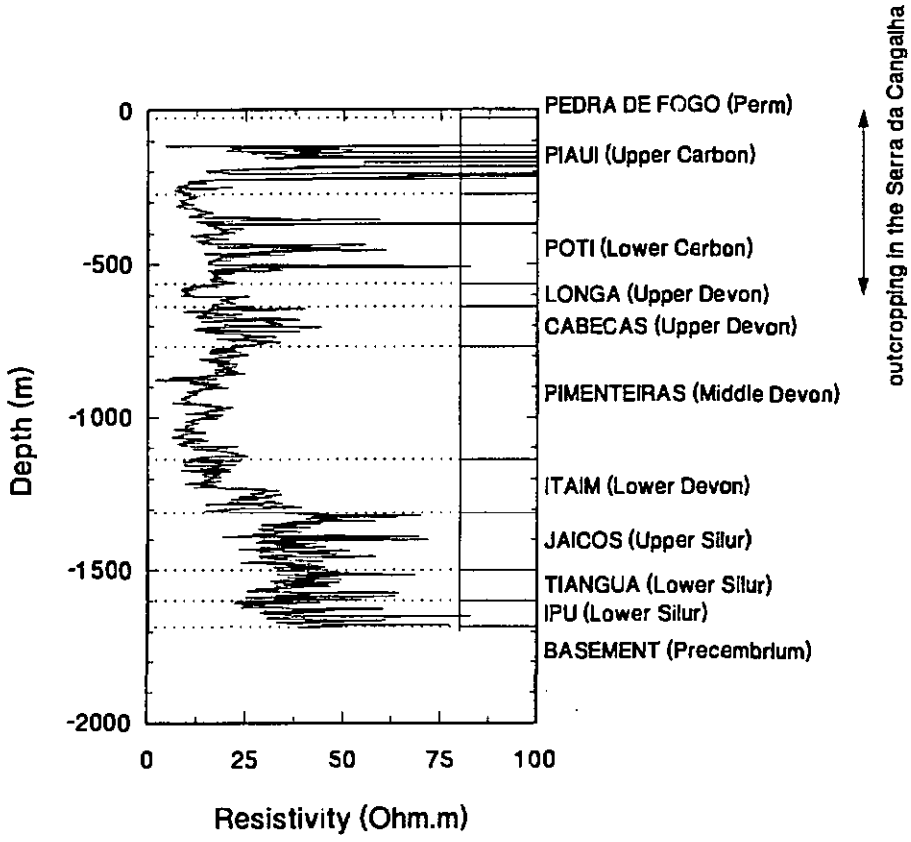
0
-500
-1000
-1500
-2000
Depth (m)
0
25
50
75
100
Resistivity (Ohm.m)
PEDRA DE FOGO (Perm)
PIAUI (Upper Carbon)
POTI (Lower Carbon)
LONGA (Upper Devon)
CABECAS (Upper Devon)
PIMENTEIRAS (Middle Devon)
ITAIM (Lower Devon)
JAICOS (Upper Silur)
TIANGUA (Lower Silur)
IPU (Lower Silur)
BASEMENT (Precembrium)
outcropping in the Serra da Cangalha

Figure 13.

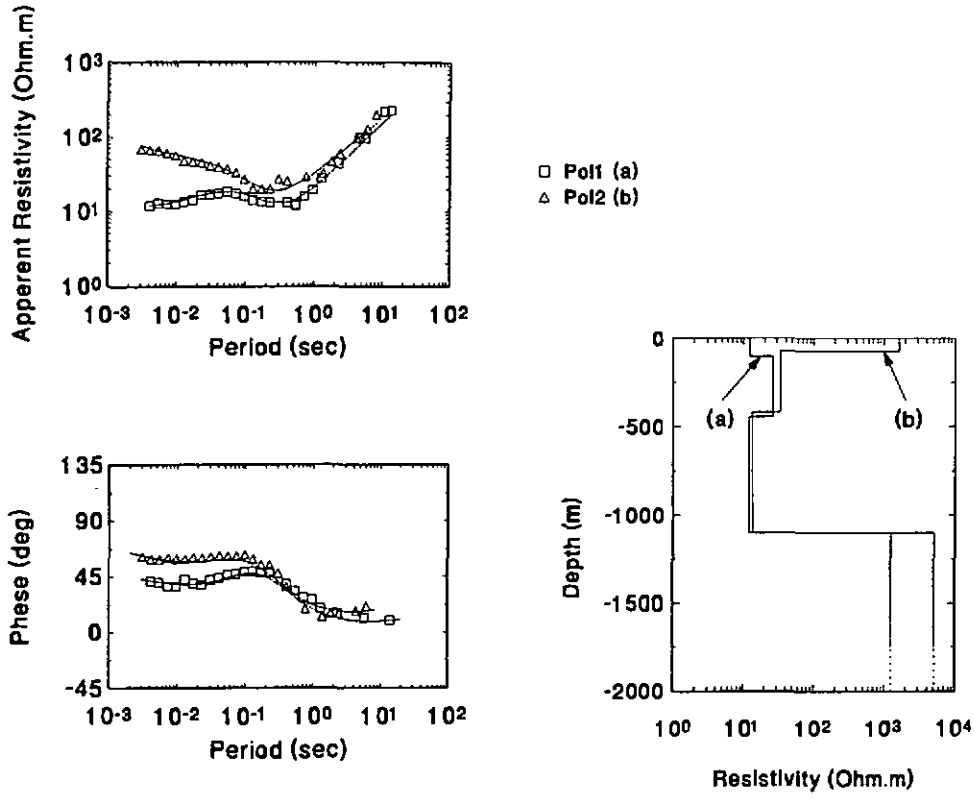
Apperent Resistivity (Ohm.m)
10³
10²
10¹
10⁰
10⁻³ 10⁻² 10⁻¹ 10⁰ 10¹ 10²
Period (sec)
Pol1 (a)
Pol2 (b)
Phese (deg)
135
90
45
0
-45
10⁻³ 10⁻² 10⁻¹ 10⁰ 10¹ 10²
Period (sec)
Depth (m)
0
-500
-1000
-1500
-2000
(a)
(b)
10⁰ 10¹ 10² 10³ 10⁴
Resistivity (Ohm.m)

Figure 14.

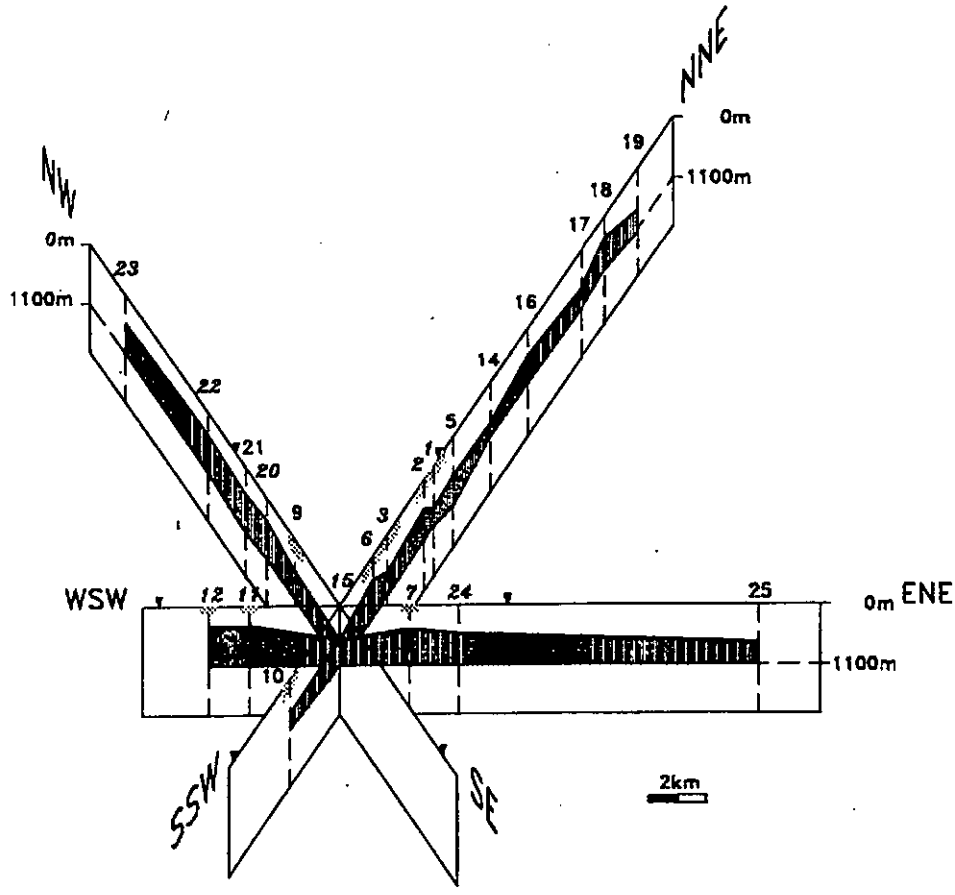
NNE
0m
1100m
NW
0m
1100m
WSW
0m ENE
1100m
SSW
SE
2km
23
22
21
20
19
18
17
16
14
12
11
10
9
6
5
3
2
1
15
7
24
25

Figure 15.

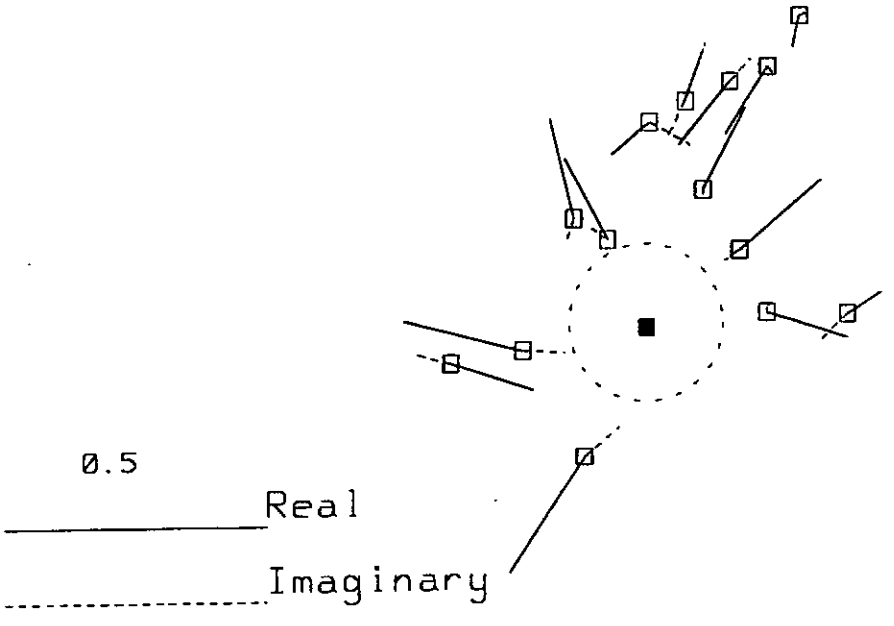

Figure 16.

This dissertation comprises the following four papers. A copy of the full text of the dissertation is at the Library of the Geology Institute and another one at the Main Library of the University of Neuchâtel.

Masero, W., P.-A. Schnegg, and S. L. Fontes, 1994. A magnetotelluric investigation of the Araguainha impact structure in Mato Grosso-Goiás, cenral Brazil, *Geophys. J. Int.*, **116**, 366-376.

Masero, W., and P.-A. Schnegg, 1994. Magnetotellurische Untersuchungen eines Meteoritenkraters, *Protokoll Kolloquium Elektromagnetische Tiefenforschung*, Höchst im Odenwald, 114-120.

Fischer, G., and W. Masero, 1994. Rotational properties of the magnetotelluric impedance tensor: the example of the Araguainha impact crater, Brazil, *Geophys. J. Int.*, **119**, 548-560.

Masero, W., P.-A. Schnegg, and S. L. Fontes, 1995. Magnetotelluric investigation of the Serra da Cangalha impact crater, Northeast Brazil, 13 pp., 3 tables, 16 figures, submitted to *J. Geomag. Geoelectr.*